Aalto University
School of Engineering

Muhammad Junaid Akhtar

Development of Guidelines for the Selection of Structural Profiles to Achieve Optimized Flooring Structure

Master's thesis submitted for examination of the degree in Master of Science (Technology)

Espoo, November 2017

Supervisor: Professor Luc St-Pierre
Thesis Advisor: Dr. Simo Koponen

Author Muhammad Junaid Akhtar

Title of thesis Development of guidelines for the selection of structural profiles to achieve optimized flooring structure

Degree program Master of Science in Mechanical Engineering

Major/minor Solid Mechanics **Code** ENG25

Thesis supervisor Dr. Luc St-Pierre
Assistant Professor, School of Engineering, Aalto University

Thesis advisor Dr. Simo Koponen
Senior Specialist, Plywood Application Development, UPM Plywood Oy

Date 26.11.2017 **Number of pages** 92 + 16 **Language** English

Abstract

The objective of this thesis is to develop finite element modelling approach for the bonded flooring structure. It shall act as a base for developing design models to study the effects of different structural profiles, materials, and to perform design optimisation. Improvements in the structural design of semi-trailers are needed to cope-up with strict emission regulations, reducing fuel cost and improving payload capacity.

In this study, a finite element modelling approach was developed for bonded flooring structures. Scaled-down models representing different zones of semi-trailer were modelled and simulated for ISO 1496-1 (1990) floor strength and stiffness test. The simulations were validated through experiments performed at the facility of UPM Plywood Oy in Lahti, Finland. Based on the comparative study of finite element simulations and experiment results, critical parameters in the finite element models were investigated. The data acquired from the scaled-down models was used to comprehend the effect of different ply lay-up on the model displacement. Scaled-down models including common structural profiles used in semi-trailers were used to develop a comparative study to comprehend the effect of geometrical profiles on lightweight construction. The scaled-down models were generated with three different spans i.e. 300 mm, 400 mm, and 500 mm. As a result, it was concluded that the I-Profile was a suitable choice for small and medium span whereas Z-Profile was an optimum choice at long span i.e. 500 mm. Scaled-down models with I-profile as a cross member was simulated to understand the application of lightweight materials in design process.

FE modelling approach developed for scaled-down models was applied to the partial (full-width) and full-scale models. These models were then simulated for ISO 1496-1 (1990) floor strength/stiffness and freight load case respectively. Weight reduction of about 5.28% was achieved in the cross members using partial models. Longitudinal beams contributed to more weight reduction. In the ISO 1496-1 (1990) forklift wheel-load case, it was concluded that the preliminary redesign of the flooring structure provides weight reduction of 3.82%. And, it increase in the model stiffness by 2.88% in partial models. Full-scale semi-trailer model with plywood yielded 9.47% less deformations in comparison to chassis-only model for freight load case. Therefore, it was concluded to use plywood panels in the finite element simulations for improved optimisation. The outcome of this thesis would be beneficial for semi-trailer designers in early design process. And, it shall also improve overall design process of the bonded floor semi-trailers.

Keywords Bonded flooring, Structural profiles, Finite Element Analysis, Semi-trailer chassis, Plywood, Adhesive bonding.

Acknowledgement

This master's thesis was commenced by UPM Plywood Oy with a vision to develop bonded floor semi-trailers for the next-generation transportation vehicles. UPM Plywood Oy is continuously striving to provide the industry with the state of the art solutions and premium products. Bonded flooring solutions for semi-trailers is one such product.

First, I would like to express my special gratitude towards my thesis advisor Dr. Simo Koponen (UPM Plywood Oy), who gave me the opportunity to perform my master's thesis on this subject. I would like to thank him for his professional guidance, constant support, and motivation. Secondly, I would like to extend my great appreciation towards my university supervisor Professor Dr. Luc St-Pierre (Aalto University) for providing me valuable suggestions and feedback throughout the thesis.

In addition, I would like to thank Mr. Sami Uuksulainen and Mr Juha Patovirta for entrusting me with this project. I gained valuable experience during last six months. I would also like to express my appreciation to Mr. Heikki Marttila for providing all the necessary technical/non-technical support whenever needed during this thesis.

Finally, I would like to thank my parents, siblings, and friends for their direct/indirect support. And, motivation throughout my project work.

Espoo, 26.11.2017

Muhammad Junaid Akhtar

Table of Contents

Acronyms and Symbols

Entries are presented in alphabetical order by first shown in uppercase letters, lowercase letters, and then finally, Greek letters or other symbols. Connection with the subscription is a good present to their units. Units are used primarily in the SI system of units. If other units are used, they transform the SI system presented.

AISI	American Iron and Steel Institute
ISO	International Organization for Standardization
EN	EUROPÄISCHE NORM
EAA	European Aluminium Association
GCW	Gross Combination Weight
FE	Finite Element
FEM	Finite Element Model
FEA	Finite Element Analysis
FOS	Factor of Safety
RHS	Rectangular Hollow Section
I	Second Moment of Area
S	Section Modulus
A	Profile Area
G	Shear Modulus
E	Elastic Modulus
v	Poisson's Ratio
ρ	Density
Φ^{e}_{b}	Shape Factor in Bending
C_m	Cost of Material
m	Metre
mm	Millimetre
km	Kilometre
MPa	Mega Pascal
g	gram
kg	kilogram
E_{XX}/E_{11}	Elastic Modulus of the veneer along the X-axis
E_{YY}/E_{22}	Elastic Modulus of the veneer along the Y-axis
E_{ZZ}/E_{33}	Elastic Modulus of the veneer along the Z-axis
G_{XY}/G_{12}	Shear Modulus of the veneer along the XY plane
G_{XZ}/G_{13}	Shear Modulus of the veneer along the XZ plane
G_{YZ}/G_{23}	Shear Modulus of the veneer along the YZ plane
U_{XY}/U_1	Poisson's Ratio of the veneer along the XY plane
U_{XZ}/U_1	Poisson's Ratio of the veneer along the XZ plane
U_{YZ}/U_{23}	Poisson's Ratio of the veneer along the YZ plane
S_{11}	Local Direct Stress in X – direction
$TSHR$	Transverse Shear Stress

"There is, in nature, perhaps nothing older than motion."

Galileo Galilei

1 Introduction

1.1 Background

Humans are always on the move. They wish to travel faster and farther with immense reliability to deliver valuable resources and products to distant lands. The availability of different modes of the transportation to deliver products creates an opportunity for consumers/suppliers to choose a more reliable, comfortable, and profitable technology. This encourages development companies to innovate, develop and improve the existing technologies. And, with the ease of the computational power, it has increased interest towards the use of predictive techniques in transportation industry as well. In the 21st century where the technological advancement is progressing with the immense speed, the optimal designs to reduce weight and efficient use of resources are of prime importance in every engineering domain including transportation industry. According to Braess & Seiffert (2005), new developments in the field of transportation will be based on advanced materials, manufacturing technology and innovative structural design to achieve conceivable lightweight products with improved functionality and recyclability. The development of such products is driven by systematic application of computational methods, experimental verification and quality assurance.

The improvement in the structural design of the land-based transportation methods is desirable to improve fuel consumption efficiently which directly results in the reduction of carbon dioxide (CO_2) emissions. It is estimated that 4.7% of the total carbon footprint in the United Kingdom is generated by the land-based transport vehicles (Department for Transport, 2012). The fuel consumption of the freight vehicles depends on many factors including engine efficiency and vehicle weight. The structural design regulations for the freight vehicles are limited which provides enormous room for innovation and improvement (Galos, 2017). The studies conducted by Brooke & Evans (2009) showed that 10% weight reduction could improve the vehicle fuel efficiency by 5 to 8%. It corresponds to approximately 12.5 g/km by reducing the vehicle weight by 100 kg. Weight reduction directly corresponds to higher payloads as these vehicles are usually limited by total weight, i.e. freight weight plus vehicle weight (SSAB, 2015). According to the Seiffert & Walzer (1984), 50% of the goods are transported by trucks and trailers in the Germany as shown in figure 1.1.

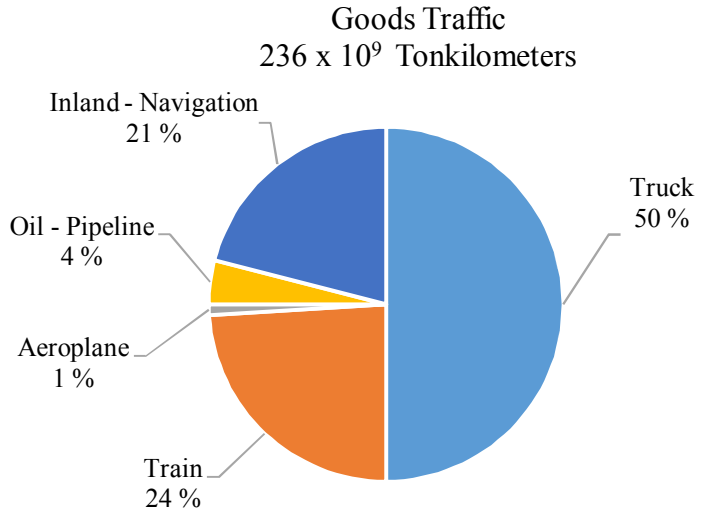

Figure 1.1: Contribution to the traffic in the Germany by different means of transportation (Seiffert & Walzer, 1984).

This thesis has been done in cooperation with UPM Plywood Oy with an aim to provide basic guidelines to perform design improvements for semi-trailer flooring structure. One such way is to use bonded flooring structures which uses adhesives instead of bolts to connect vehicle floor to the primary structure. The design of bonded floors needs the development of suitable plywood coatings and adhesive along with improved semi-trailer structural design to achieve lighter, stiffer, and durable. The optimum design and the use of the materials with minimum wastages demands a close cooperation of all the stakeholders involved in the vehicle development process. The development of next-generation transportation vehicle shall be able to cope with the increasing emission regulations, especially in Europe. Freight vehicles are the most popular mode of transportation due to high flexibility and frequency to transport various kinds of products. It has good weather independence and speed of shipping as shown in table 1.1.

Table 1.1: Qualitative evaluation of various freight transportation systems *(Braess & Seiffert, 2005)*

Serial No.	Item	Railway	Road traffic	Aircraft	Ship
1.	Mass transport	High	Low	Low	High
2.	Speed	Medium	Medium	High	Low
3.	Flexibility	Low	High	Low	Low
4.	Weather independence	High	Medium	Low	Medium
5.	Environmental impact	Medium	Low	Low	Medium
6.	Transport frequency	Medium	High	Low	Low
7.	Variability	Medium	High	Low	Low

1.2 Research Problem

The traditional semi-trailer flooring uses screws or bolts to fix the plywood panels as shown in figure 1.2 (left). According to Assembly (2011), the load distributed by mechanical fasteners is concentrated near the screw/bolt location rather than distributed over the entire connection region. Also, the application of the mechanical fastening such as screws/bolts requires special considerations like maintaining the minimum edge distance, resealing any machine or sawn edges to protect the panels from moisture etc. It requires labour to make drill holes and extensive inventory the assembly process. In a typical semi-trailer, around 200-300 screws are used to install plywood panels on the chassis which are one of the critical sources of increased corrosion, noise, and vibrations of semi-trailer. The application of mechanical fasteners for plywood panel connection reduces the durability and increases the maintenance cost in semi-trailers (Adhesives & Sealants Industry, 2010). In addition to that sometimes the screws become loose which can damage the freight thus causes economic loss to the transportation companies (Dow Automotive Systems, 2017).

To overcome the problems mentioned above, as an alternative, the bonded flooring structure is being developed. The method uses adhesives as a joining mechanism between floor panels and semi-trailer chassis as shown in figure 1.2 (right). The bonded floor creates exciting prospects for the future designs and development of semi-trailer flooring as it requires a lower number of components. The final product is stiffener and durable structure because of improved chassis to plywood panel interaction. But, it is essential for the development of bonded flooring solutions to develop the methodology for design and computational tools of bonded joints. These procedures shall be established through finite element methods (FEM) and experimentally validated. It is important to understand the behaviour of the plywood, adhesives, and structural profiles in a bonded flooring structures.

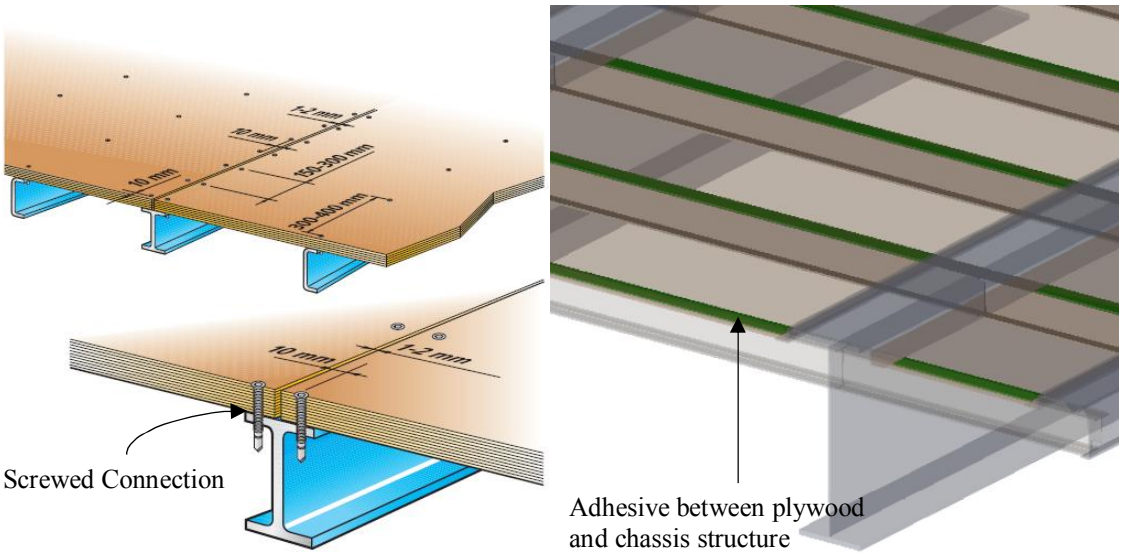

Figure 1.2: Plywood panel screwed with the chassis structure on the left (Veistinen & Pennala, 1999) and the CAD model of plywood floor bonded with the chassis structure on the right.

The bonded flooring structure comes with few design constraints such as the addition of three-millimetre adhesive between the plywood panel, and semi-trailer chassis means the use of thinner floor panel. According to Galos, et al. (2016), the maximum thickness available for the panels in semi-trailers is approximately 30 mm. The plywood panels in the bonded flooring should be about 27-28 mm. The reduced thickness of plywood pane needs to be studied from strength and stiffness point of view. It shall meet ISO 1496-1 (1990) forklift wheel-load requirements as shown in figure 1.3.

It is essential to ensure that plywood panels have enough strength to avoid local damages as shown in figure 1.3 (left) and the bonded joints shall not experience any failure. The overall floor stiffness for bonded plywood panel under forklift loading needs to be satisfactory as shown in figure 1.3 (right). These design methods need to establish using computational methods and experimental verification to create a reliable design method. This work shall demonstrate certain aspects of the design process by examples and discussion on the outcome of the FEM results. This work aims to provide designer assistance in the early design stage. In this study, focus has been on the modelling and simulation of bonded flooring structure.

Figure 1.3: Plywood panel damaged by the forklift wheel-load (left) and semi-trailer floor stiffness measurement as per ISO 1496-1 (1990) (right). Image courtesy UPM Plywood Oy.

Forklift wheel-load can produce local floor damages as shown in figure 1.3. But, it could result in catastrophic failures if the chassis structure is not properly maintained as shown in figure 1.4.

Figure 1.4: Box semi-trailer structure under forklift weight (Robson Forensic, 2017).

1.3 Research Objectives

The objectives of this thesis research work are as follows:

- Develop a suitable finite element modelling approach for the bonded flooring structures
- Validate finite element models through experimental testing
- Investigate critical parameters effecting the FE models
- Develop a procedure for selection of structural profiles for bonded floors
- Perform optimisation studies of semi-trailer flooring structures

1.4 Scope and Structure

In this thesis, the emphasis is on the viable modelling approach for bonded flooring structure of semi-trailers. The author has tried to model and simulate cases for forklift loading condition with the available data. The outcome of the thesis shall be used as starting point for trailer designers to analyse complex designs and perform the required simulations in development of new generation optimised semi-trailers. The study is based on the linear elastic models with static conditions. Boundary nonlinearity is included in some models due to frictional contacts. The material properties are estimated from the publicly available literature and technical documents provided by UPM Plywood Oy. The CAD models were generated in the SolidWorks 2016, and FE calculations were executed in ABAQUS CAE.

Chapter 2 explains the literature material needed for this thesis based on the journal articles, companies' reports, publications etc. It introduces semi-trailers and its components, materials, and bonded flooring structure. The advance trends in semi-trailer development and structural design approach are also discussed.

Chapter 3 is the heart of the thesis. It explains the methodological approach used in this work. It describes the elements selection approach and mesh convergence tests for the components used in the trailer design. A comparison between the experimental results and FE simulations is made. Based on the scaled-down models and experimental

verification, a conclusion is made on the FEM approach and expected deviation for real-life results.

Chapter 4 covers the details of the design studies performed in this thesis. Effects of different structural profiles with varying span are studied. The influence of lightweight material on the weight optimisation and model response is investigated. The partial (full-width) models are made and tested for forklift load case. The full-scale semi-trailer model is tested for freight loading and compared with the non-bonded case (chassis-only). The effect of shape factor on the weight reduction is also studied.

Chapter 5 explains the conclusions on the selection of structural profiles for the bonded flooring structure based on the FE simulations. And, it provides recommendations for future developments.

2 Literature Review

The aim of this study to present the information needed to understand semi-trailers, flooring arrangement, and loading conditions in general. It describes the structural components and materials used in the development of semi-trailers. It provides information to the reader that is considered useful in the design process and future trends in semi-trailer designs.

2.1 Semi-Trailer

2.1.1 Overview

A semi-trailer is a trailer that does not have the front wheel, and it is moved around with the help of the truck. It is widely used in transporting the materials and supplies. The chassis of semi-trailers forms the primary entity that maintains the safety of the whole structure by efficiently carrying and distributing the loads during operation. According to Patil & Deore (2015), a typical semi-trailer chassis is a ladder frame. The name ladder frame comes due to its resemblance to the ladder structure as shown in figure 2.1. It consists of the two longitudinal beams with several cross members (cross-beams) at specific locations. The chassis structure is formed by connecting cross members that are regularly positioned in the high load regions to form a rigid structure. The longitudinal beams are usually I or C profile beams. The cross members are open or closed profiles based on the manufacturer's design method (Fitch, 1994). 73% percent of the total semi-trailer weight comes from the chassis structure, and improved designs can help in the weight reduction (Prucz, et al., 2013).

The structural design of semi-trailers is based on bending strength and stiffness for an applied loading conditions. The longitudinal beams provide bending strength and stiffness of the structure. The bending stiffness is usually more important as compared to bending strength. Local reinforcements can be added to improve bending stiffness. The torsional rigidity of the ladder frame is low due to small torsion constant of the open profiles of longitudinal beams and cross members. It shall be calculated correctly as very low torsional stiffness will generate high angle of twist from applied torque. It can dislodge the freight resulting in damaging the trailer (Fenton, 1976). It is essential to increase the torsional stiffness of the overall structure as it also improves ride comfort and handling (Happian-Smith, 2002).

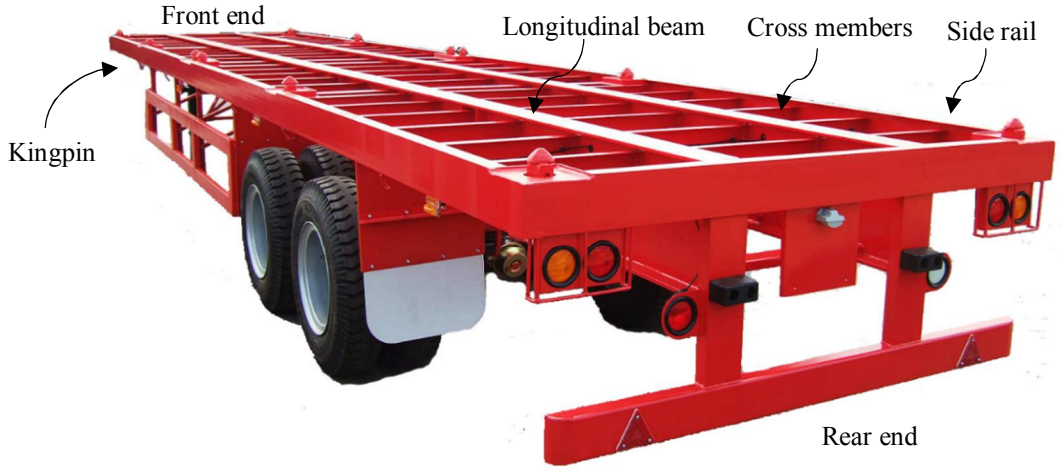

Figure 2.1: Typical flatbed semi-trailer chassis consists of two longitudinal beams connect with cross members at various locations. Image courtesy to Qingdao CIMC Special Vehicles Co. Ltd.

Semi-trailer chassis can be divided into five different zones based on the structural arrangement and loading faced by chassis as shown in figure 2.2. Zone – 1 is the rear side of semi-trailer that typically experiences dynamic axle loads. It undergoes the maximum number of loading cycles, and fatigue performance of the structure is significant in this zone. Zone – 2 is the area where wheels of semi-trailer are connected. The presence of wheels allows an insufficient space for cross members. It experiences standard loads that include forklift wheel-load and freight load. Zone – 3 is considered as the standard construction of semi-trailer chassis that have regular cross members and standard loading conditions. Zone – 4 is the neck area of semi-trailer where longitudinal beam height is reduced to make enough space for connection with the truck. It experiences standard loads that include forklift wheel-load and freight load. Zone – 5 is the kingpin area of semi-trailer. It provides a connection point for semi-trailer and the truck. It supports the front end of the trailer and takes a considerable amount of freight load but no forklift wheel-load.

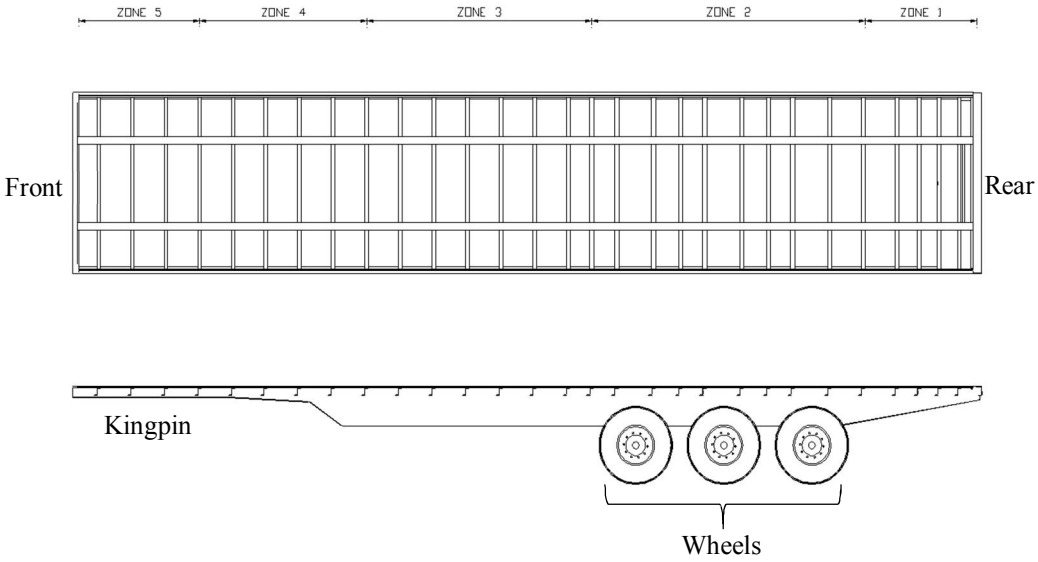

Figure 2.2: Typical semi-trailer chassis divided into five zones based on the structural variation.

2.1.2 Semi-trailer flooring arrangement

Semi-trailer chassis is usually covered with the plywood panel to provide a flat surface. According to Veistinen & Pennala (1999), semi-trailers chassis is constructed for two different panel arrangements, i.e. longitudinal and transverse arrangement as shown in figure 2.3. In the longitudinal panel arrangement, cross members are below the longitudinal beams usually by 30 mm (Galos, et al., 2016). In the transverse panel arrangement, cross members are the same height as the longitudinal beams.

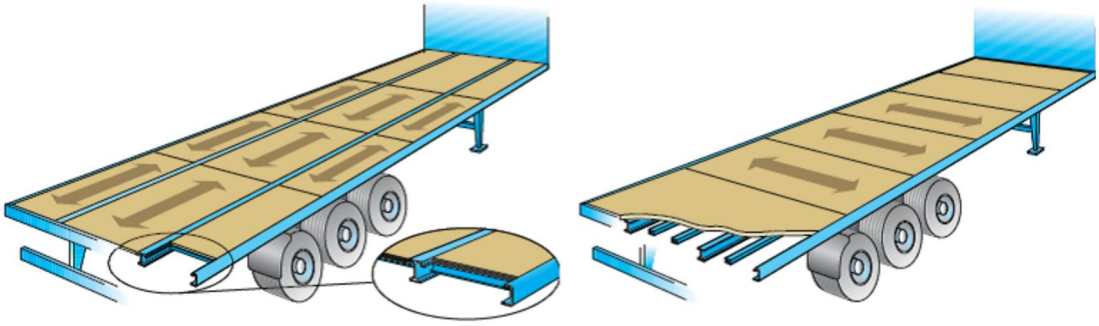

Figure 2.3: Longitudinal panel arrangement (left) and transverse panel arrangement (right) as reported by Veistinen & Pennala (1999). The arrows in the figure show the plywood strongest direction.

2.1.3 Semi-trailer loading conditions

A semi-trailer experiences several types of static and fatigue loadings during product life cycle. These loads have global as well as local effects on the vehicle structure. It is essential to have information about the nature and impact of these loads to improve the performance of the trailer design. According to Ghazaly (2014), semi-trailer mainframe should be able to support loads from the vertical, longitudinal, lateral, and torsional loads during the transportation of freight. Semi-trailer shall be able to handle loads generated during turning, braking, road variation and dynamic instability as shown in figure 2.4.

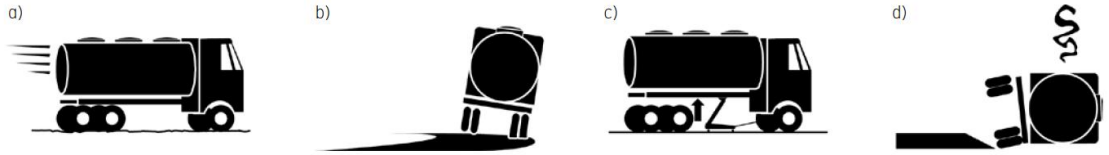

Figure 2.4: Different mode of loading face by the trailer structure during product life cycle. a) Fatigue loading b) Elastic (twisting) deformations during service, c) Total freight load during stationary and in-service d) Stability when operating (SSAB, 2015).

According to Seyfried, et al. (2015), the primary mode of deformation in the commercial vehicles is longitudinal bending due to vertical loads. The dynamic loading caused by the road irregularities is converted into a static load with an impact factor. The value of 1.3 is usually taken for the commercial vehicle in the Western Europe. The freight load depends on semi-trailer rating based on gross combination weight (GCW). In this thesis, GCW of the semi-trailer model is assumed to be approximately 38 – 40 ton, which makes the freight load about 30 – 32 ton.

2.1.3.1 ISO 1496-1 (Floor Strength Test)

Semi-trailers flooring is rated based on the ISO-1496-1 floor strength test. Floor strength test is conducted to prove that the floor of semi-trailer can withstand loading of forklift wheels, while loading/unloading of freight. The typical load class for floor strength are 7,200 kg and 5,460 kg axle loads, i.e. 3,600 kg and 2,730 kg wheel-load respectively. It is usually represented by 180 x 80 mm flat area with rubber pads at the bottom to replicate tyres. After the test, if the panel has no permanent deformations, the load class of the floor is defined based on applied loading (ISO 1496-1, 1990). According to Galos (2017), the deflection is usually measured from the side of the wheel, i.e. top of the plywood panel. Forklift loading experienced by semi-trailer floor during loading/unloading of the freight is shown in figure 2.5.

Figure 2.5: Forklift wheel-load on the semi-trailer floor (Krone, 2017).

2.2 Materials in Semi-Trailers

Materials play a significant role in improving the overall performance of the transportation vehicles. The selection of materials depends on structural and non-structural properties of the material. It is driven by some important objectives like usage of energy-saving materials, recyclability of the materials, reduced wastage of the materials, enhanced durability and increased comfort. The selection of materials for mainframe of semi-trailer depends on torsional stiffness, structural stiffness, operational durability, manufacturability, material weight, corrosion resistance, ease of repair and economy (Braess & Seiffert, 2005). Some of the conventional materials used in the development of semi-trailers are explained as follows.

2.2.1 Plywood

2.2.1.1 Overview

Plywood is an engineering wood material that consists of multiple thin layers of wood known as veneers. In the construction of plywood, veneer layers are glued together to form a flat sheet (UPM Plywood, 2017). It is an engineered wood product that has reasonably uniform properties compared to solid timber. The uniform properties are due to reduction of grain anisotropy. According to Ivanov, et al. (2008), plywood products are extensively used in the structural applications due to its resistance to progressive failures in cracking and breaking. The primary raw material for plywood products made in Finland is birch which is a hardwood and spruce which is a softwood (Finnish Forest Industries Federation, 2002).

Plywood products are widely used in the construction and transportation industry such as containers for LNG in shipbuilding and flooring structure in semi-trailers (UPM Plywood, 2017). Birchwood is the preferred choice for the vehicles flooring due to its uniform consistency, superior strength, stiffness, and durability. Also, birch plywood has excellent surface hardness, easy to coat surface, gluing and peeling properties (Finnish Forest Industries Federation, 2002). In this study, birch veneers are considered suitable for the plywood panels.

2.2.1.2 Birch plywood panel as a vehicle flooring

Plywood panels in vehicle flooring provide a flat, stiff, and durable surface for the freight to be loaded and transported (Prucz, et al., 2013). According to Galos (2017), that plywood is an excellent material for semi-trailer decking due to its renewable and recycling properties. The carbon emission value during the production of plywood panel are much lower as compared to steel, aluminium, and plastics. Finnish birch plywood is the most common material used as flooring for semi-trailers in Europe.

2.2.1.3 Manufacturing process of Finnish plywood

Plywood panels with required mechanical properties are manufactured after a series of sequential steps as shown in figure 2.6. The process starts with the soaking of the logs in the warm water; then they are debarked and cut in the required dimensions. After that, the logs are peeled by a rotary lathe machine into thin veneers with a nominal thickness of 1.50 mm (corresponding to a layer thickness of 1.40 mm in final plywood panel). The veneers are then trimmed, dried, and sorted out. During sorting stage, plywood panels

are separated based on defects and joint. The veneers are then stacked together with the ply layup depending on the design requirement. The stacked veneers are bonded together by applying adhesive along with heat and pressure to make plywood. The plywood panel is then sanded by 0.30 mm from each side and density graded. Phenol impregnated paper is hot-pressed on the faces, and the side edges are painted with acryl-based paint to reduce environmental degradation during service life. In the hot-press, the top side has wire-mesh, square or hexagonal pattern plate to improve friction (Galos, 2017).

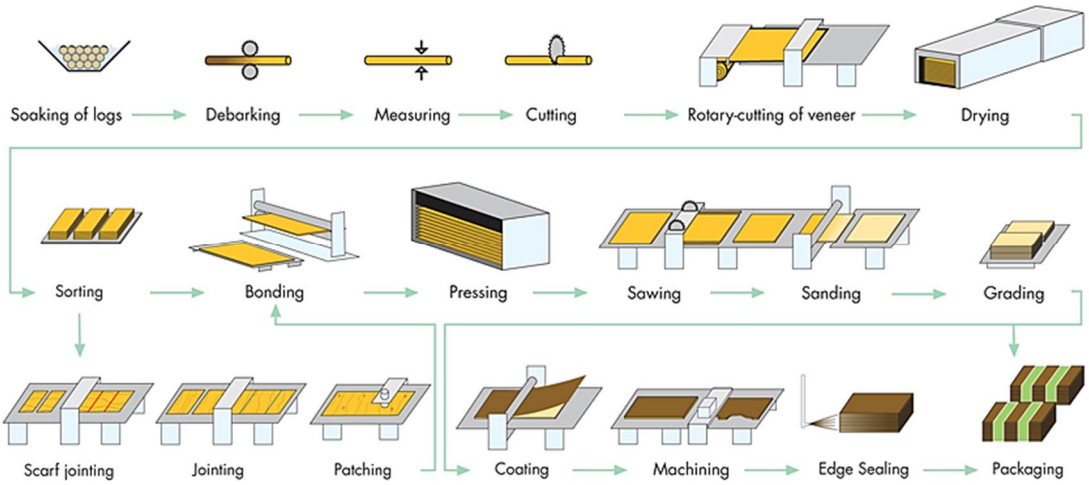

Figure 2.6: Typical schematics of plywood manufacturing process (UPM Plywood, 2017).

It is essential to design the chassis structure while keeping the standard panel sizes. It helps in reduction of material wastages which reduces the overall cost of semi-trailers. The standard panel dimensions from plywood panels manufactured by UPM Plywood Oy are shown in table 2.1.

Table 2.1: Some common sizes of birch plywood panels *(UPM Plywood, 2017)*

Serial No.	Dimension [mm^2]
1	1220 x 2440
2	1250 x 2500
3	1500 x 2500
4	1500 x 3000
5	1525 x 3050
6	1525 x 3660

2.2.1.4 Mechanical characterisation of Plywood Panel

The plywood panels used in this thesis are WISA-Trans by UPM. It is a slip and wears resistant plywood panel for trucks and trailers. The face (topside) of the panel is coated with brown (RAL 8017) phenolic resin impregnated multi-layer laminate with the high-friction pattern as shown in figure 2.7. The backside (reverse) is printed with phenolic moisture barrier, and the edges are protected by Acryl-based paint.

Figure 2.7: WISA-Trans Plywood panel (UPM Plywood, 2017).

The veneers in the plywood panel have two principal directions that are parallel to the grain direction or longitudinal direction (1) and tangent to the annual growth rings (2) due to rotary peeling of the log as shown in figure 2.8. The plywood panels are made of multiple layers of veneer arranged in a specific order to achieve desired mechanical properties based on the loading requirement (Ivanov, et al., 2008). The length of plywood (L) is in the face veneer direction of the panel. The recommended range for the length of the panel is from 1200 mm to 1500 mm for improved production efficiency (UPM Plywood, 2017).

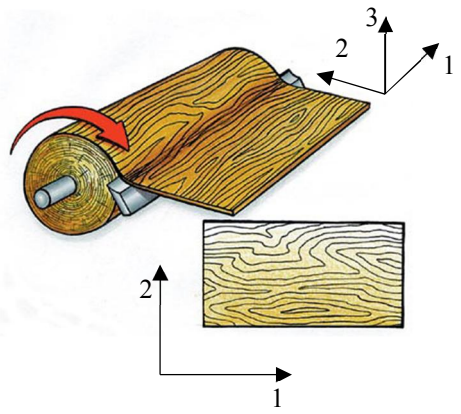

Figure 2.8: The orthotropic properties of veneer layer (Canex Group, 2010).

Referring to figure 2.8, Axis-1 is in the longitudinal direction of the grain fibres that forms the length the panel. Axis-2 is the tangential direction of the log which forms the width of the panel. And, Axis-3 is in the radial direction of the wood that forms the thickness of the veneer.

According to Veistinen & Pennala (1999), the response of the plywood panel in the vehicle flooring is based on the plate theory. The applied loading is predominately perpendicular to the floor; hence, it is a bending dominated problem. It is recommended that the plywood panels should be supported by all four edges to achieve full loading capacity. Table 2.2 shows standard arrangement of veneers in the plywood panel and its mechanical properties. It shows the effect of plywood thickness and the impact of veneer construction (ply layup) on bending stiffness of plywood. And, it illustrates the complexity of optimisation and selection of proper plywood panel. Second moment of area is divided by the specimen width to make independent of specimen width.

Table 2.2: Veneer arrangement for plywood panels used in vehicle flooring and the effect of construction on bending stiffness *(UPM Plywood, 2017)*

Sr. No.	No. of plies	Construction	t	I/b	$E_{11}I \times 10^6$	$E_{22}I \times 10^6$
			[mm]	[mm^4/mm]	[Nmm^2/mm]	[Nmm^2/mm]
1	20	|-|-|-|-|--|-|-|-|-|-|	27.40	1714	15.8	13.3
2	20	|---|-|-|--|-|-|-|---|	27.40	1714	11.0	18.2
3	20	|||-|-|-|--|-|-|-|||	27.40	1714	22.1	7.1
4	22	|-|-|-|-|-|--|-|-|-|-|-|	30.40	2295	21.0	18.0
5	22	|---|-|-|-|--|-|-|-|---|	30.40	2295	14.8	24.3
6	22	|||-|-|-|-|--|-|-|-|||	30.40	2295	28.9	10.2

| (Veneer crossed-grain direction); – (Veneer longitudinal grain direction)

where,
t = thickness
I/b = second moment of area per section width
$E_{11}I/b$ = bending stiffness per section width parallel to the face veneer grain direction
$E_{22}I/b$ = bending stiffness per section width perpendicular to the face veneer grain direction

The veneer properties of plywood panel are calculated using Steiner's theorem (parallel axis theorem) applied to layered composites. It states that the bending-stiffness of the plywood is composed of the weighted-moduli of the elasticity of individual veneer layers. In this approach, Poisson's ratios are ignored (Öchsner & Merkel, 2013). In this thesis, two different ply layup (construction) are used in the simulations and experiments i.e. 'oriented' and 'special' construction. The details of the ply layup are UPM Plywood Oy confidential informaion.

According to Finnish Forest Industries Federation (2002), the surface grades and coating of the plywood panels have insignificant effect on the structural performance of the panel. Therefore, it is not considered during the structural calculations. The plywood material behaves in a linear elastic manner when the applied load is close to the design load. The maximum limit (design) value for bending strength in second veneer (bottom-face) is around 90-95 MPa. The rolling shear strength in the middle layer is around 4.0-4.5 MPa for wheel-load cases. And, the allowable strength in heavy transport vehicles is usually taken as 1.05-1.10. The deflection of the plywood panel consists of the bending and shear deformations. The deformation due to shear stresses in a short-spanned structure is one-third of the total deformation (UPM Plywood, 2017).

According to UPM Plywood (2017), the failure of the plywood panels is predominantly in bending. The failure depends on the span of the supports and thickness of the plywood panel. It is reported that long-spanned thin plywood panels experience a bending failure whereas short-spanned thick plywood panel fails in shear. Shear failures are difficult to observe as the failure happens in the middle layers. As there is no visual identification, therefore, such panel ultimately fails in bending.

2.2.2 Structural Steel

Structural Steel is the key material in many engineering applications due to its strength and stiffness. It is an iron-carbon alloy where carbon quantity is usually ranges from 0.15-0.30%. The carbon quantity has a significant impact on the properties of the steel alloy e.g. increasing the carbon content, increases the yield strength but decreases the weldability and ductility of the material. High strength to weight ratio and its ease of availability makes structural steel a vital choice in structural applications. Structural steel has uniform and distinct properties which are easy to predict (Aghayere & Vigil, 2009).

Structural steel is widely used in the construction and transport industry. The most common steel grade used in semi-trailers is S355 with the yield strength (f_y) of 355 MPa. The structural profiles are manufactured through hot or cold rolling process depending on the geometrical shape. Some of the standard shapes used in semi-trailer chassis are shown in figure 2.9.

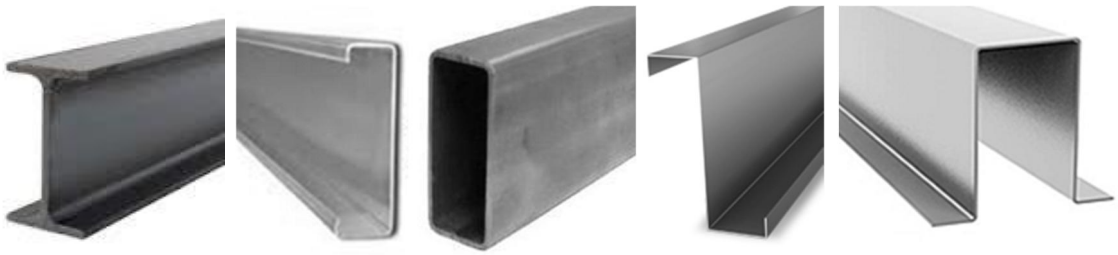

Figure 2.9: Common steel profiles used in semi-trailer designs. From left to right: I, C, Box, Z, and Omega profile.

2.2.3 Adhesive

The structural adhesive used in this thesis is the polyurethane-based adhesive that offers high strength, toughness, and excellent fatigue resistance. Polyurethane resins provide high adhesion and weathering resistance (Frisch & Reegen, 1984). The adherence is defined as the bonding of the two-different component with the presence of the interfacial layer that operates in the elastic domain. According to Zachariah (2006), adhesives failure occurs in two different ways as briefly explained below:

a. Adhesive failure is the failure of the material to stick to the substrate
b. Cohesive failure is the structural failure of the adhesive material

Adhesives provide significant benefits regarding applicability to join different elements, vibration damping, increased component stiffness and load distribution of the structure (Braess & Seiffert, 2005). According to Bassler, et al. (1992), one of the significant benefits of using adhesive fixation is that they can be easily modified to meet the requirements of the structural loads. And, these can be developed with unique characteristics and performance.

The adhesive material is assumed to be isotropic and homogeneous material. The mechanical properties of the adhesive material are estimated based on the information available in the report by Sika Services AG (2006). It states that the shear modulus of adhesive is between 1 to 10 MPa. In this thesis, shear modulus is assumed to be 3 MPa.

2.3 Design Considerations in Semi-Trailer Application

The ladder frame design of semi-trailer has a sufficient bending stiffness but a low torsional stiffness that can be improved by using the close profile for cross members instead of open profiles (Happian-Smith, 2002). The design of the structure near the point of load application should be cautiously formulated, and structure discontinuity should be avoided. The load shall be distributed over the entire structure as much as possible. The cross members should be connected at the full depth of the longitudinal beams to transfer maximum torque, if possible. (Fenton, 1996). The cross members shall be connected to the web of the longitudinal beams, as the flanges (top or bottom) are highly stressed regions when loaded at full capacity. During the design, these regions should be free from any welding or holes to avoid any failure (Fitch, 1994).

The structural design of the heavy-duty vehicles is based on three fundamental design criteria i.e. stiffness, strength and durability as reported by Zehnder, et al. (2011). The structural profiles should be selected based on stiffness and strength parameters. Stiffness depends on the geometrical shape and elastic modulus of the material whereas strength depends on the yield or ultimate strength of the material. The use of high-strength structural steel enables to design thinner and lighter structure, but the stiffness of the component is compromised. In selecting the profile, the moment of inertia, especially around the main loading direction, contributes significantly to the bending stiffness values of the profile. The stiffness of the structure plays a significant role in the efficient carrying of loads (Keeler & Kimchi, 2014). In this study, the focus is on the stiffness of the bonded flooring structure. Bending and torsional rigidity are two critical parameters that shall be improved in the design process.

2.3.1 Factors improving bending stiffness

According to the Braess & Seiffert (2005), bending resistance of the structure in response of the applied loads can be improved by:

a. Increasing the section depth of the longitudinal beams
b. Adding reinforcements in the critical locations

2.3.2 Factors improving torsional stiffness

Torsional loads are generally generated by road irregularities that can lead undesirable vibration and noise as shown in figure 2.10. According to the Braess & Seiffert (2005), the structure shall have high torsional stiffness. It can be achieved by:

a. Optimized connections between structural beams
b. Section profile of the longitudinal beams and cross beams
c. Optimized weld locations
d. Additional cross members
e. Additional reinforcements

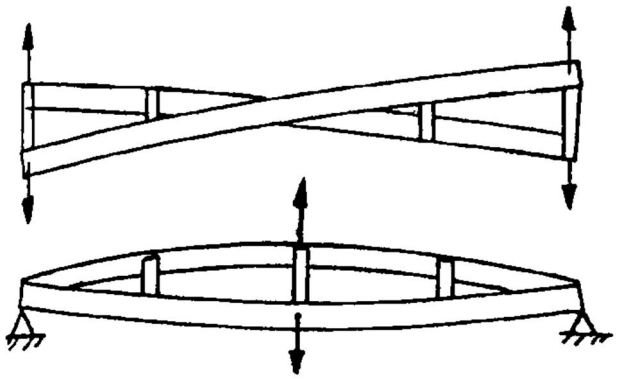

Figure 2.10: Exaggerated twisting of the simplified chassis structure torsional loads (Fenton, 1996).

According to Aghayere & Vigil (2009), the open profiles in the beam application are categorised by two types of elements: stiffened and unstiffened element. Stiffened elements are supported at both edges in direction of the applied loads whereas unstiffened elements have one unsupported edge as shown in figure 2.11. It is recommended by American Iron and Steel Institute (AISI) that the width to thickness ratio of unstiffened elements should not exceed 60 as reported by Fenton (1996).

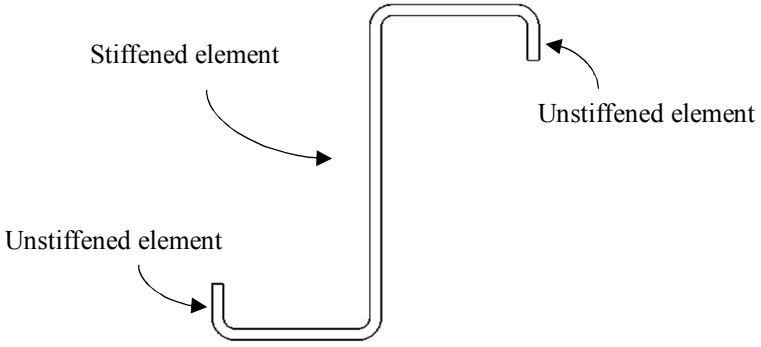

Figure 2.11: The unstiffened element is only supported for one edge and is prone to local instabilities.

In this study, forklift wheel produces bending and twisting loads on the cross members depending on location of wheel. Therefore, cross member needs to be evaluated based on the profile bending stiffness and resistance to twisting loads.

2.4 Future Trends in Semi-Trailer Design

Vehicle design process has significantly transformed over the years. In the past, only static analyses and crashworthiness were considered as significant design objectives. In the modern trends, dynamic structural design for the vehicle development plays a significant and substantial role. Modern design requirements focus more on the ride comfort (Braess & Seiffert, 2005). Torsional stiffness in semi-trailers directly affects the ride-comfort, and it is listed as one of the future demands in transportation industry by Seiffert and Walzer (1984) as shown in figure 2.12.

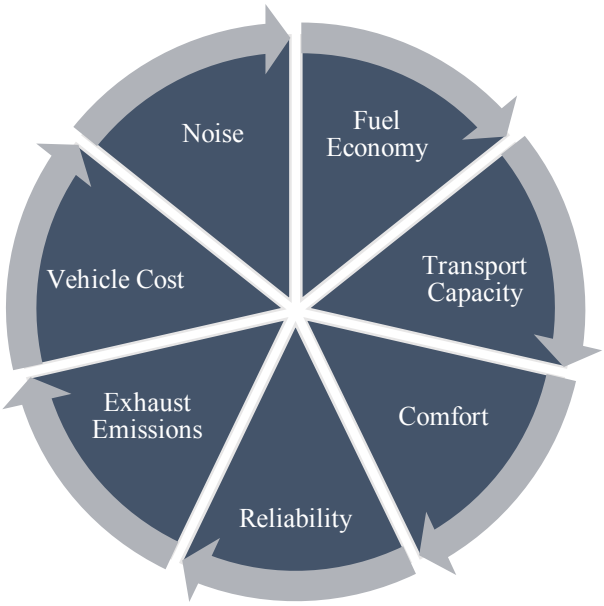

Figure 2.12: The future demands in the vehicle development (Seiffert & Walzer, 1984).

2.4.1 Application of advanced materials in the frame design

In transportation industry, low carbon steels are being replaced by the combination of steels and aluminium alloys as shown in figure 2.13. According to Mallick (2010), several factors influence the selection process for the materials apart from weight reducing potentials such as cost, durability, safety, processing, and manufacturing. High strength steel is commonly used to achieve weight reduction in the modern semi-trailers (SSAB, 2015). But, the aluminium material is also gaining importance in the automotive and transport industry as a reliable alternate material for structural steel.

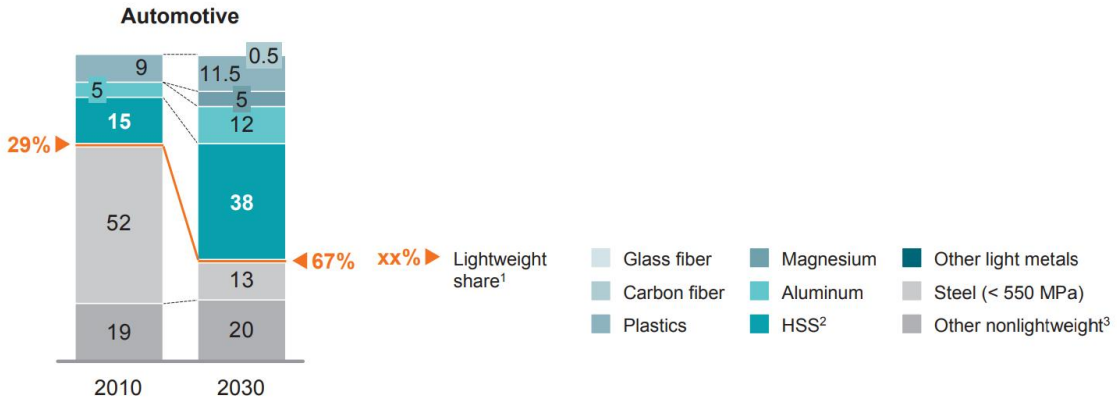

Figure 2.13: The future application of lightweight materials in the automotive industry. Image courtesy to McKinsey and Company.

Aluminium material is predominantly considered as a weight saving material in the structural design process. A study was performed by Institut fur Kraftfahrzeuge to estimate the weight reduction capabilities of aluminium and steel materials. They performed weight optimisation for 26 different components using both materials. The study concluded that the weight reduction of analysed part for the aluminium was between 14 to 49% whereas for structural steel it was 11%. Because, a very thin high-strength steel loses its stiffness that hinders overall structural performance of the components (Federation of Aluminium Consumers in Europe, 2010).

The comparison of strength and stiffness values for aluminium and steel alloys are shown in figure 2.14 as reported by European Aluminium Association (EAA). The application of aluminium alloys also requires redesigning e.g. 20 to 40% higher beam sections and smooth transitions to achieve superior results. The studies were performed on the standard beam section 'double T' using FEM. The comparison was based on the equal strength and equal stiffness. The report concluded that 'at equal strength', beams made from aluminium alloys are 58% lighter than standard steel beam. And, it was 40% lighter than high strength steel. At equal stiffness, the aluminium alloy beam was about 50% stronger than standard steel. But, it was less strong as compared to high-strength steel (Zehnder, et al., 2011).

DEFINITION			
	Standard steel	High strength steel	Aluminium alloy
Yield strength (MPa)	350	760	250
E-Modulus (MPa)	210000	210000	70000
Density (kg/m³)	7800	7800	2700

EQUAL STRENGTH						EQUAL STIFFNESS					
	Standard steel		High strength steel		Aluminium alloy		Standard steel		High strength steel		Aluminium alloy
Strength	1	=	1	=	1	Strength	1	<	2.17	>	1.54
Stiffness	1	>	0.30	<	0.56	Stiffness	1	=	1	=	1
Weight	1	>	0.71	>	0.42	Weight	1	=	1	>	0.55
Section height	1	>	0.65	<	1.18	Section height	1	=	1	<	1.40

Figure 2.14: Weight optimised design comparison of aluminium alloy with standard and high strength steel (Zehnder, et al., 2011).

The selection of aluminium alloys based on cost becomes competitive in the lightweight semi-trailers application as shown in table 2.3.

Table 2.3: Cost comparison of steel, aluminium and its alloys used in the vehicle design *(Happian-Smith, 2002)*

Material	Cost/tonne (£)
Steel and steel alloys	200 – 1800
Aluminium and aluminium alloys	1000 – 1500

Fenton (1996) emphasised on the design of vehicle based on the structural efficiency of the engineering material as shown in figure 2.15. It points to the use of aluminium and magnesium alloys in the transportation applications.

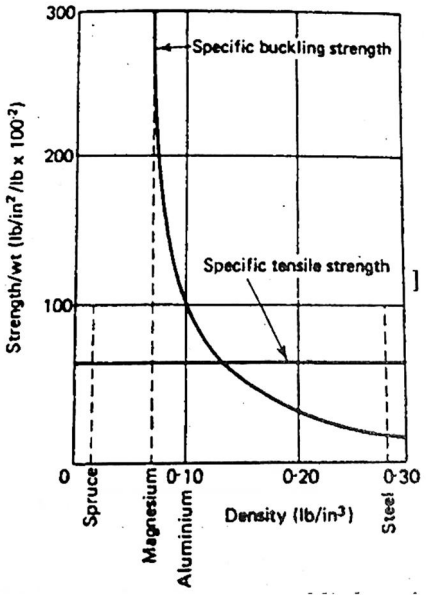

Figure 2.15: Structural efficiency of lightweight materials (Fenton, 1996).

2.4.2 Application of bonded joints in the flooring structure

The bonded flooring solution is one of the emerging trends in semi-trailer designs. It reforms the traditional semi-trailer design principles as it relies on the chemical connection between the floor and semi-trailer frame structure (chassis). According to Adhesives & Sealants Industry (2010), bonded flooring technology eliminates the need for the mechanical fasteners like screws and bolts for the flooring installation. Adhesive joints improve the structure durability, rigidity and acoustic characteristics while providing excellent corrosion resistance. The UPM Plywood Oy in collaboration with Dow Automotive Systems has developed next-generation semi-trailer with a fully bonded structure as shown in figure 2.16.

Figure 2.16: Plywood floor bonded with the semi-trailer chassis (Adhesives & Sealants Industry, 2010).

According to report by WISA Plywood (2013), the results of the full-scale prototype model of the fully bonded semi-trailer requires a very little maintenance as the adhesive joints seem to be robust. The improved rigidity of structure allows the driver to have comfortable handling. Structural adhesives reduce joint stresses by transmitting stresses

over the entire connection area thus eliminating the stress concentrations (Assembly, 2011). It was reported by Bassler, et al. (1992) that the use of adhesive also reduces the noise and vibrations characteristics of the vehicle, which improves the ride comfort. Bonded joints are less sensitive to corrosion and in some cases; the bonded elements act as a sealant to protect other components (Sika Services AG, 2006).

Structural adhesives in the plywood flooring creates a better interaction between the plywood panel and semi-trailer chassis. This type of connection improves the stiffness and strength of the overall structure. The physics of the bonded flooring is analogous to the behaviour concrete-steel composite slabs used in the civil applications where the connectors transfer shear loads between the components that results in improved strength and stiffness. According to the Couchman, et al. (1999), the structure response lies between zero composite interactions to full composite interaction depending on the effectiveness of joining mechanism as shown in figure 2.17. As per their findings, composite interaction could increase the stiffness by 20-30 %.

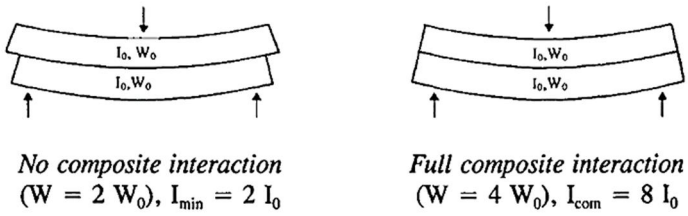

Figure 2.17: According to the (Couchman, et al., 1999), the interaction between two component lies between two extreme scenarios.

According to Assembly (2011), load distributed by mechanical fasteners is concentrated near the screw/bolt location rather than distributed over the entire connection region. The bonded connection provides better interaction characteristic in comparison to the mechanical fasteners such as screws, bolts etc. Mechanical fasteners tend to be loosely fitted in the trailer floors, and it becomes loose over time. According to Bassler, et al. (1992), the torsional stiffness of the structure is improved between 10 – 30% in the weld-bonded joints. The improvement also depends on the type of adhesive used. The use of low modulus adhesive had a lower increase in the torsional stiffness of the structure.

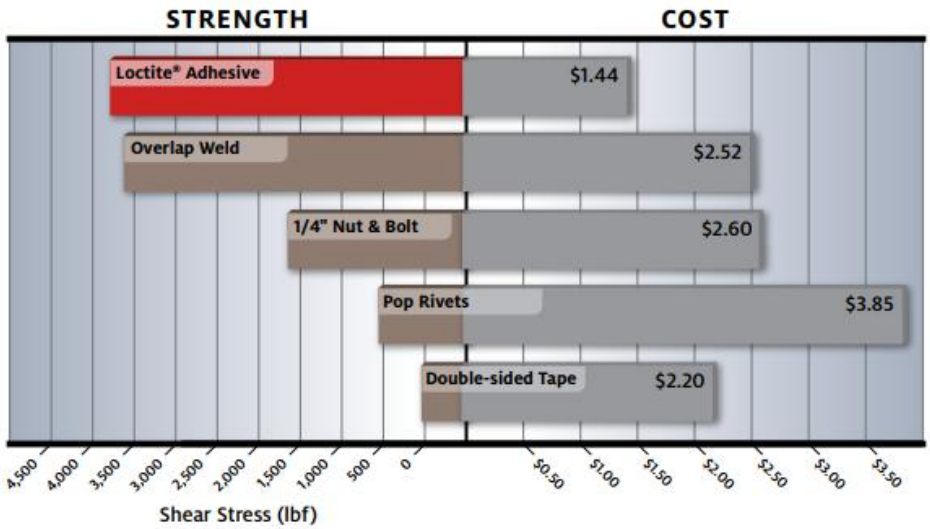

Figure 2.18: Structural adhesives have superior strength and lower cost in comparison to mechanical fastening techniques as reported by Henkel Corporation (2013).

According to Assembly (2011), the use of adhesive bonding is more cost-efficient as compared to instant assembly techniques as shown in figure 2.18. Instant assembly techniques consist of the screws, rivets, two-sided tapes and so on. As per the article, the conventional mechanical fastening is more popular because one does not need to wait for structural adhesives to cure for next processes. Whereas, instant assembly techniques require more skilled labour, surface preparation and specific location points that increase the overall cost of the assembly process. The bonded joints are much more economical and cleaner as compared to other fastening methods. It helps in reducing the number of components in the assembly and directly adds to reducing the weight of overall structure as documented by Sika Services AG (2006). It is reported by Assembly (2009) that Henkel engineers installed the wooden floor using adhesive on the trailer-frame in the 10% of the time that they normally take to install the panels with mechanical fastening.

3 Methodical Development of FE Models

3.1 Introduction

It is essential to develop a robust procedure for analysing optimised flooring structure which can be later used to create more accurate design models. The outline of the methodical steps used to develop FE models and design studies are shown in figure 3.1. Chapter 3 focuses on selection procedure of the reliable FE elements along with mesh convergence studies for each component of the bonded flooring structure. During the study, scaled-down models were developed in the SOLIDWORKS 2016 as shown in figure 3.2 and imported to ABAQUS CAE as a 'step' file. Scaled-down models represent different zones of the chassis. The scaled-down models were simulated in order to comprehend model response for ISO 1496-1 (1990) floor strength test. The simulations were then compared with experimental tests conducted at UPM Plywood, Lahti, Finland. Outcome of the comparative studies gave valuable insight on the modelling strategy and to understand the effect of various simulation parameters on the overall results. The effect of plywood layup on model displacement was also studied.

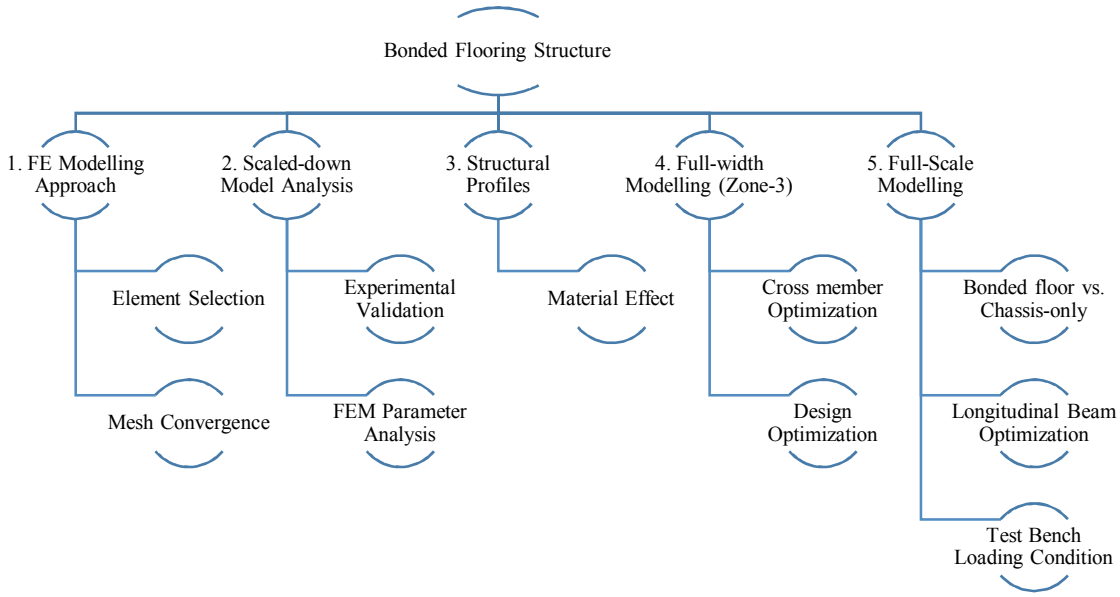

Figure 3.1: Process flow in developing methodical approach for optimised flooring structure.

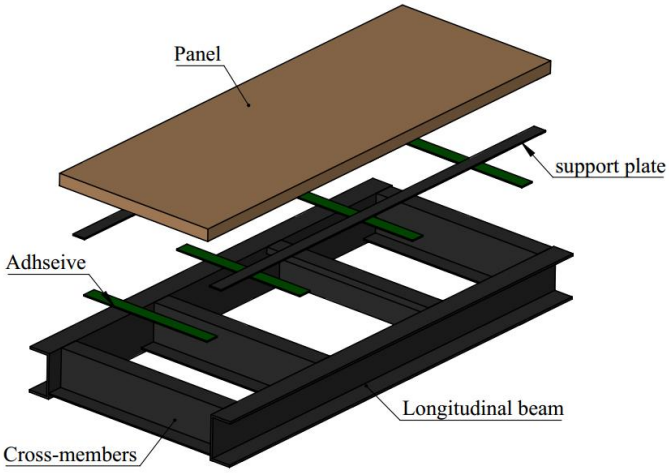

Figure 3.2: Scaled-down model representing chassis zone.

3.2 Finite Element Modelling Approach

The Finite Element Analysis (FEA) or Finite Element Method (FEM) is a numerical technique used to approximate complex engineering problems. FEM has a significant value in the design and development of the new products. FEM relies on division of the complex problem/object into a system of simple algebraic equations to give approximate results. This technique is called discretization, and it is useful in solving complex real-life problems (Madenci & Guven, 2015). The selection of suitable FE modelling approach is the first step in the FE modelling process as the accuracy of the results depends on the accuracy of FE modelling in predicting the physical problem. The FE simulations shall be able to replicate the physical behaviour of the structure with good approximation. Typically, accuracy depends on the quality (type of element and shape) and quantity (mesh element size) of elements used in the simulation process. A compromise shall be made to select computationally viable solution while performing FE analysis. Realistic model of semi-trailer is a complex geometry. And, it is recommended to perform simplifications in the design, element selection, and element size to reduce computational time (Fenton, 1996). According to the Peng & Yong-hai (2010), the non-critical elements shall be ignored. Elements having little contribution to the strength and stiffness of the structures shall be simplified to have a better mesh quality and low number of elements. The elements for the plywood panel, adhesive and frame structures were selected based on the available literature material and are described in section 3.2.1 – 3.2.3.

3.2.1 Elements for plywood panel modelling

The plywood panel was developed using 'layer-wise composite model' that means that each veneer was separately defined by its orientation and direction. Orthotropic nature of plywood panels can be modelled in ABAQUS CAE using three main elements: conventional shell, continuum shell or solid composite elements as shown in figure 3.3.

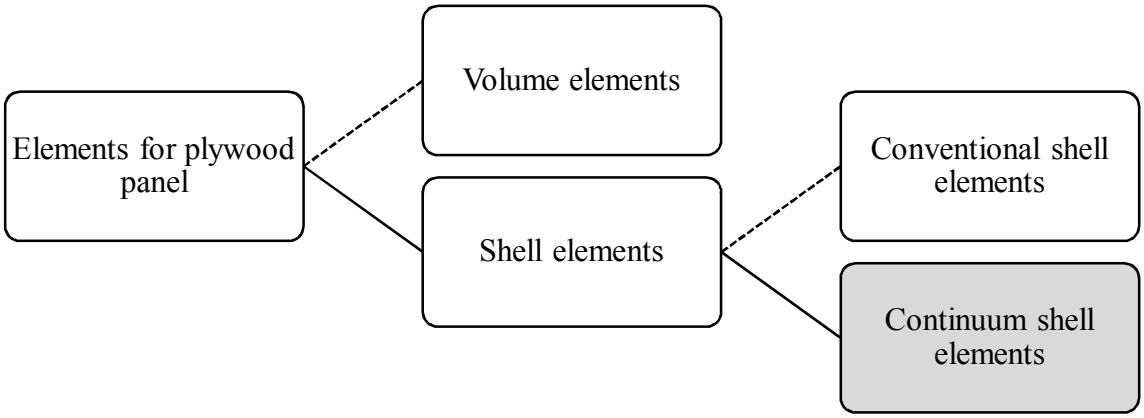

Figure 3.3: Suitable elements available in ABAQUS CAE for the plywood panel.

Continuum shell elements employ layer-wise composite theory and discretise 3-dimensional geometry. The kinematic behaviour and constitutive behaviour of continuum shell elements are like conventional shell elements as they are also established on the shell

theory. Continuum shells elements have only displacement degrees of freedom like continuum solid elements and suitable for large strain analysis. It is important to define stacking direction for continuum shell elements (ABAQUS, 2016). Stacking direction is defined in the thickness direction as shown in figure 3.4. In addition, one element shall be used in the thickness direction of the continuum shell element. Ply lay-up is defined in terms of relative thickness in continuum shell elements. Whereas, absolute thickness is defined in conventional shell elements. Continuum shell elements are computationally more efficient when compared to solid elements despite being modelled as brick elements (ABAQUS, 2016). Continuum shell elements have been previously used in research by Ivanov, et al. (2008) for the progressive failure of plywood panels during compact tension tests.

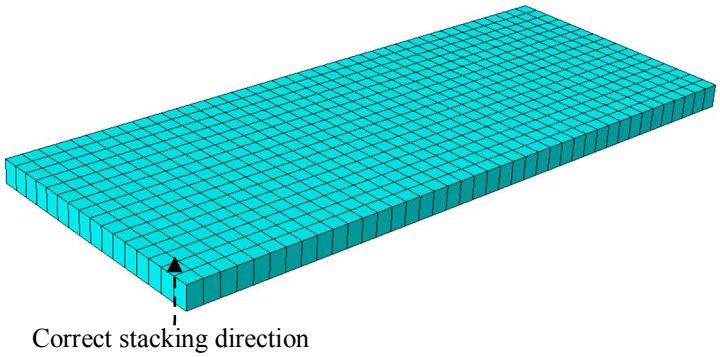

Figure 3.4: Desired stacking direction. And, one element is used in the thickness direction for plywood panel modelled using continuum shell elements.

Conventional shell elements discretise the structure at the reference surface of the geometry i.e. often mid-surface. It is generally more convenient to define the reference surface as a top or bottom surface of the CAD model (ABAQUS, 2016). Four-node shell elements were used by Labans & Kalniņš (2011) in modelling plywood sandwich panels with corrugated core. The suitable elements for modelling layer-wise plywood panels are documented in the table 3.1.

Table 3.1: Suitable elements for plywood modelling in ABAQUS CAE

Element type	Code	Notes
Continuum shell elements	SC8R	• 8-node hexahedron element with three degrees of freedom (displacement only). • Elements allow finite membrane deformation. And, large rotations that makes them effective in modelling nonlinear geometric analysis. • Suited for two-sided contacts.
Conventional shell element	S4R	• 4-node quadrilateral element with six degrees of freedom (three displacements and three rotations). • Robust elements. • Provides suitable response in most applications.

The difference between continuum and conventional shell elements is shown in figure 3.5.

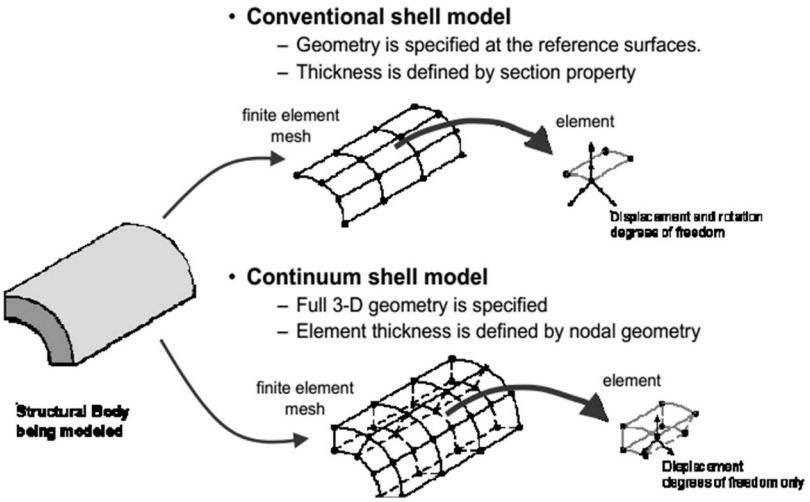

Figure 3.5: Comparison between conventional shell and continuum shell (ABAQUS, 2016).

In this study, continuum shell elements were used to model plywood panel due to its superior bending response, a possibility to use two-sided contact, and ease of modelling.

A comparative study was also performed to comprehend the plywood response with different element type as documented in Appendix 1.

3.2.2 Elements for adhesive joint modelling

Adhesive joints are used to connect two or more different components with a glue-like material having a finite thickness (ABAQUS, 2016). Adhesive material in this application was used to connect semi-trailer chassis with the plywood panel (semi-trailer floor). Adhesive elements in the FE analysis can be modelled using volume, shell or spring elements as reported by Sika Services AG (2006). The selection process of finite elements for adhesive components is shown in figure 3.5.

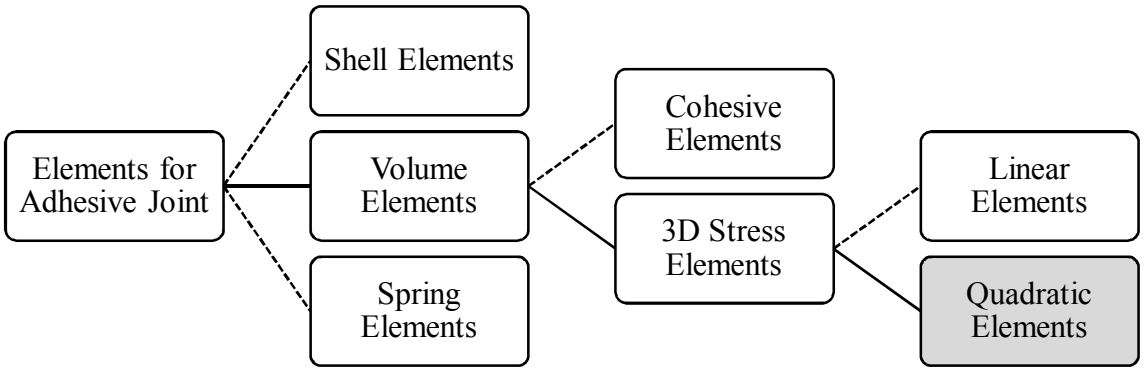

Figure 3.6: Element selection process for adhesive joint.

Shell elements are not considered in these simulations as they are not recommended in the case of two-sided contacts for 3D models (ABAQUS, 2016).

Spring elements are more efficient in comparison to volume elements as they can be modelled using large elements. This reduces the computational cost of modelling (Sika Services AG, 2006). Usually, it is assumed that spring elements have uniform performance throughout the applied area. Spring elements were not used in this thesis as many different iterations were performed, and that the spring elements are scale-depended. The stiffness parameters for the spring elements can be defined as:

$$\text{Stiffness}_{\text{Shear}} = K_s = G_a \times \frac{A}{d}$$

$$\text{Stiffness}_{\text{Tension/Compression}} = K_{tc} = E_a \times \frac{A}{d}$$

where,
G_a – Shear modulus of the adhesive
E_a – Young's modulus of the adhesive
A – Area of the bond face
d – Thickness of the adhesive

Volume elements provide better accuracy as they are well equipped to represent both tensile and compressive stresses. It is recommended to use at least one second-order (quadratic) elements. Or, two linear elements through the thickness of the adhesive for optimum compromise between modelling accuracy and computational time (Sika Services AG, 2006). Bogdanovich & Kizhakkethara (1999) discussed three different types of elements for adhesive modelling, i.e. 8-node linear brick elements, 20-node (second-order) brick elements and 27-node full LaGrange brick elements.

Volume elements in ABAQUS CAE can be modelled using cohesive elements and continuum solid (linear or quadratic) elements. They can be used for adhesive modelling if the adhesive material has sufficient thickness (ABAQUS, 2016). Sadowski, et al. (2011) used 8-node cohesive elements in their studies to simulate the damage and failure of aluminium bonded plates that were reinforced through rivets. The suitable elements in this application are briefly explained in table 3.2.

Table 3.2: Suitable elements for adhesive joints in ABAQUS CAE

Element type	Code	Notes
Cohesive element	COH3D8	• 8-node brick elements. • These elements with continuum approach can be used in situations where adhesive has finite thickness. • Shall be used with a TIE constraint in the assembly to demonstrate perfect bonding (Diehl, 2004).
Second-order elements	C3D20R	• 20-node brick elements. • Quadrilaterals and hexahedra as they provide more accurate results. • Recommended by Sika Services AG (2006).

A comparative study was performed to check the response of modelling of 3 mm thick adhesive with cohesive elements and second-order continuum solid elements. The overall model response was similar as shown in Appendix 2. Second-order hexahedron elements (C3D20R) are used in this thesis.

3.2.3 Elements for frame structure modelling

Chassis structure forms a major backbone of a semi-trailer which undergoes bending and twisting loads. It is important to select elements on the basis of the type of loading. The thickness of the metal components in a semi-trailer chassis vary from 2 mm to 15 mm. Therefore, element type and number of elements becomes important to maintain computationally viable models. Also, element shape e.g. aspects ratio is important while defining the elements in the thickness direction of the structural profile. The element selection process used in this study for frame structure is shown in figure 3.7.

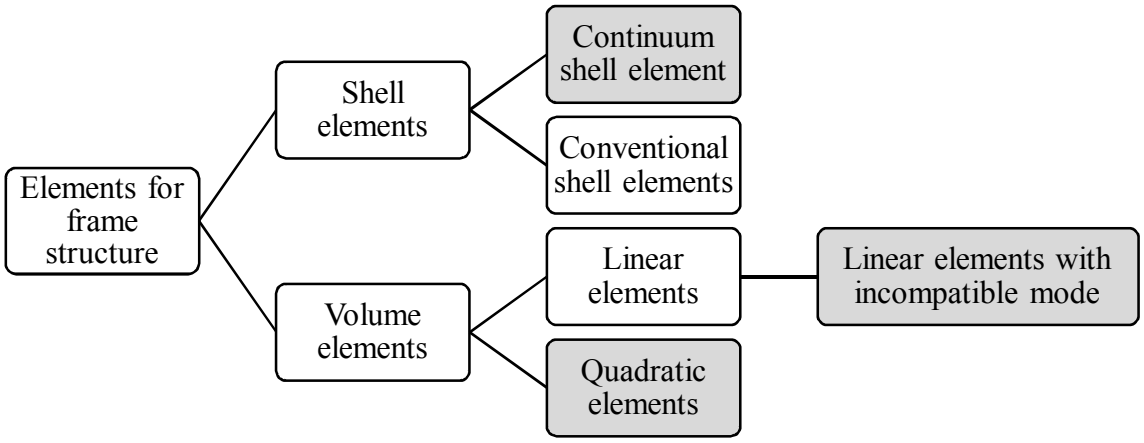

Figure 3.7: Selection of elements for semi-trailer chassis.

The modelling of metal components can be achieved using volume (solid) or shell elements. The frame components having two-sided contact shall be modelled with continuum (solid) elements or continuum shell elements. In addition, continuum elements provide ease in the modelling of 3D assemblies, but they are computationally expensive in comparison to shell elements.

The default continuum elements in ABAQUS CAE is C3D8R which is an 8-node linear brick element with reduced integration. According to Qiuli Sun (2006) 8-node linear elements are stiff to capture bending response accurately due to shear-locking effect. He emphasized on using four elements through the thickness direction to overcome shear-locking effect. Or, to use incompatible mode linear elements such as C3D8I as these elements reduces the shear-locking effect.

According to LEAP Australia (2017), it is recommended to use solid-shell elements in ANSYS for semi-trailer chassis. Solid-shell elements is same as continuum shell elements in ABAQUS CAE.

The suitable elements in this application i.e. bending dominated problem are explained briefly in table 3.3.

Table 3.3: Suitable elements for bending dominated problems in ABAQUS CAE

Element type	Code	Notes
Incompatible mode elements	C3D8I	• First-order linear elements with improved bending behaviour. Incompatible mode eliminates parasitic shear stresses that makes first-order elements too stiff in the bending related problems. • Comparable to the second-order elements while being more cost-efficient elements. • Elements performance highly dependent on the shape of the elements. These elements lose accuracy if the elements are distorted/parallelogram in shape.
Second – order elements	C3D20R	• These elements can generate quadratic displacement fields that allows them to reproduce excellent bending response. • Elements are less sensitive to element distortions especially trapezoidal distortion. • Computationally expensive.
Continuum shell elements	SC8R	• Effective in the modelling of slender structures with bending dominated problem • Computationally efficient. • Potential application: longitudinal beams and cross beams in semi-trailers.
Conventional shell elements	S4R	• Exceptionally well in capturing in-plane bending behaviour. • Computationally very efficient.

During this study, incompatible mode linear elements are selected for scaled-down models as they are computationally effective and suitable for this application. And, continuum shell elements were used in the modelling of longitudinal beam for full-scale model.

A comparative study is performed to understand the response of using conventional shell and continuum elements as documented in Appendix 3.

3.2.4 Mesh convergence studies

Mesh convergence is performed to accurately predict displacements and stresses while keeping the optimum number of elements. Stress and strains are more laborious to converge as they depend on the displacement gradients (ABAQUS, 2016). According to Peng & Yong-hai (2010), the increase in the number of elements increases the precision, but the computational cost also increases tremendously. It is recommended to use large elements where the shape is more regular and small-sized elements in the transition zones. The geometrical configuration can be simplified by removing fillets for the components to make the meshing simple. Weld-lines were not modelled in the frame structure for the same reason. It shall be noted that the inclusion of sharp edges in model gives rise to singularities, but overall response of the model should remain same. That is why stresses close to the edges are ignored. It was decided to perform the mesh convergence studies based on model displacements (U_Z). As, it is the parameter recorded during experimental

validation. But, stresses are also considered for plywood panel during mesh convergence to accurately predict plywood stresses in scaled-down models. Mesh was considered as converged when the relative difference between two displacements was less than 5%.

3.2.4.1 Mesh convergence studies for plywood panel

A continuum shell plywood panel having 20 plies in the oriented layup with face veneer in Y-axis direction was modelled and simulated. The dimensions of the plywood panel were 1000 × 400 × 27.40 mm. The mechanical properties of birch veneer used in the simulations are shown in the table 3.4.

Table 3.4: Mechanical properties of birch veneer

Property	Value
Density (ρ)	680 kg/m^3
Elastic Modulus (E_{XX})	16400 MPa
Elastic Modulus (E_{YY})	620 MPa
Elastic Modulus (E_{ZZ})	1100 MPa
Shear Modulus (G_{XY})	910 MPa
Shear Modulus (G_{XZ})	1180 MPa
Shear Modulus (G_{YZ})	110 MPa
Poisson's Ratio (υ_{XY})	0.433
Poisson's Ratio (υ_{XZ})	0.483
Poisson's Ratio (υ_{YZ})	0.406

where,
X – parallel to the wood grain direction
Y – Tangential wood direction
Z – Radial wood direction (thickness direction of the plywood)

A linear static analysis was performed where the plywood panel was loaded with a 36 kN force applied as a uniform pressure load on the wheel plate (steel) with dimension 80 × 180 mm replicating the ISO 4096-1 (1990) forklift wheel. And, the bottom edges were in pinned constraint ($U_X = U_Y = U_Z = 0$) as shown in figure 3.8.

Interaction between wheel plate and plywood panel were in tied constraint, where wheel plate (bottom-face) was selected as slave surface and plywood panel (top-face) as master surface. The thickness of the wheel plate was kept at 0.10 mm to keep the effect of the steel plate on the plywood deformations to a minimum level.

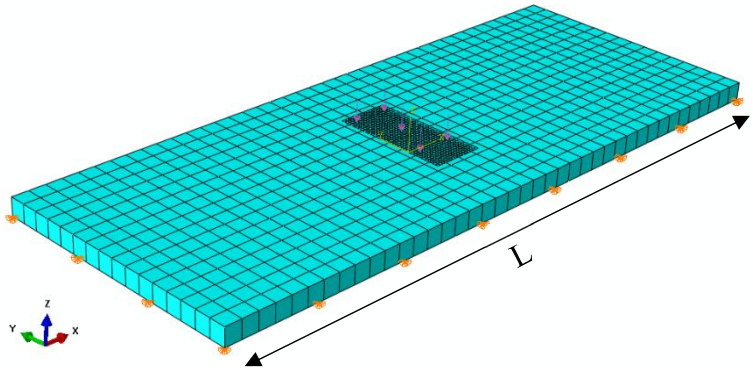

Figure 3.8: A meshed plywood panel with loading and boundary conditions.

The mesh for plywood panel was varied in the length direction as shown in figure 3.8 and corresponding values for displacement (U_Z) and Stress (S_{11}) for the bottommost layer is recorded as shown in figure 3.9 and 3.10 respectively.

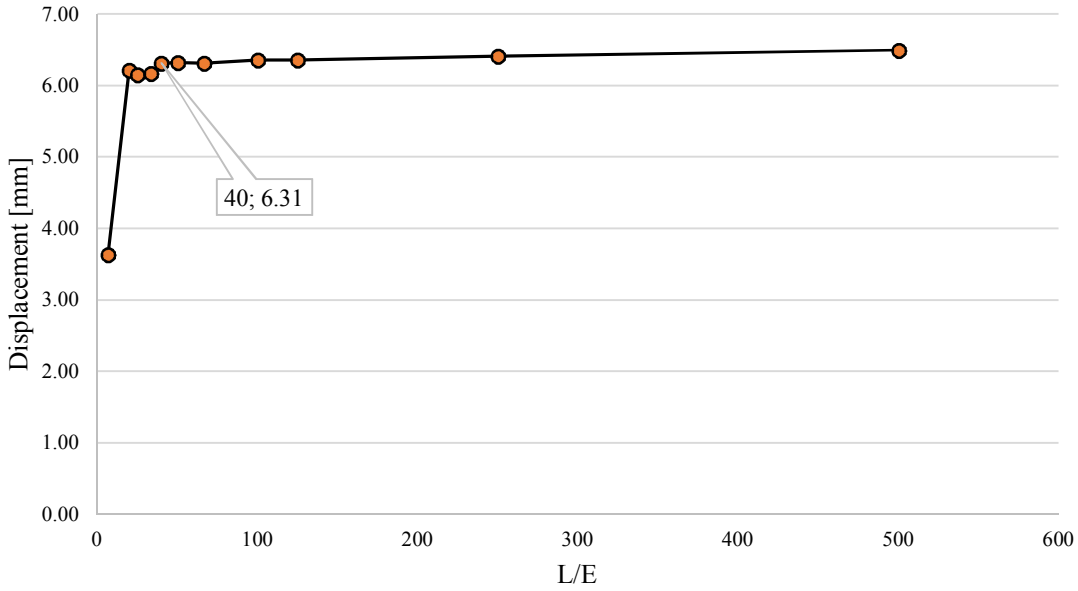

Figure 3.9: Mesh convergence plot for vertical displacement of plywood panel.

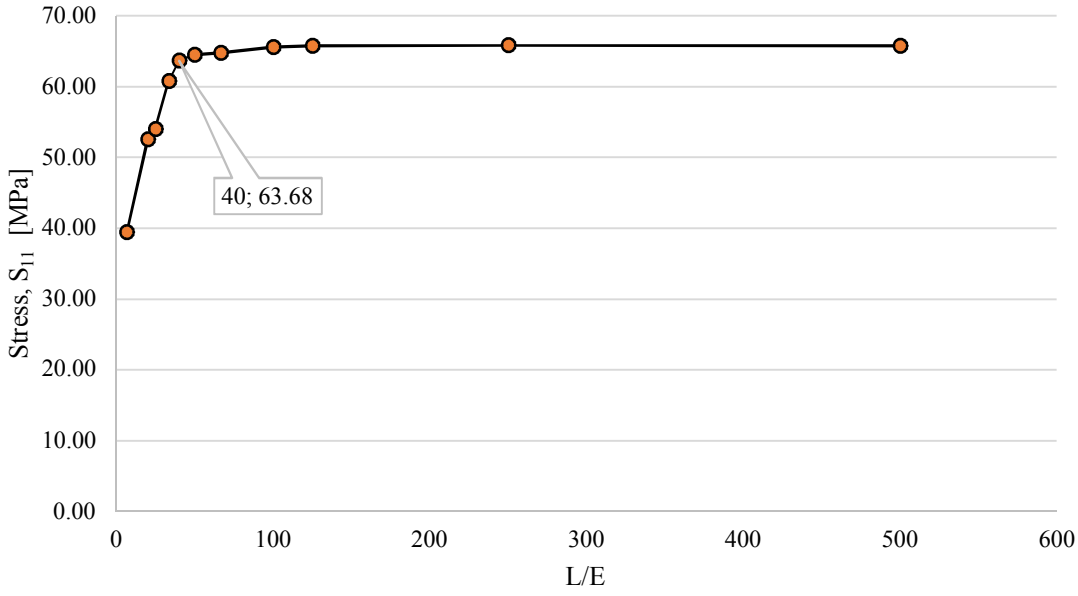

Figure 3.10: Mesh convergence plot for Stress (S_{11}) for bottommost layer of the plywood panel.

The mesh of plywood panel was converged at 25 mm. And, it was calculated by following equation:

$$\frac{\text{Lenght (plywood panel)}}{\text{Element size}} = \frac{L}{E} = \frac{1000}{E} = 40$$

3.2.4.2 Mesh convergence study for adhesive

The adhesive joint was modelled using second-order brick elements (C3D20R) with only one element through the thickness direction. Dimensions of the adhesive component were 400 x 32 x 3 mm where 32 mm was considered as the length (X-axis) of the adhesive component. The material properties of the polyurethane-based adhesive are shown in the table 3.5.

Table 3.5: Mechanical properties of adhesive material

Property	Value
Density (ρ)	1250.00 kg/m^3
Elastic Modulus (E)	7.80 MPa
Shear Modulus (G)	3.00 MPa
Poisson's Ratio (υ)	0.30

In table 3.5, the elastic modulus is calculated using following solid mechanics equation:

$$E = 2 \times G\,(1 - v)$$
$$E = 2 \times 3\,(1 - 0.30)$$
$$E = 7.80\ \text{MPa}$$

Model for adhesive convergence studies was developed from the previous model of section 3.2.4.1 as shown in figure 3.11. The adhesive material is connected to the plywood panel using tied constraints as adhesion failure is not considered in this study.

A linear static analysis was performed with a load similar to section 3.2.4.1. And, the bottom-face of the adhesive component was in pinned constraint ($U_X = U_Y = U_Z = 0$). The element size in the width direction (Y-axis) was maintained at 10 mm. Because, the deformations in the Y-axis direction are small as compared to other directions.

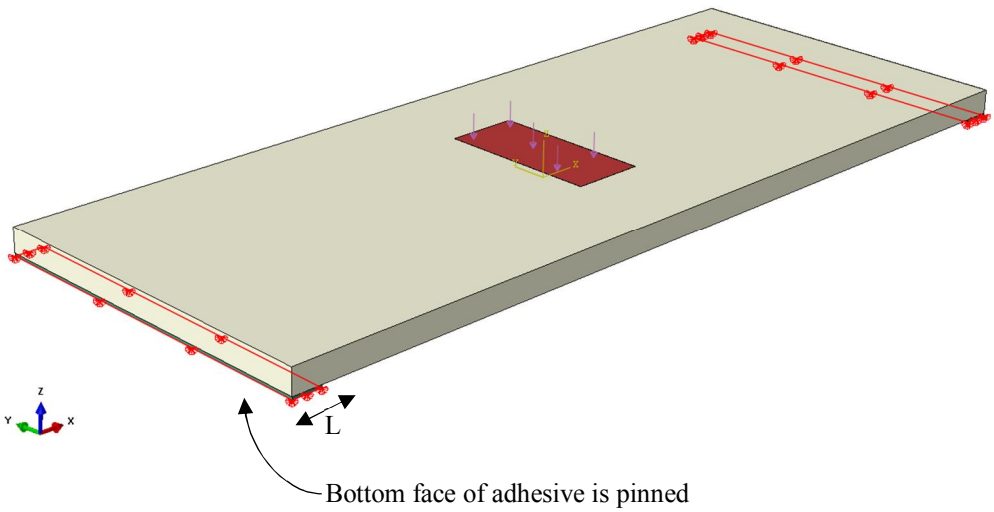

Figure 3.11: Loading and boundary conditions for mesh convergence studies of adhesive.

In the first convergence studies as shown in figure 3.12, elements along the length of the adhesive were varied. The effect of adhesive material element size on the overall model displacement was small. But, element size of 6 mm was selected to keep right aspect ratio and more than one element in the length direction.

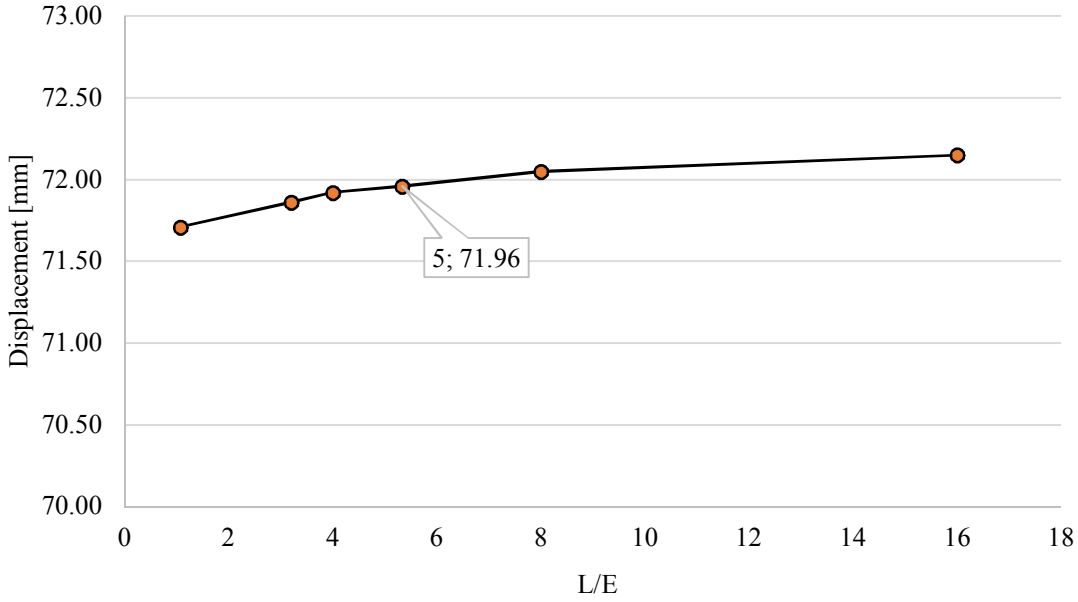

Figure 3.12: Effect of varying elements size in the length direction of the adhesive.

The element size in the length direction of adhesive material used in the simulations was 6 mm. And, it was calculated by following equation:

$$\frac{\text{Lenght (adhesive)}}{\text{Element size}} = \frac{\text{L}}{\text{E}} = \frac{32}{\text{E}} = 6.4 \approx 6 \text{ mm}$$

In the next convergence studies as shown in figure 3.13, the number of elements through the thickness is increased while keeping the element size in the length direction to 6 mm. As expected by the recommendation of Sika Services AG (2006), there was negligible effect on the overall displacements.

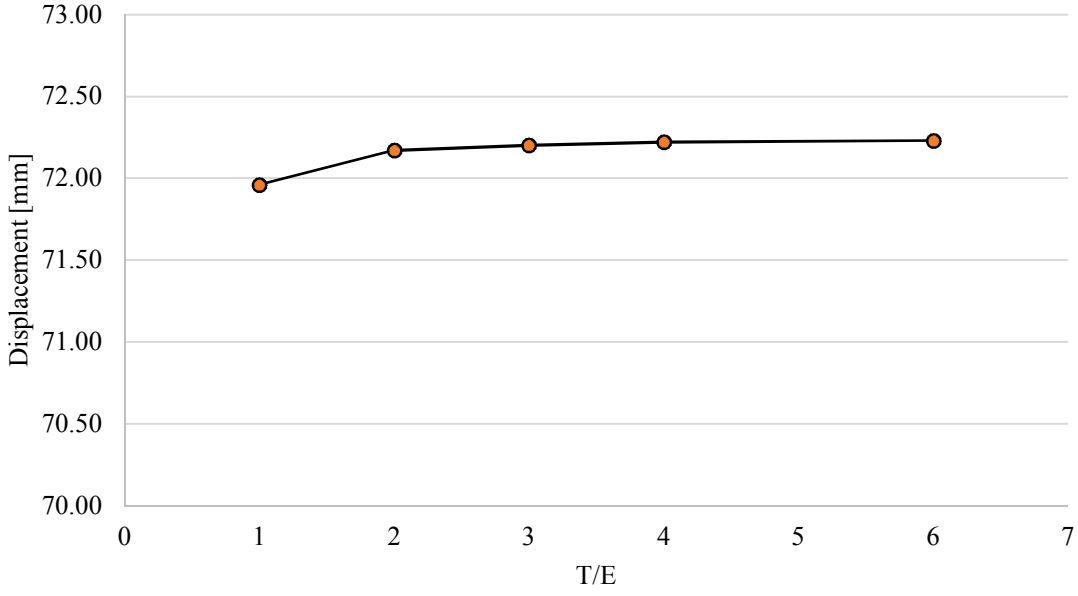

Figure 3.13: Effect of varying elements size in the thickness direction.

3.2.4.3 Mesh convergence study for steel components

The structural components of semi-trailer chassis mainly consists of longitudinal beams and cross members. The length of these components is significantly large compared to the profile thickness. As discussed previously, linear continuum element with incompatible mode (C3D8I) elements is the most suitable choice in these applications.

The mechanical properties of isotropic homogenous structural steel shown in table 3.6 are taken from AustubeMills (2015).

Table 3.6: Mechanical Properties of Structural Steel

Property	**Value**
Density (ρ)	7850 kg/m^3
Elastic Modulus (E)	200 GPa
Shear Modulus (G)	80 GPa
Poisson's Ratio (υ)	0.25

A linear static analysis was performed with a load similar to section 3.2.4.1. And, the sides of the steel profile were in pinned constraint ($U_X = U_Y = U_Z = 0$). A simplified model with cross members similar to the actual model was used as shown in figure 3.14.

The element size of the steel components in the Y-axis was kept at 15 mm whereas the element size in the web area was kept at 10 mm. The convergence studies were performed only on the flanges. The flange dimension of the cross member (z-profile) was 43 mm.

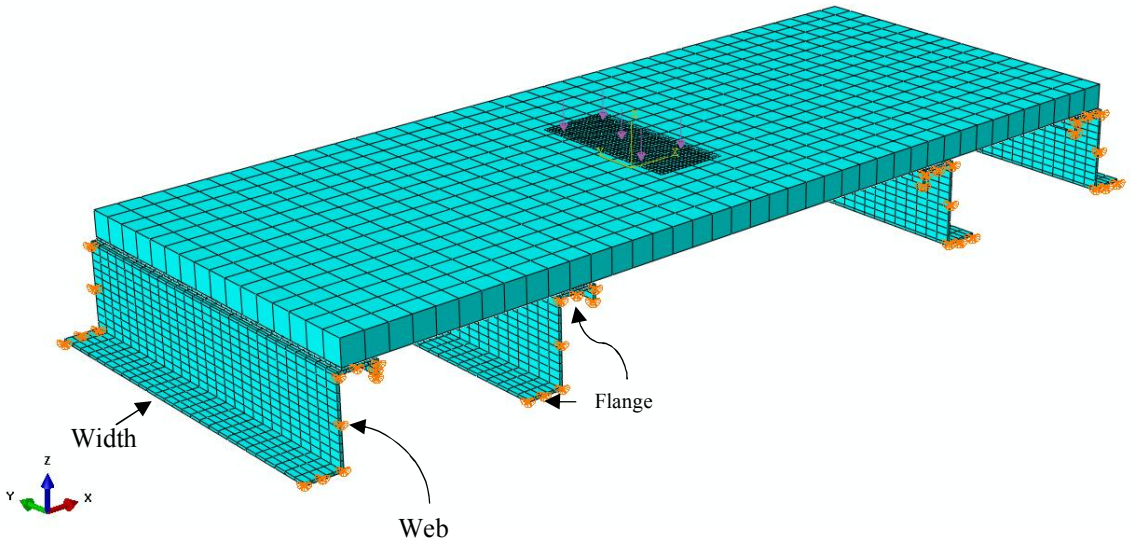

Figure 3.14: Simplified model of all the components of the flooring structure. Pinned constraint is applied on the sides of the steel components.

Figure 3.15 shows the model displacements with varying flange element size. It shows that the mesh converged at around 8 to11 mm where *'F'* is flange length.

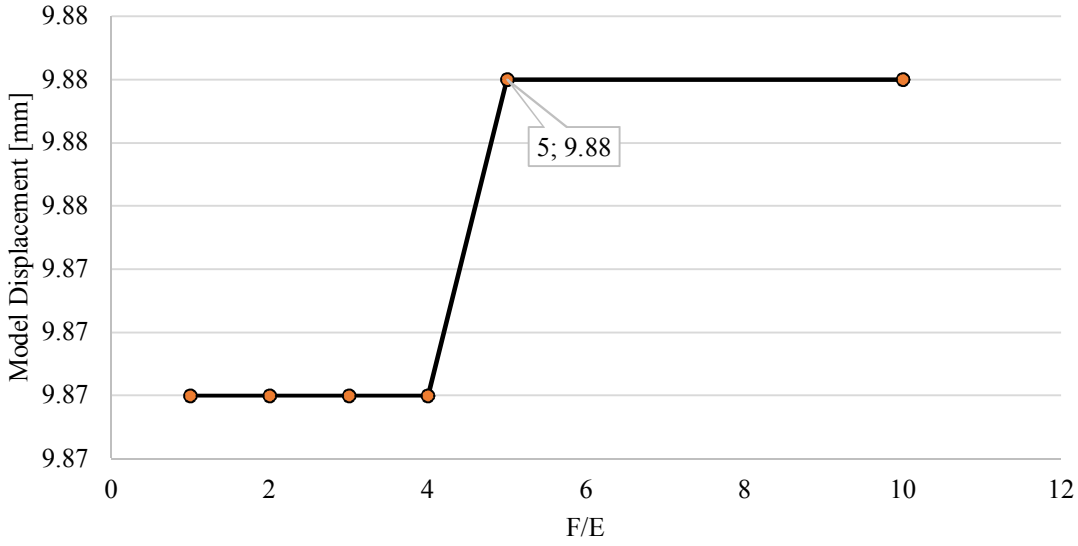

Figure 3.15: Mesh convergence with model displacement shows that the elements size of the flange should be around 8 mm.

Figure 3.16 shows the cross-member displacements with varying flange element size. It shows that the mesh converged at around 8 to 11 mm where *'F'* is flange length. Therefore, the element size was kept at 10 mm during these simulations.

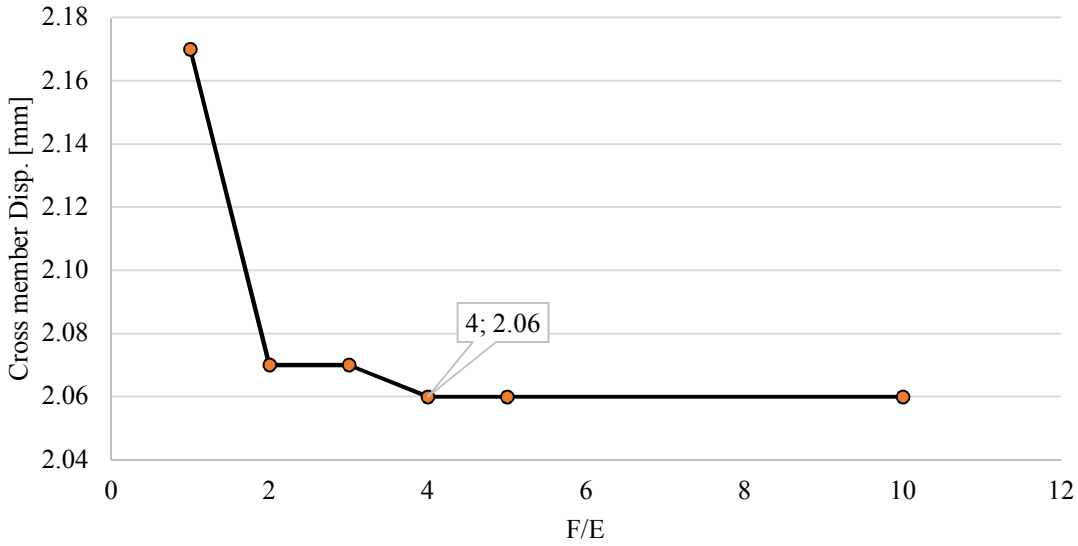

Figure 3.16: Mesh convergence with profile displacement shows that the elements size of the flange should be around 10 mm.

C3D8I element models were also compared with shell (S4R) elements to verify the overall model displacements. The percentage difference between the two models was 1.61%.

3.3 FEM: Scaled-down Models

3.3.1.1 Overview

In the design process, it is common to develop scaled-down models or to perform FE analysis on the small parts/assemblies as full-scale models are computationally expensive. Scaled-down models for bonded flooring structure was modelled in SOLIDWORKS and then imported as step file in ABAQUS CAE. The continuum models were used in the simulations due to two-sided contact, good accuracy, and ease of modelling.

Twenty-eight different simulations were performed. The variations in the simulations were due to load location, model geometry, plywood ply construction and boundary conditions. All models consisted of plywood panel, longitudinal beams, cross members, support plates and adhesive. Exploded view of the model-2 is shown in figure 3.17. The plywood panel was bonded with cross members using adhesive. Support plates were placed between cross members and plywood panel to ensure that the plywood panel had reasonable support from all sides. The cross members were fully-welded with longitudinal beams to form a stiff structure. The components are hereby explained briefly:

- Plywood panel was made of 20 birch veneers with a total thickness of 27.40 mm after sanding 0.30 mm from each face. Face veneer was in the transverse direction, i.e. Y-axis in the model. Two different plywood constructions (Oriented and Special) were used named as mentioned in section 2.2.1.

- Longitudinal beams, cross members, and support plates were made of steel.

- Polyurethane-based adhesive material was used to bond the floor.

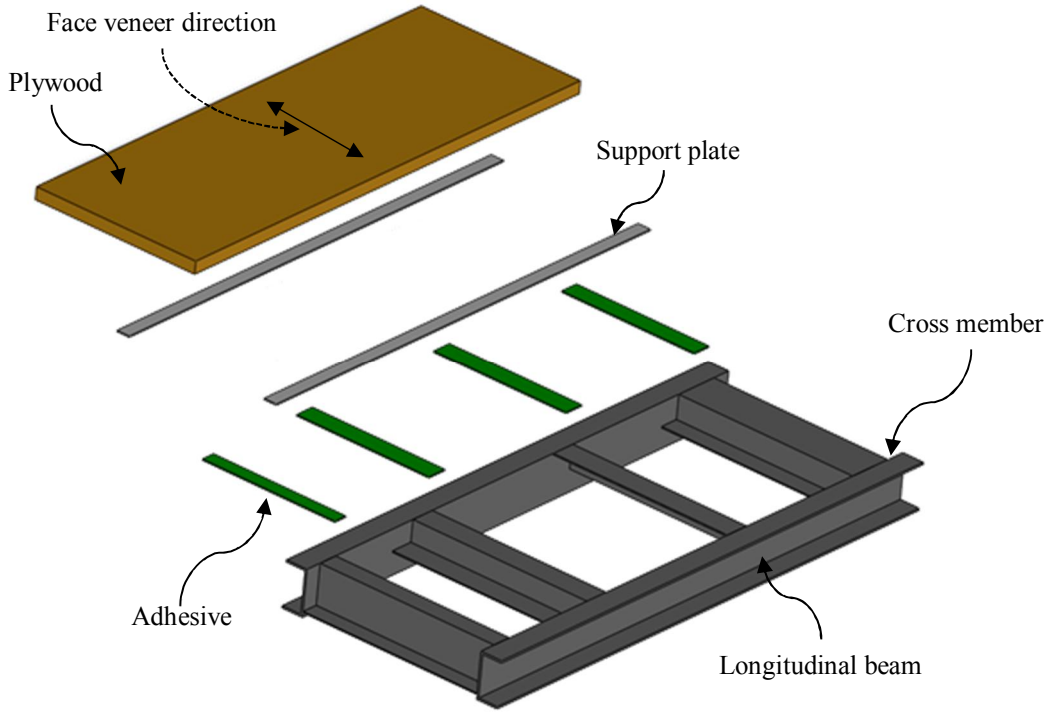

Figure 3.17: Exploded view of model-2. Other variants of the model consist of different cross member profiles and different spans.

Three different models representing the various zones of semi-trailers were used in the simulations and experiments. Figure 3.18 shows section-view of the three different models used for scaled-down models.

a. Model-1 shows the regular construction of the chassis (zone-3).

b. Model-2 represents the wheel area of the chassis (zone-4). Therefore, smaller z-profiles are used in the middle.

c. Model-3 shows the regular construction along with the panel edge location. Hence, omega profile is used at one end of the frame.

Detail drawings of the scaled-down models is presented in Appendix 4.

The models were loaded at three distinct locations represented by the arrows in figure 3.18. In each model, centre loading is represented by C whereas A is the next larger span and B has always the smallest span.

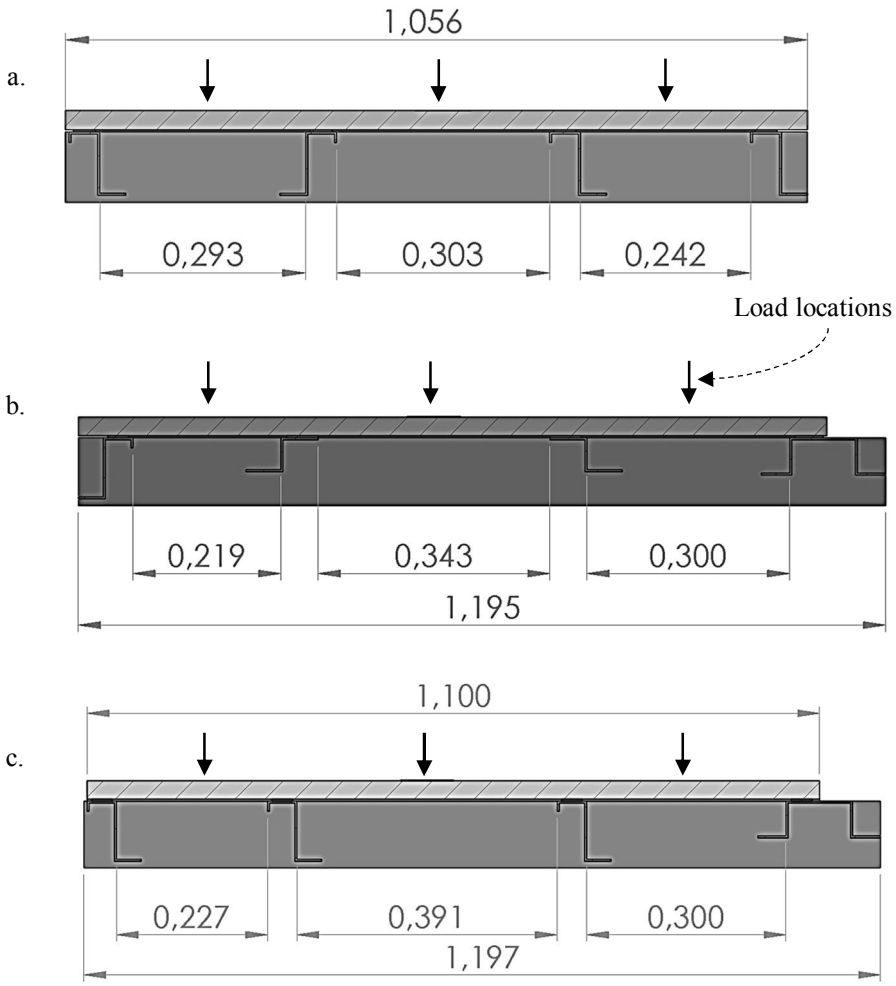

Figure 3.18: (a) Model-1 (b) Model-2 (c) Model-3 shows the difference in the configuration of the cross members. The arrows show loading locations at which models were analysed. Centre loading is represented by C whereas A is the next larger span and B has always the smallest span.

3.3.1.2 Modelling process in ABAQUS CAE

As discussed in 3.3.1.1, step models were imported ABAQUS CAE in groups to make the pre-processing less time-consuming e.g. all cross members were imported as one part/group. Fillets and rounds were removed from the model. Removal of fillets will generate some notch stresses in the simulation due to sharp corners (Baguley & Hose, 1997). Thus, those notch stresses will be ignored in the results. The components were further partitioned to have better mesh quality as shown in figure 3.19.

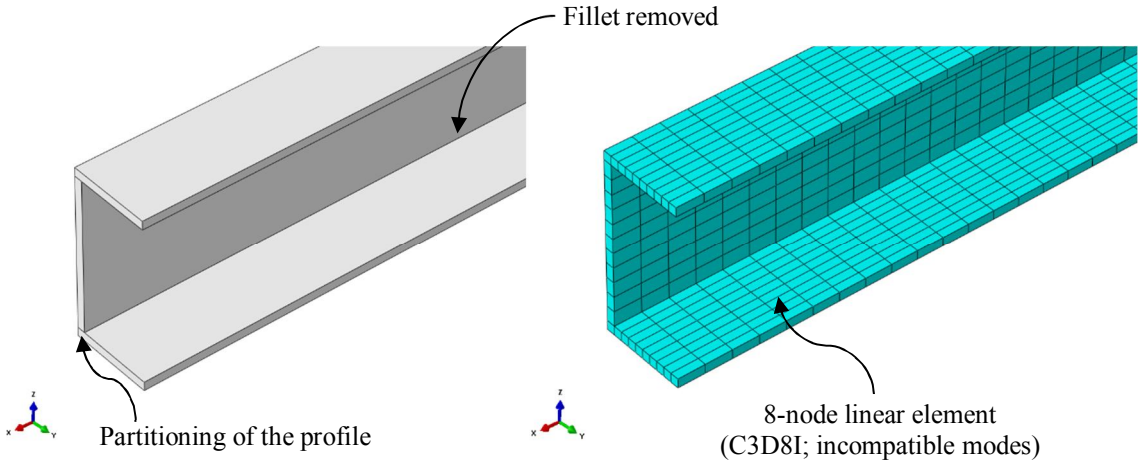

Figure 3.19: Solid modelling of longitudinal beam. The beam is divided into in the small segments for hexagonal mesh elements.

Loading and boundary condition of the model is shown in figure 3.20. Two different boundary conditions were during the simulations named as 'partial support models' and 'full support models'. In partial support models, longitudinal beams were restrained at the bottom face in the Z-axis direction as shown in figure 3.20 (a). Whereas, in the full support model, longitudinal beams along with support plate bottom-face were restrained at the bottom face in the Z-axis direction as shown in figure 3.20 (b). Forklift wheel-load of 36 kN was applied in the form of pressure (total force) load at the 180 × 80 mm wheel plate.

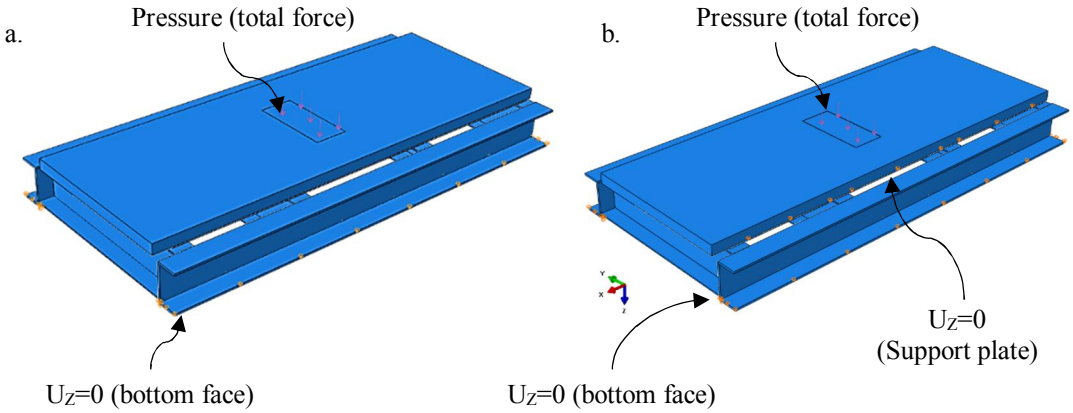

Figure 3.20: (a) Partial support model (b) Full support model.

Interaction between the model components is shown in figure 3.21. Cross members were welded with the longitudinal beam (c-profile), therefore, they were modelled as 'Tie' constraint. Forklift wheel and plywood panel were also modelled as 'Tie' constraint where forklift wheel plate bottom surface was a slave surface and plywood panel top surface were defined as a master surface. Support plates in the model were defined as frictional constraint with the cross members and plywood panel. 'Tangential Behaviour'

was modelled with penalty formulation having frictional coefficients values as shown in table 3.7:

Table 3.7: Frictional coefficient of the contact region

Contact Region	Frictional Coefficient
Steel-Panel (S-P)	0.01
Steel-Steel (S-S)	0.5

'Normal behaviour' was modelled using Pressure-Overclosure as 'Hard' contact and with separation after contact was allowed.

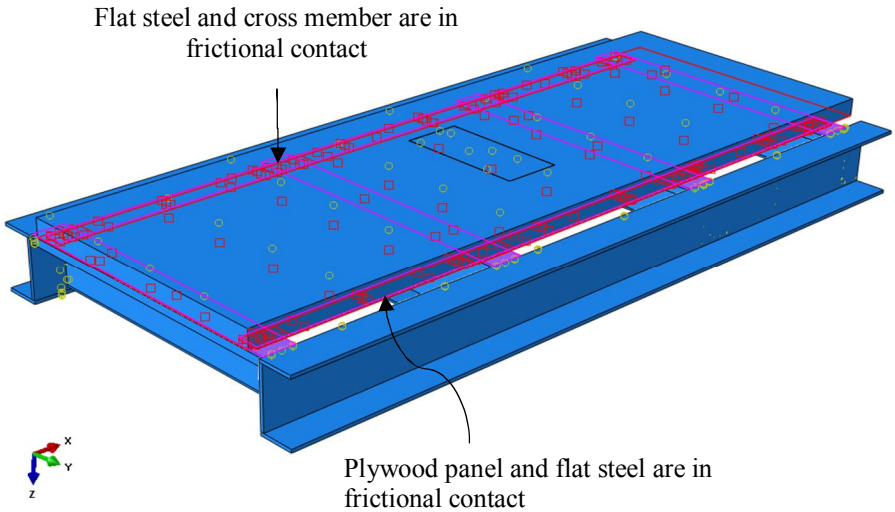

Figure 3.21: Boundary nonlinearity is introduced in the model due to frictional contacts between plywood-flat steel and flat steel-cross members.

A nonlinear static analysis was created in the *Step* module of ABAQUS CAE. The presence of frictional contacts makes this model boundary nonlinear problem (ABAQUS, 2016). Initial increment size was kept at 0.01, minimum increment size at $1e^{-10}$ and maximum increment size at 0.05. The total number of increments were kept at 10000.

Hex dominated mesh was generated for all the components of the model as shown in figure 3.22. Element size was based on the mesh convergence studies as previously discussed. Forklift wheel plate modelled with higher mesh density as the slave surface needs to have a higher mesh density (ABAQUS, 2016).

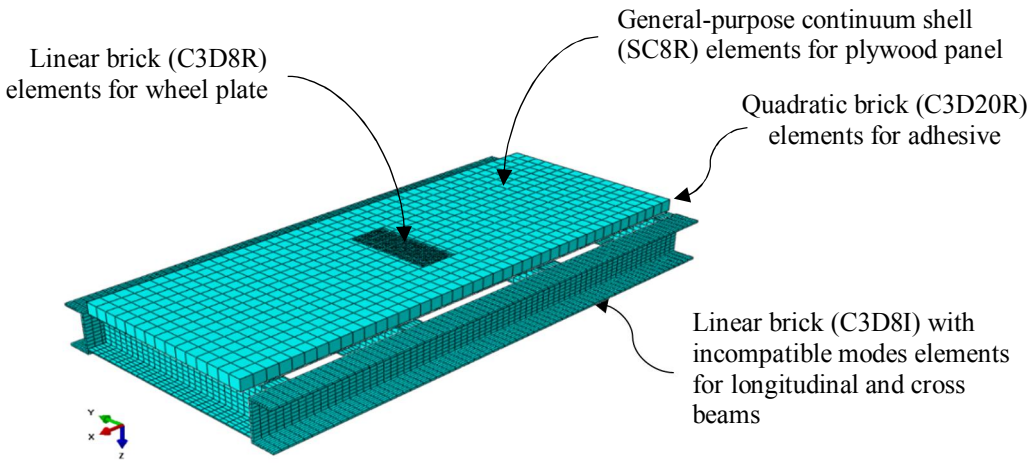

Figure 3.22: Mesh element types for model components.

3.3.1.3 Simulation results

The results accumulated from the simulations are presented in table 3.8. It contains the model maximum displacement (U_Z), normal stresses (S_{11}) for the first and second veneer from the bottom-side of the plywood panel. The transverse shear stress ($TSHR_{13}$) at the middle veneer i.e. ply 10. The simulations names are based on model type, panel layup, support type and load location e.g. **M1-SPL-FS-PL-C** stands for model-1, special ply, full support, and wheel-load at C.

- Model type: M1 (model-1), M2 (model-2), M3 (model-3)
- Plywood layup: SPL (special), ORN (oriented)
- Support: FS (full support), PS (partial support)
- Load location: A, B, C (as mentioned in figure 3.17)

Table 3.8: FE simulation results of scaled-down models

Sim. No.	Simulation Name	Model Displacement	S_{11} First Ply	S_{11} Second Ply	$TSHR_{13}$
		[mm]	[MPa]	[MPa]	[MPa]
1	M1-SPL-FS-PL-C	5.33	90.60	58.10	3.63
2	M1-SPL-FS-PL-A	5.25	89.20	61.38	4.10
3	M1-SPL-FS-PL-B	4.68	79.31	58.60	3.58
4	M1-SPL-PS-PL-C	6.30	68.53	66.32	3.80
5	M1-SPL-PS-PL-A	5.92	69.95	68.98	4.33
6	M1-SPL-PS-PL-B	5.08	65.12	63.18	3.64
7	M1-ORN-FS-PL-C	5.26	86.15	59.58	3.48
8	M1-ORN-FS-PL-A	5.20	85.01	62.87	3.91
9	M1-ORN-FS-PL-B	4.67	76.06	60.52	3.44
10	M2-SPL-FS-PL-C	6.03	103.10	57.75	3.65
11	M2-SPL-FS-PL-A	5.56	94.57	62.08	3.51
12	M2-SPL-FS-PL-B	4.69	79.39	58.29	4.16
13	M2-SPL-PS-PL-C	8.12	73.34	71.67	3.96
14	M2-SPL-PS-PL-A	6.55	73.34	71.57	3.64
15	M2-SPL-PS-PL-B	5.07	67.06	61.86	4.26
16	M2-ORN-FS-PL-C	5.87	96.54	58.76	3.50
17	M2-ORN-FS-PL-A	5.47	89.58	63.31	3.37
18	M2-ORN-FS-PL-B	4.66	75.98	60.23	3.97
19	M3-SPL-FS-PL-C	6.03	104.80	63.07	3.54
20	M3-SPL-FS-PL-A	5.36	91.09	62.45	3.43
21	M3-SPL-FS-PL-B	4.49	76.04	58.00	4.15
22	M3-SPL-PS-PL-C	8.23	71.61	73.83	3.81
23	M3-SPL-PS-PL-A	6.39	74.70	76.61	3.55
24	M3-SPL-PS-PL-B	4.72	64.52	65.12	4.19
25	M3-SPL-PS-PL-CE	11.15	32.24	111.70	7.80
26	M3-ORN-FS-PL-C	5.87	96.59	59.67	3.35
27	M3-ORN-FS-PL-A	5.40	88.90	67.93	3.29
28	M3-ORN-FS-PL-B	4.55	74.80	64.21	3.90

Figure 3.22 shows the stress values for face veneers of plywood panels. The stress plot shows that some of the panels will fail due to high stresses (veneer cracking). According to Finnish Forest Industries Federation (2002), the surface grades of the plywood panels has an insignificant effect on the structural performance of the panel. It shall be noted that face veneer is not used as a structural layer, but it has an impact on the degradation of plywood against humidity and moisture.

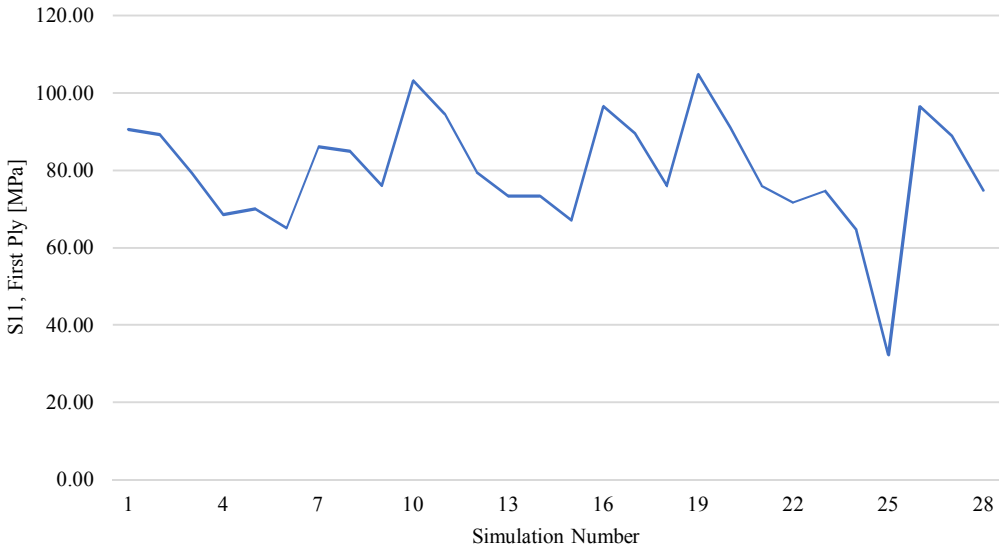

Figure 3.23: Normal stress (S_{11}) for face veneer layer (bottom-face) of the panels under wheel-load.

The bending strength of veneers in the plywood panel is around 90 – 95 MPa. Simulation number 25 (edge loading condition) fails in shear shown in figure 3.25. And, it is not considered for bending strength. The plot in figure 3.24 shows that plywood panels are safe for second veneer failure. The minimum factor of safety (FOS) for the second ply comes out to be 1.18 for simulation number 23 (M3-SPL-PS-PL-A) as shown in the equation below:

$$\text{FOS} = \frac{\text{Maximum bending strenght}}{\text{Stress generated}} = \frac{90.00\ [\text{MPa}]}{76.61\ [\text{MPa}]} = 1.18$$

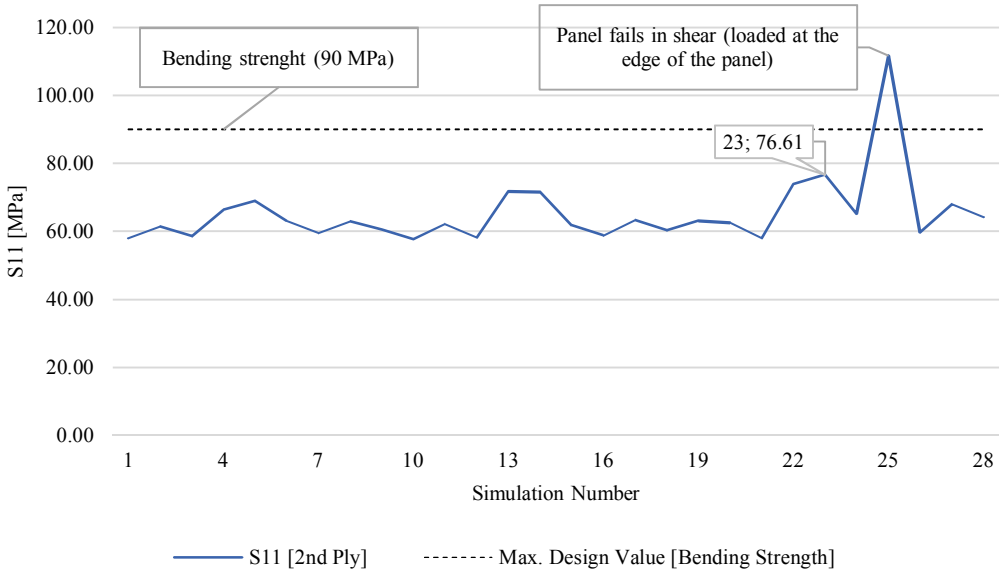

Figure 3.24: Normal stress (S_{11}) for second veneer layer (bottom-face) of the panels for wheel-load. According to UPM Plywood (2017), the maximum design value for bending strength is 90-95 MPa.

It can be seen in figure 3.25 that the only simulation number 25 (edge loaded case) failed due to shear. It was observed in the experiments as well. The shear stress values for result of the panels are close or below design values. Therefore, shear failure was not observed in the experiments. The FE simulations results can be seen in figure 3.26 and 3.27.

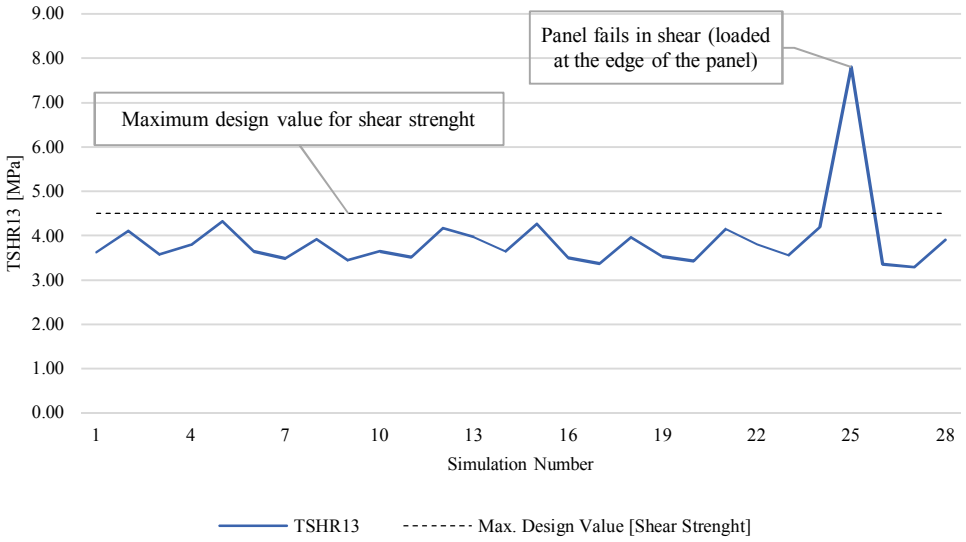

Figure 3.25: Transverse shear stress ($TSHR_{13}$) for middle veneer layer of the panels. The recommended design value for rolling shear strength is 4.0-4.5 MPa (UPM Plywood, 2017).

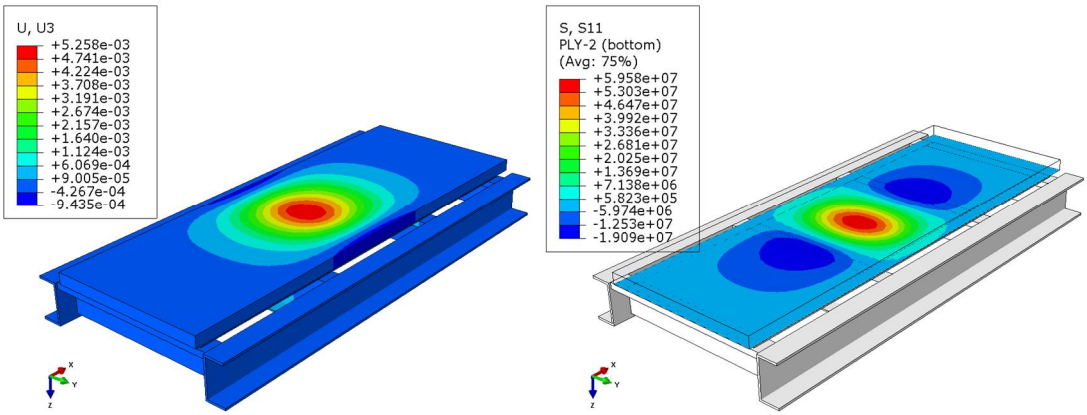

Figure 3.26: Vertical displacement for M1-ORN-FS-PL-C comes out to be 5.26 mm (left). Second ply stress (S_{11}) value comes out to be 59.58 MPa (right).

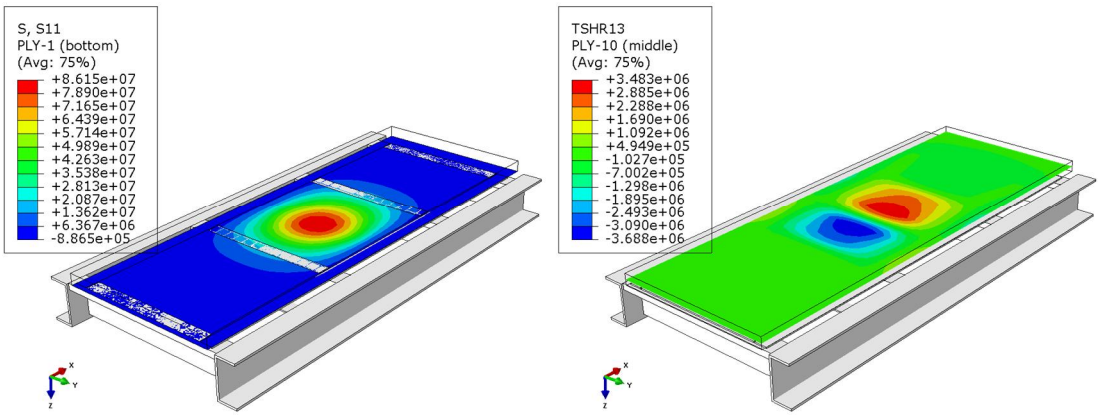

Figure 3.27: First ply stress (S_{11}) value comes out to be 86.15 MPa (left) where shear stress is around 3.48 MPa for the M1-ORN-FS-PL-C (left).

3.4 Experimental Validation of Scaled-down Models

The FE simulations were validated through experiments conducted at UPM Plywood facility in Lahti, Finland. In total, thirty-one experiments were performed in accordance to the ISO 1496-1 (1990) as shown in figure 3.28.

The panels were loaded two times. Firstly, the panels were loaded with the proof load i.e. approx. 36 kN and the load-displacement measurements were recorded. Then, the same panels were loaded till the failure load. The load rate was kept at 0.60 kNs^{-1}. The panel failure was estimated by the load-displacement curve.

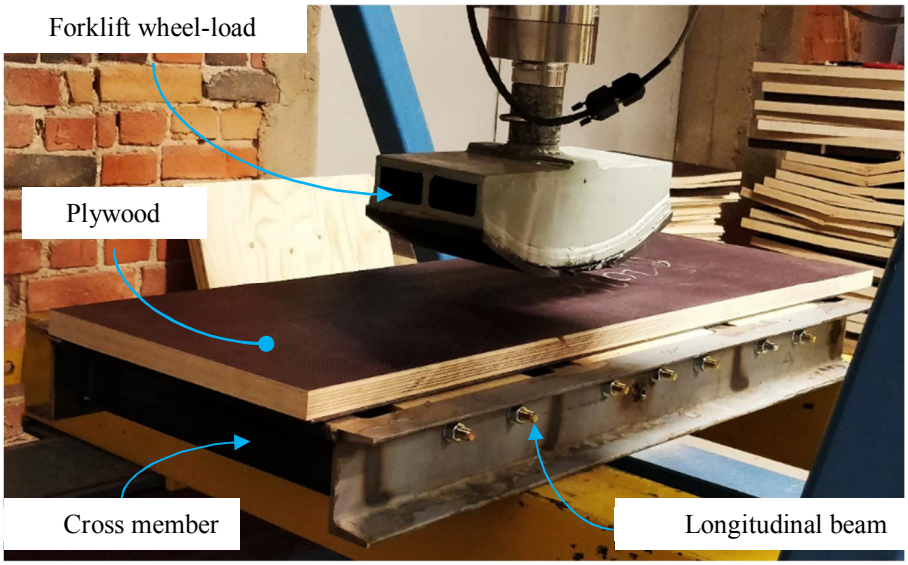

Figure 3.28: Experimental setup for scaled-down model testing according to ISO 1496-1 (1990).

During the experimental testing, two displacement sensors were used. One sensor was used to measure plywood displacement and the other sensor was used to measure cross member flange displacement as shown in figure 3.29. The wooden blocks in the figure represent full support condition in the FE simulations whereas wooden blocks were removed to replicate partial support model.

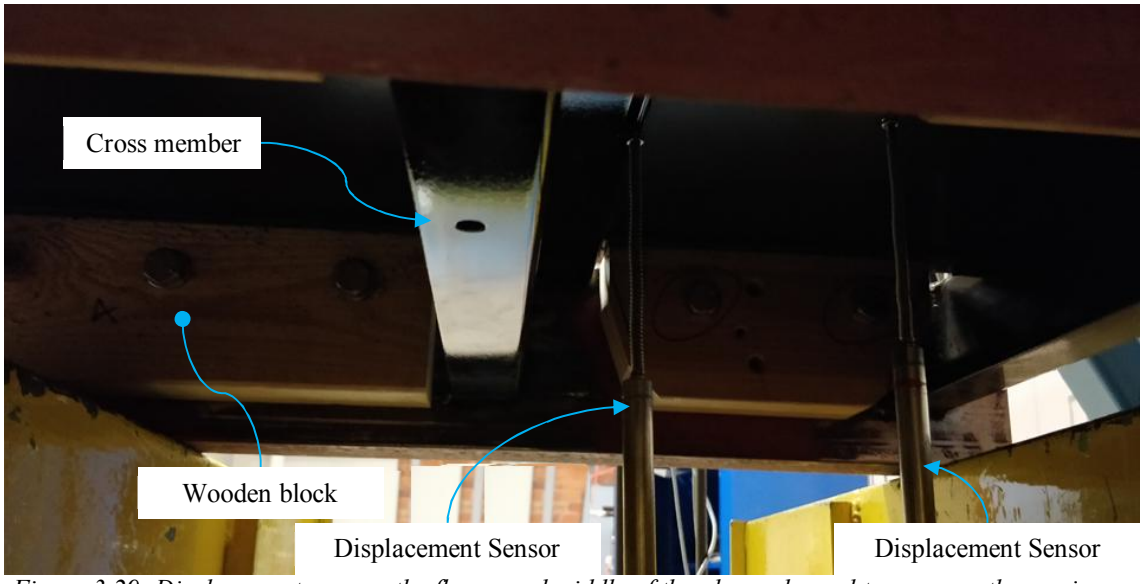

Figure 3.29: Displacement sensors the flange and middle of the plywood panel to measure the maximum displacement under proof and ultimate failure load.

Figure 3.30 shows load-displacement curve for the scaled-down model under proof load i.e. approx. 3600 kg. Displacement at proof load was estimated according to EN 789 (2004). The standard suggests to use section of graph between 0.1Fmax (≈ 500 kg) and 0.4Fmax (≈ 2730 kg) for a linear regression. It was perfomred to consider linear elastic deformations of panel after the normal service load i.e. 2730 kg for semi-trailer floors. As, there is a chance of increased plastic deformations after service load. After regression, a linear interpolation function was used as shown below:

$$w_3 = 3600 \times \frac{w_2 - w_1}{L_2 - L_1}$$

where
w_1 – displacement at L_1 i.e. approx. 500 kg
w_2 – displacement at L_2 i.e. approx. 2730 kg
w_3 – displacement at 3600 kg

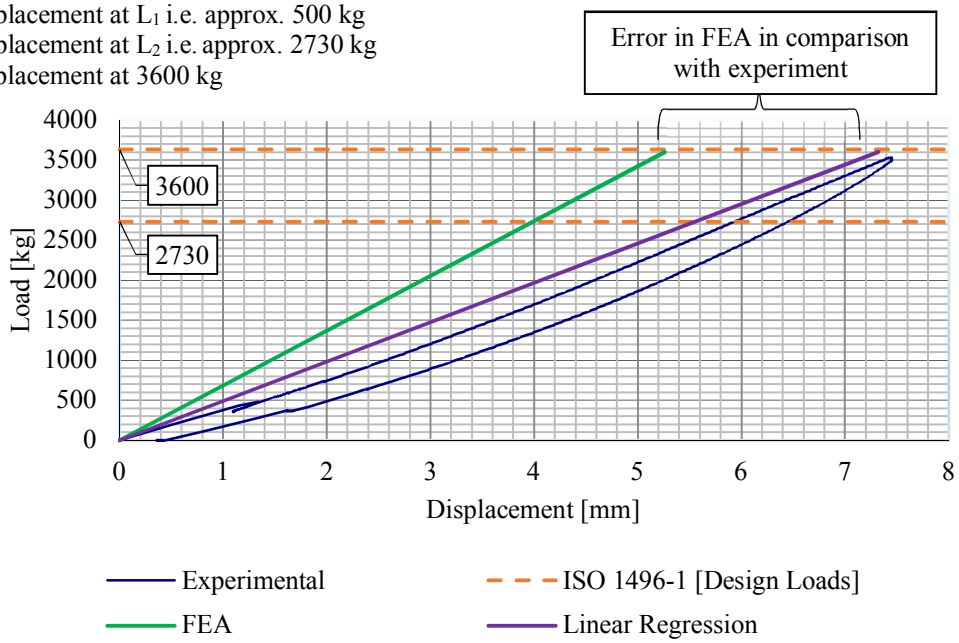

Figure 3.30: Load-displacement curve of M1-ORN-FS-PL-C plywood panel. The difference in the slope of FEA and Linear regression suggests further investigation of the causes of this variation.

Figure 3.31 shows that plywood panel response for the experiment M1-ORN-FS-PL-C under ultimate loading. The response of the plywood panel is overall nonlinear. But, it is observed that the panel behaves linearly close to the design loads as suggested in section 2.2.1.4. The capacity of the panel is almost twice the proof load i.e. 7380 kg.

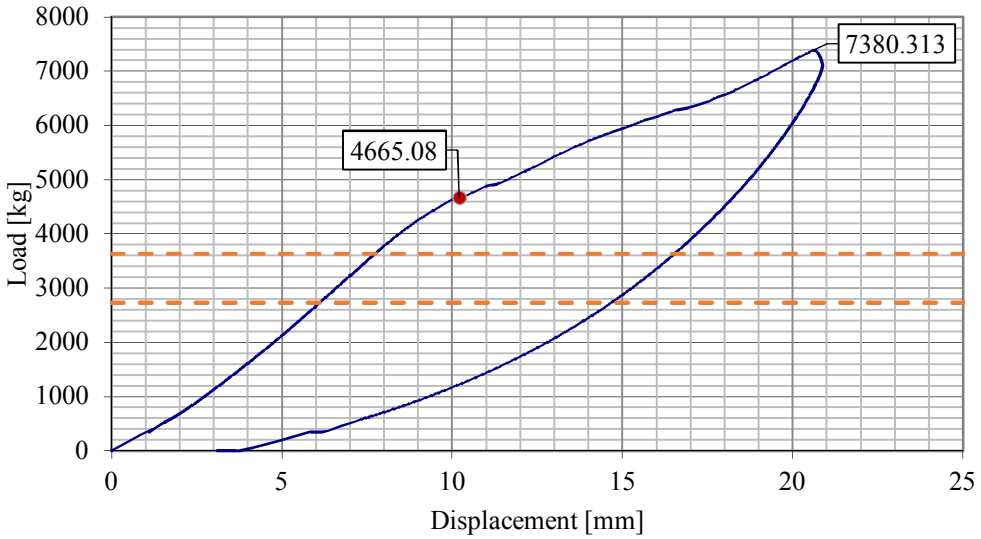

Figure 3.31: Load-displacement curve shows the first visible veneer failure occurred at 4465.08 kg (45.76 kN) during ultimate panel loading. Plywood panel has almost twice the load capacity i.e. 7380 kg.

Table 3.9 shows the comparative displacement for FEM and experimental model interpolated for 1000 kg load. It also shows plywood panel failure load and face veneer condition after proof loading. Minor surface cracking in the experiments is corresponds closely with the result in figure 3.23 for face veneer stresses (S_{11}).

In the model-1 (simulation/experiment 1 – 6), fixed support simulations with special ply arrangement have higher stress values compared to the partially supported models. This is validated by the experiments that the fixed support models are experiences more first ply failure compared to the partial support models. This shows the FE models are quite close in predicting the experiments.

Table 3.9: FEM and experimental results at 1000 kg load

Exp. No.	Experiment	FEM Disp. per 1000 kg	Model Disp. per 1000 kg	Panel Condition after Proof Load (35.5 kN)	Veneer Failure Load
		[mm]	[mm]		[kN]
1	M1-SPL-FS-PL-C	1.48	2.08	1st veneer (surface) crack	
2	M1-SPL-FS-PL-A	1.46	1.90	Minor crack on coating	
3	M1-SPL-FS-PL-B	1.30	1.49	1st veneer (surface) crack	
4	M1-SPL-PS-PL-C	1.75	2.30	No cracking	
5	M1-SPL-PS-PL-A	1.64	2.10	No cracking	
6	M1-SPL-PS-PL-B	1.41	1.72	No cracking	
7	M1-ORN-FS-PL-C	1.46	2.03	Minor crack on coating	45.76
8	M1-ORN-FS-PL-A	1.44	1.92	No cracking	48.11
9	M1-ORN-FS-PL-B	1.30	1.73	No cracking	44.72
10	M2-SPL-FS-PL-C	1.68	2.85	Minor crack on coating	
11	M2-SPL-FS-PL-A	1.54	2.30	No cracking	
12	M2-SPL-FS-PL-B	1.30	2.05	No cracking	
13	M2-SPL-PS-PL-C	2.25	3.00	1st veneer (surface) crack	
14	M2-SPL-PS-PL-A	1.82	2.51	1st veneer (surface) crack	
15	M2-SPL-PS-PL-B	1.41	1.74	Minor crack on coating	
16	M2-ORN-FS-PL-C	1.63	2.36	Minor crack on coating	54.97
17	M2-ORN-FS-PL-A	1.52	2.05	Minor crack on coating	45.40
18	M2-ORN-FS-PL-B	1.29	1.83	No cracking	57.61
19	M3-SPL-FS-PL-C	1.68	2.70	No cracking	
20	M3-SPL-FS-PL-A	1.49	2.30	1st veneer (surface) crack	
21	M3-SPL-FS-PL-B	1.25	1.62	No cracking	
22	M3-SPL-PS-PL-C	2.29	3.80	No cracking	
23	M3-SPL-PS-PL-A	1.78	2.76	No cracking	
24	M3-SPL-PS-PL-B	1.31	1.80	1st veneer (surface) crack	
25	M3-SPL-PS-PL-CE	3.10	5.80	Shear failure	
26	M3-ORN-FS-PL-C	1.63	2.28	Minor crack on coating	43.44
27	M3-ORN-FS-PL-A	1.50	1.96	Minor crack on coating	41.84
28	M3-ORN-FS-PL-B	1.26	1.66	No cracking	57.15

FE simulations are compared for model deflections with experiments at 1-ton load as shown in figure 3.32. FEA models predict 20-30% lower displacement in comparison to experiments. It is reported by UPM that percentage error for only plywood models are around 10 – 15% due to variation in the plywood properties in different batches.

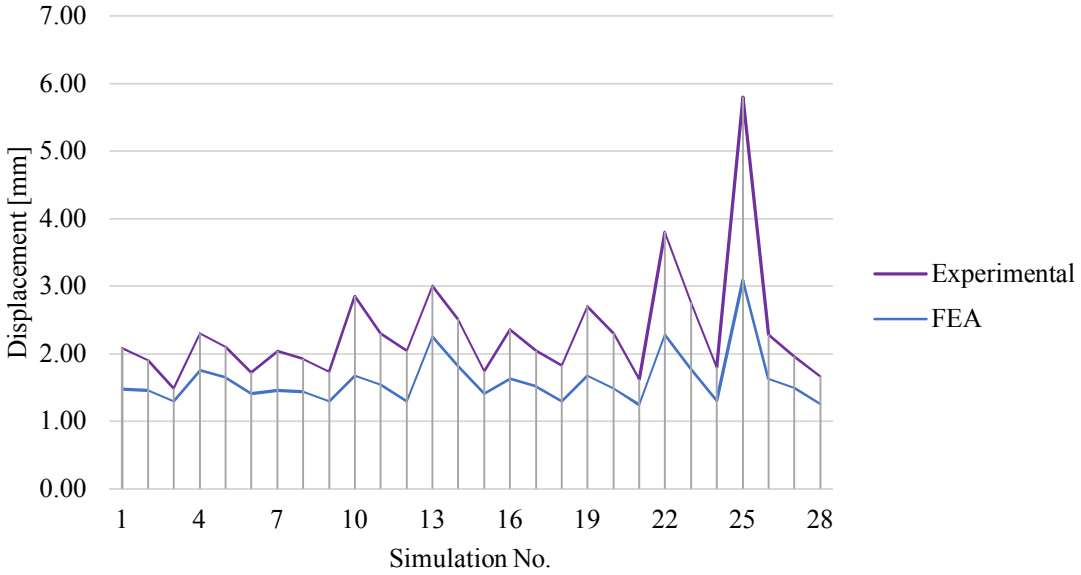

Figure 3.32: The plot showing comparison of model displacements (Uz) between experimental and FE simulations for 1-ton load

It is important to determine critical parameters for the cause of deviation to further develop FEA approach. Some of this deviation can be related to following issues:

a. Material properties of the plywood and adhesive material
b. Finite elements response to the applied loading
c. Variation in the experiments
d. Plywood damage behaviour
e. Quality of adhesive joint

It was noted that there was some variation in the experiments as well. In the experiments, two tests were performed on the model-2 (M2-SPL-PS-PL) showed maximum of 18.75% deviation (load location B) as shown in figure 3.33.

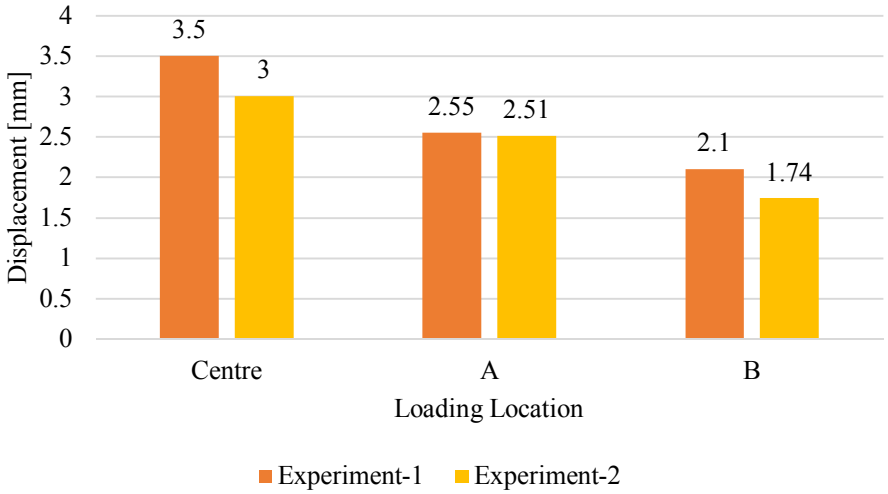

Figure 3.33: The maximum variation in the experiments came out to be around 18.75% which can be attributed to adhesive bond-line behaviour and plywood properties.

Figure 3.34 shows the M1-ORN-FS-PL after loaded at location A, B, and C. It was reported that the plywood had developed minor first ply cracks. The stress value in the simulations for this case was 86.15 MPa which is reasonably close to design values i.e. 90-95 MPa.

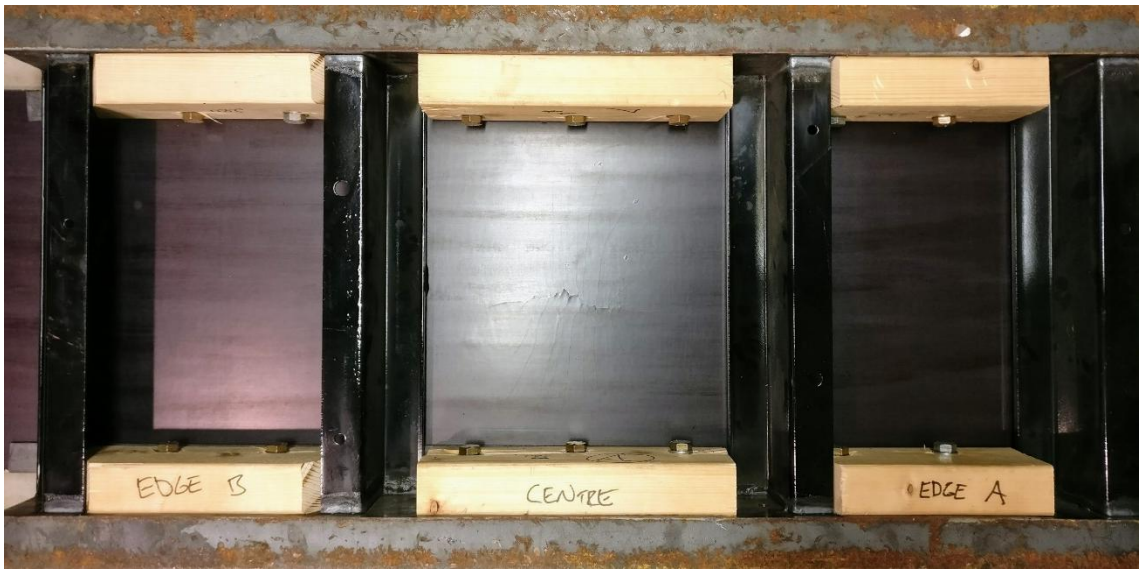

Figure 3.34: Model – 1 with full support has developed a very thin crack at the centre. This crack is mostly phenolic film.

Figure 3.35 shows M3-SPL-FS-PL after proof loaded at the location A, B, and C. There is a minor crack at the location A. For FE simulations, the S_{11} for the first ply is 91.16 MPa which is very close to the design values.

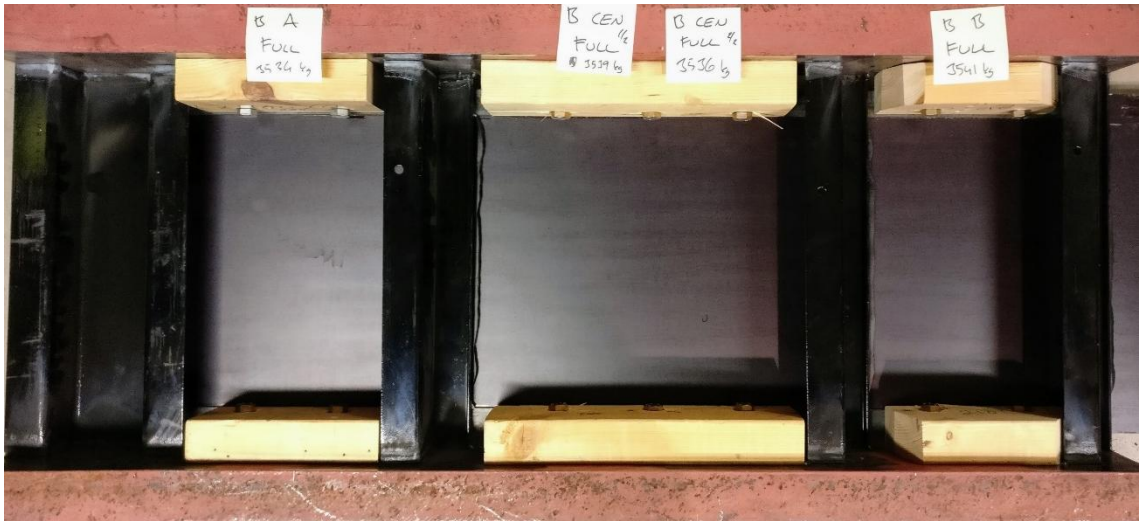

Figure 3.35: Model-3 with full support has developed a thin crack at the location A. This minor crack is mostly phenolic film.

3.5 Investigation of Critical FEM Parameters

It is desirable to figure out the sensitive and non-sensitive parameters in these finite element models. It will be helpful in determining the cause of deviation in the experimental and FE simulations. The key parameters of the FE models investigated in this study are listed below:

- Variation in shear modulus of plywood panel
- Variation in the material properties of adhesive
- Variation in the friction coefficient

3.5.1 Effect of variation in shear modulus (G_{13}) of plywood panel

According to UPM Plywood (2017), material properties of plywood vary from batch to batch production. And, it was considered important to evaluate the effect of varying shear modulus of the plywood panel on model displacements.

A comparative study was performed with two different shear modulus (G_{13}) to estimate the effect of the shear modulus. The different shear modulus (G_{13}) used in the scaled-down model analysis were 1180 and 110 MPa.

Results of the simulation for model displacement with different shear modulus values are shown in figure 3.36.

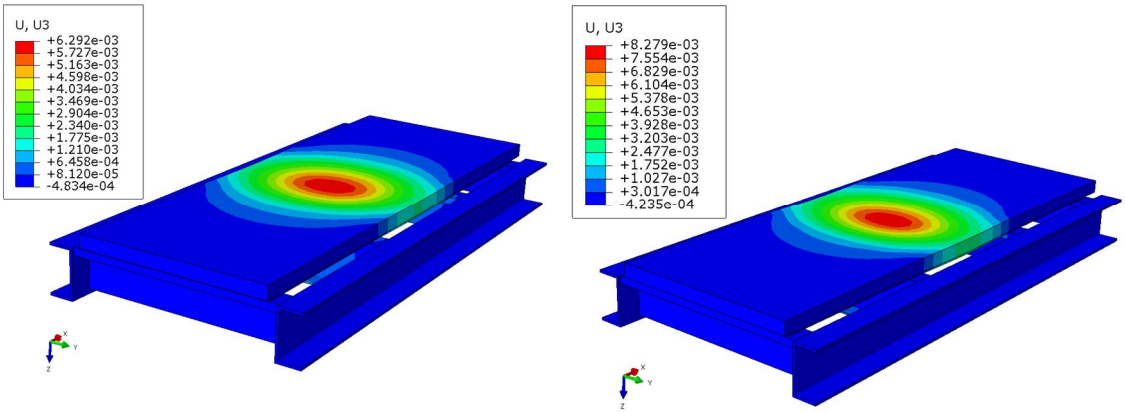

Figure 3.36: Model displacement (U_Z) with two different shear modulus (G13) for plywood panel i.e. 1180 MPa (left) and 110 MPa (right) for M1-SPL-PS-PL-C for wheel-load case.

It can be seen from figure 3.37 that the FE models are quite sensitive to the shear modulus of the plywood panel and it shall be predicted as accurately as possible. It was noticed that changing the shear modulus of the plywood panel had a substantial impact on the overall model displacement. The error with the experimental results reduced from 23.91 % to 0.04 %. Shear modulus had an inverse relation with the model displacement.

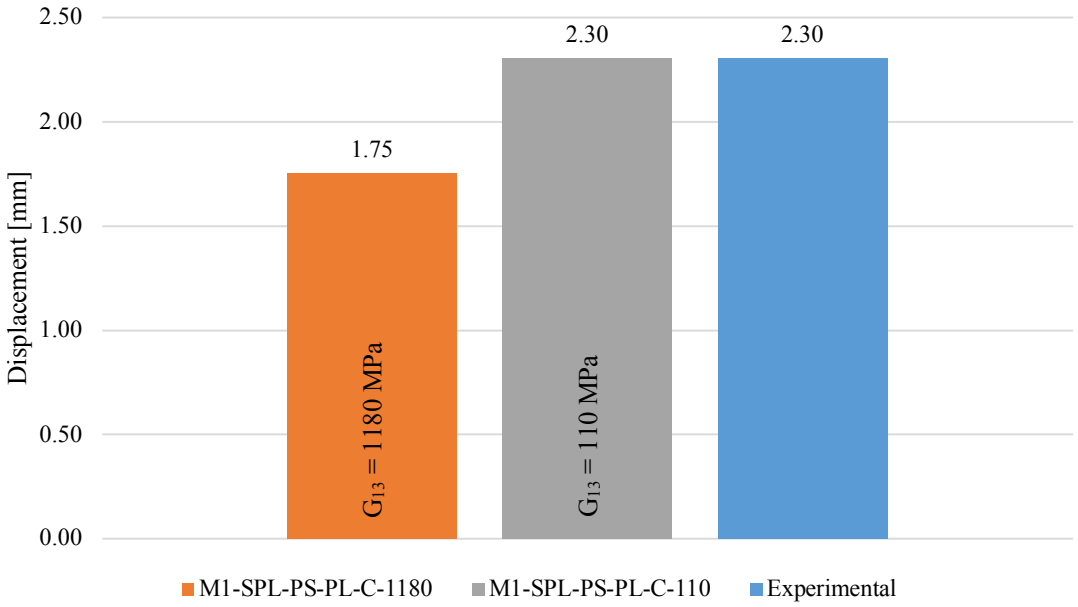

Figure 3.37: Graph showing model displacement (U_Z) at 1-ton wheel-load with different shear modulus (G_{13}) of the plywood shows significant impact on the overall displacement. G_{13} = 1180 MPa (orange) and G_{13} = 110 MPa (grey)

3.5.2 Effect of variation in elastic modulus (E) of adhesive

The adhesive material properties were estimated from the literature as mentioned in section 3.2.4.2. Therefore, it was important to comprehend the effect of material property on model stiffness. The maximum and minimum values of the elastic modulus used were 26 MPa and 2.6 MPa respectively.

The results of the simulation for model displacement with different elastic modulus of adhesive material are shown in figure 3.38.

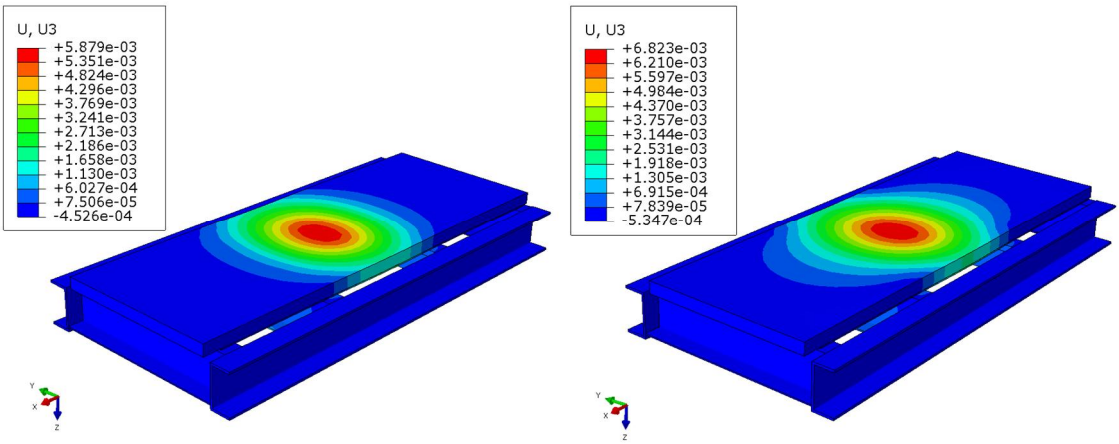

Figure 3.38: M1-SPL-PL-C-BL-MAX (left) and M1-SPL-PL-C-BL-MIN (right) shows that the applications of the stiffer adhesive material resulted in lower displacements.

From figure 3.39, it was observed that changing the elastic modulus of adhesive material had a moderate effect on model displacements. Increasing the elastic modulus, decreases the model displacement. At minimum value of adhesive elastic modulus, the percentage error was reduced to 17.39 % whereas, at maximum value i.e. 2.6 MPa, the percentage error was increased to 29.13%.

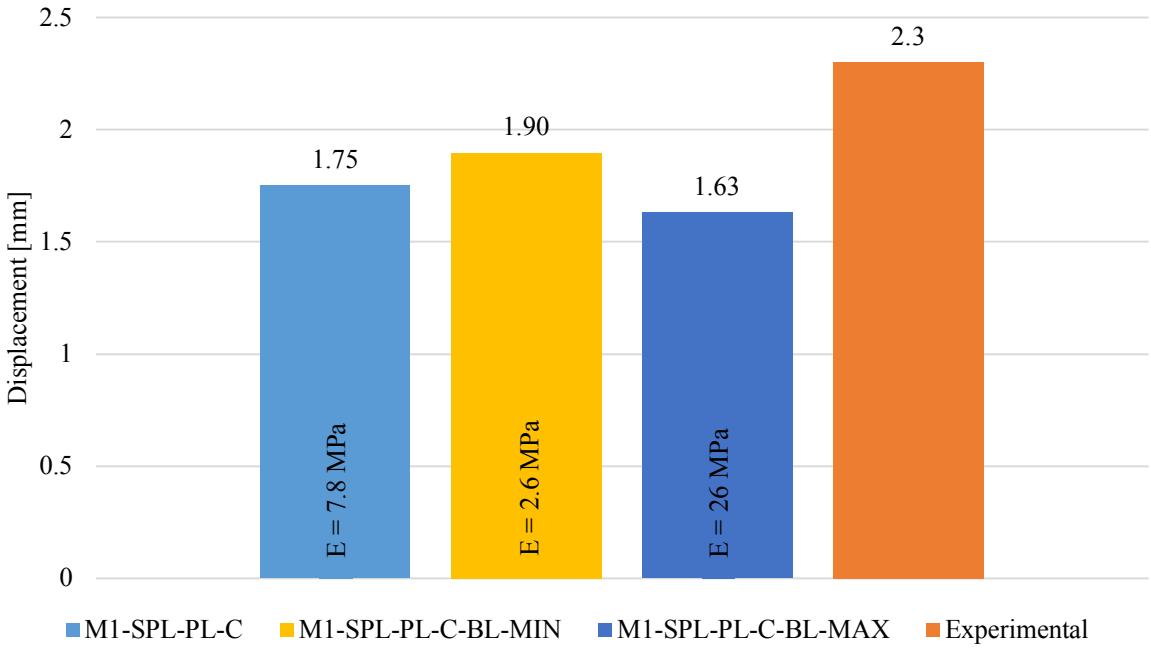

Figure 3.39: Graph showing model displacements (U_Z) with varying elastic modulus of the adhesive material at 1-ton wheel-load.

3.5.3 Effect of variation in frictional coefficients

Frictional contact between steel – steel components and between steel – plywood was also evaluated. The scaled-down model was simulated with different values of friction coefficient with minimum value of 0.01 and maximum value of 0.9.

The results of the simulation for model displacement with different elastic modulus of adhesive material are shown in figure 3.40.

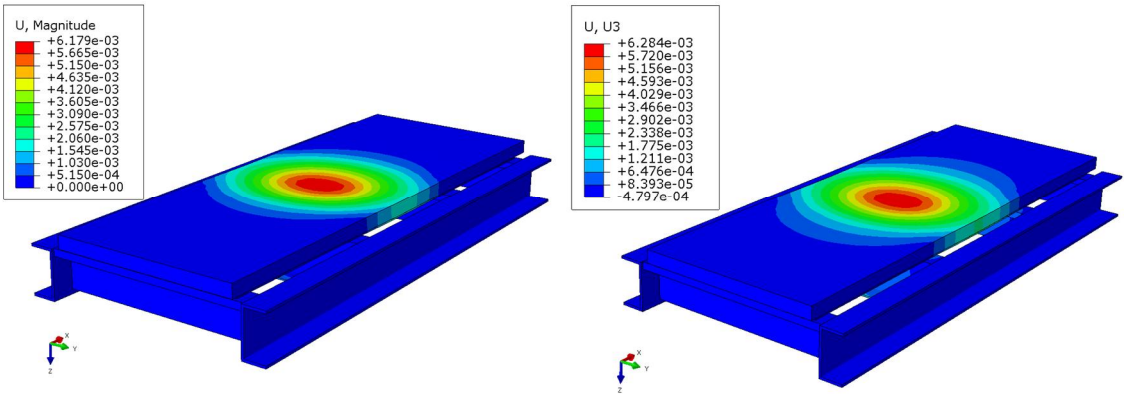

Figure 3.40: The FE simulations showing model displacements (U_Z) at the maximum (left) and minimum (right) values of the frictional coefficients.

From figure 3.41, it was noted that changing the frictional coefficient had a trivial effect on the overall model response. At the low value of frictional coefficient, model displacement was almost the same. But, at the maximum values of frictional coefficient, percentage difference between experiments and FE simulations were increased. At higher values of friction, the model was stiffer and percentage error was increased by 1.30%.

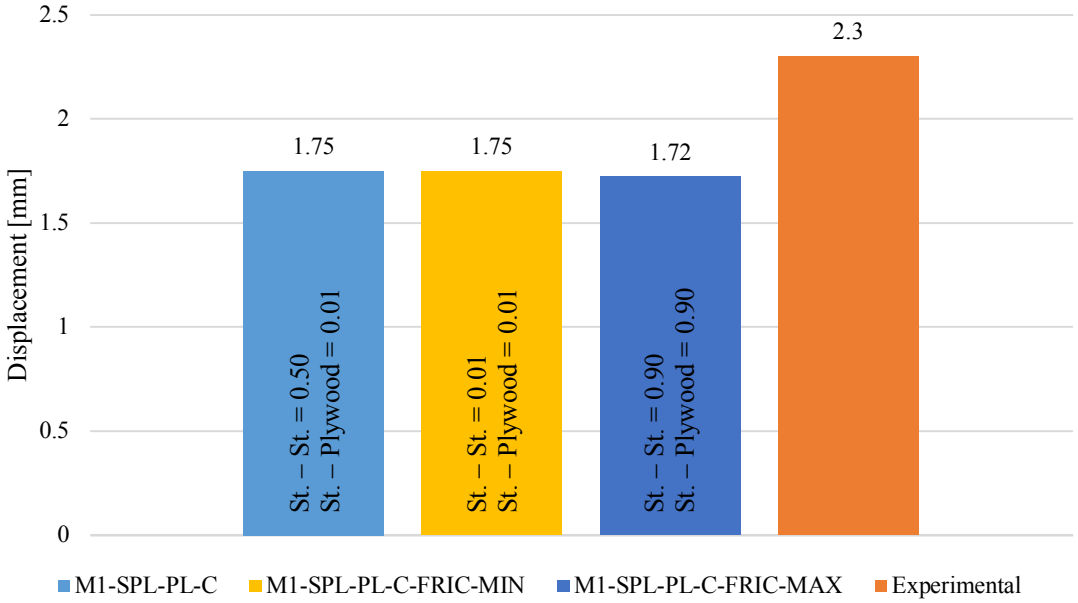

Figure 3.41: Effect of frictional coefficient on model displacement (U_Z) at 1-ton load.

It was noted that the use of fully bonded model decreased the panel displacement by 19.40%. The results of simulations for of M2-ORN-PS-PL-C for fully-bonded case are documented in Appendix 5.

3.6 Effect of Plywood Construction on the Stiffness and Strength

The arrangement of veneers in the plywood panel plays an essential role in the overall model stiffness and strength of the optimised flooring structure. Therefore, a comparative study was performed to comprehend the effects of different lay-up on the overall model stiffness as shown in figure 3.42. The data accumulated from the scaled-model simulations were used in these comparative studies. Model number and load locations are shown in each graph. In this study, oriented construction was compared with special construction.

It can be seen in figure 3.42 that oriented veneer arrangement gives 0.35 – 2.82 % lower deformations as compared to special veneer arrangement in most cases. A similar trend is also seen in the experimental results as shown in section 3.4 where oriented construction had lower model deformations.

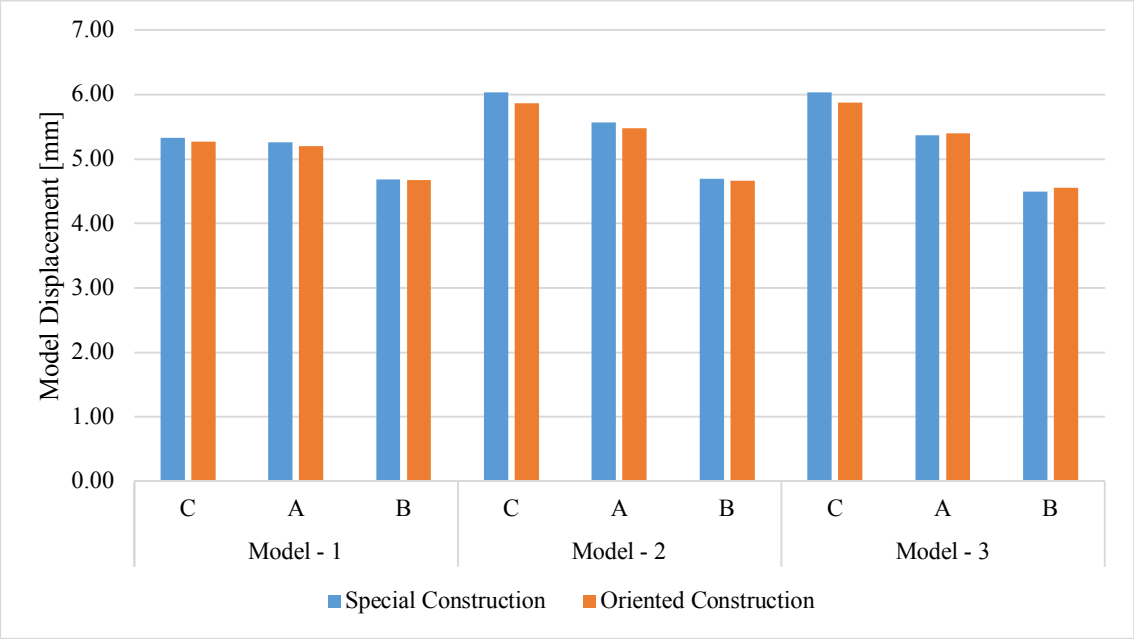

Figure 3.42: Model displacement for oriented construction versus special construction. Oriented construction has lower displacements.

The face veneer in the oriented ply arrangement gives a maximum of 8.15% lower values of the stress values as shown in figure 3.43. Lower stress values enable in avoiding the minor cracking on the bottom face of the plywood due to local loading which can increase environmental degradation of the plywood panels.

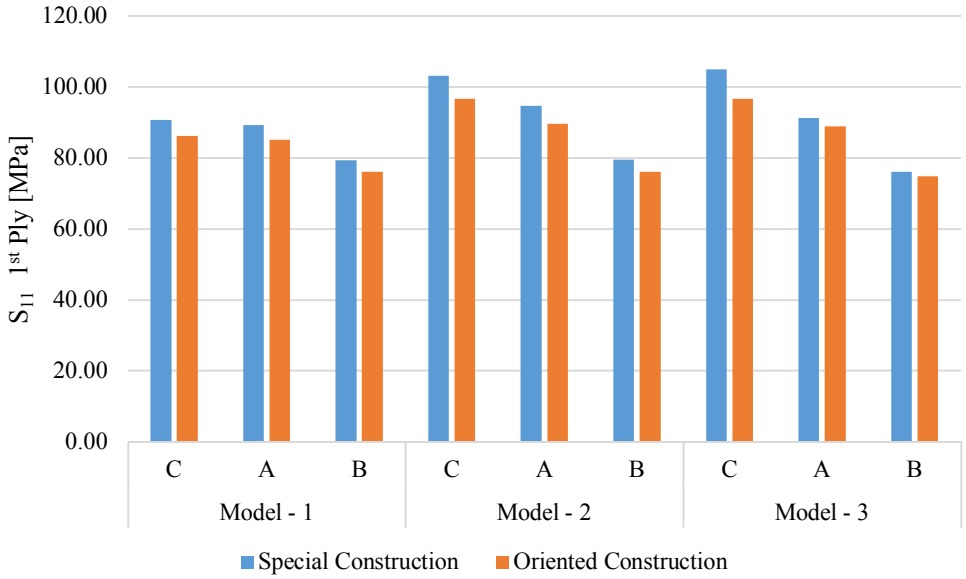

Figure 3.43: The face veneer (bottom-face) stresses for oriented construction versus special construction is shown in the graph. Oriented construction generates lower stress values for the face veneer.

According to the Veistinen and Pennala (1999), veneer layers (excluding face veneer) contributes predominantly to the structural integrity of the plywood panel. It is important to consider the stresses generated in the veneer layers for the comparative studies of different ply arrangement. It is shown in figure 3.44 that oriented ply arrangement generates slightly higher stresses in comparison to special ply arrangement.

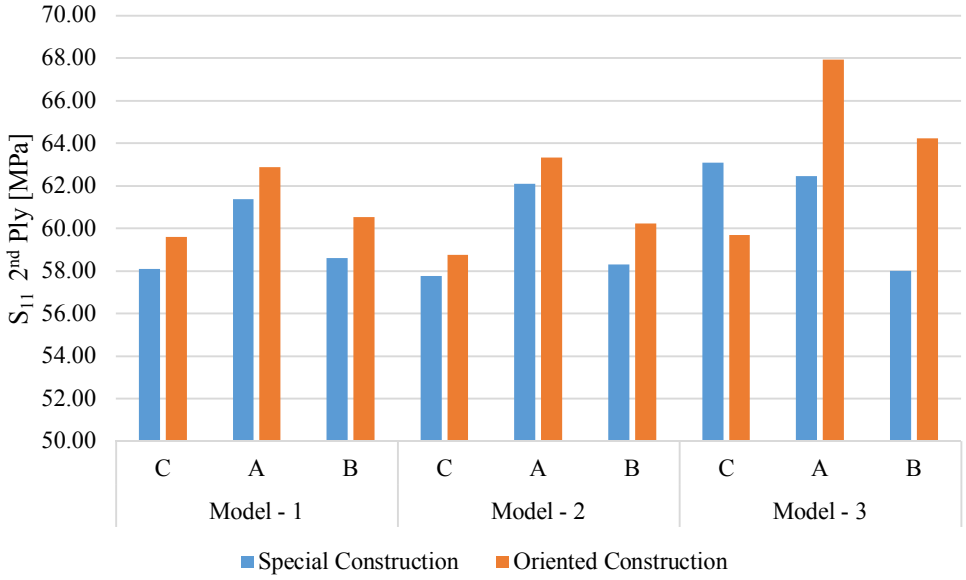

Figure 3.44: The second veneer (bottom-face) stresses for oriented construction versus special construction is shown in the graph. Oriented construction generates slightly higher lower stresses.

This research work is based on the stiffness based design. Hence, oriented ply arrangement as it gives lower values of the model displacements along with lower stress values for face veneer that makes it more resistant to moisture and humidity effects.

4 Design Studies

4.1 Introduction

Design studies were conducted with an objective to make the best use of the structural material. A comprehensive study was performed considering minimum weight, optimal shape of the beams and application of the lightweight material. According to Fenton (1996), the application of steel is influenced by the mass production and availability of steel. But, by carefully analysing the strength and stiffness of the different materials; optimum materials can be used. It is reported by National Research Council (2003) that at least 5% of weight reduction in the structural design should be achieved during the optimization process without compromising the performance of the structure.

In this chapter, the effect of structural profiles on floor deformations were observed for scaled-down models. Loading and boundary conditions were similar to section 3.3.1.2. Cross members in such loading experiences both bending and twisting loads. But, the beams in this study were mainly analysed and optimised from bending perspective. All the beams had a uniform cross-sectional area. Except, the longitudinal beam in full-scale semi-trailer model. Model deformation for each profile was recorded under varying span. As mentioned earlier, optimum choice of material can influence the overall weight and performance of the structure. Therefore, a comparative study was performed for steel and aluminium material.

Full-width models of semi-trailer were created in the SolidWorks 2016 to show that partial models can be used in early-stage design studies. Partial (full-width) models were developed for longitudinal and transverse panel arrangements. And, simulated for ISO 1496-1 (1990) floor strength test. Optimization of the frame was only performed on transverse panel arrangement model. The aim of optimization was to reduce weight of the model. Then, full-scale semi-trailer with bonded floor was modelled and analysed for uniform freight load with an objective to optimize the longitudinal beams. A comparative study was also performed to check the response of bonded flooring chassis with a chassis-only condition.

4.2 Impact of Structural Profile on Lightweight Construction

Based on the studies performed by Ashby (1991), the geometrical properties of the structural profile help in designing efficient structures. The response of the profile is influenced by the mode of loading and boundary conditions. In these studies, the cross members with four different section profiles were simulated for model displacement as shown in figure 4.1. And, three different spans (distance between two cross members) i.e. 300, 400 and 500 mm were used as shown in figure 4.2

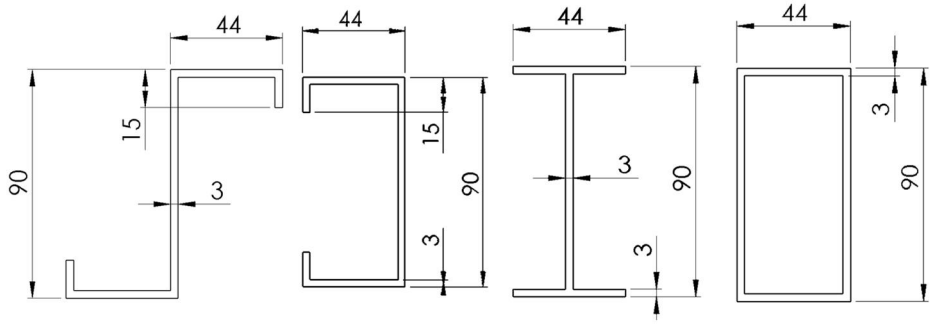

Figure 4.1: Structural profile used for comparison studies (left to right: Z, C, I, RHS)

It was intended to comprehend the scaled-down model displacement for commonly available structural profiles i.e. Z, C, I, and RHS as shown in figure 4.1. And, geometrical properties are shown in table 4.1. The profiles used in this study were idealised sections with same profile thicknesses i.e. 3 mm.

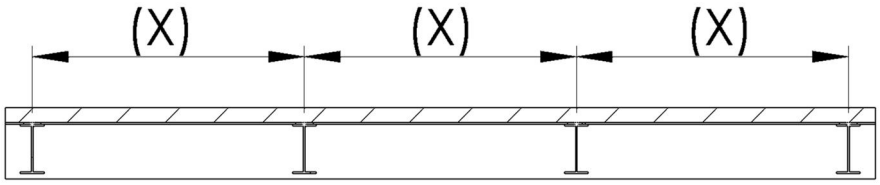

Figure 4.2: Scaled-down models were simulated at 3 different spans i.e. 300 mm, 400 mm, and 500 mm.

According to AISI recommendations, the ratio of flange width to thickness ratio of the unstiffened element of the beam profile was kept under 60 to avoid local flange instabilities *(Fenton, 1996)*. The Z and C-profile came out to be 5.00 whereas for I-profile the value was 7.33. The calculation for I-profile is shown below:

$$\frac{\text{Lenghth of the unstiffened element}}{\text{thickness of the unstiffened element}} < 60$$

$$\frac{22}{3} = 7.33 < 60$$

Table 4.1: Geometrical properties of cross member profiles

Profile	Dimensions [mm]	Mass per length [kg/m]	Section area [mm^2]	I_{XX} [mm^4]	I_{YY} [mm^4]	I_Z [mm^4]	Φ^e_b
Z	44 x 90 x 3 x 15	18.45	588	742,104	274,813	1016,917	26.96
C	44 x 90 x 3 x 15	18.45	588	742,104	155,839	897,943	26.96
I	44 x 90 x 3	16.21	516	647,928	42,781	690,709	30.56
RHS	44 x 90 x 3	24.12	768	796,104	254,776	1050,880	16.95

The cross-member profile was selected based on mass *(m)*, the second moment of area *(I)*, ability to handle twisting loads *(I_Z)* and shape factor for elastic bending. The mass of the beam was calculated by

$$m = \rho A L$$

The second moment of area *(I)* describes the shape influence on the structural profile (Ashby, 1991). The second moment of around bending axis is defined as

$$I = \int_{\text{section}} y^2 \, \mathrm{d}A$$

where; y is the normal distance from the neutral axis and A is the area of the cross section

Shape factor *(Φ)* is a dimensionless quantity which describes the efficiency of the shape irrespective of the size. Shape factor for each profile is different in each loading case i.e. bending, torsion etc. Shape factor for the elastic bending is defined as

$$\Phi^e_b = \frac{4\,\pi\, I_{XX}}{A^2}$$

where; A is the section area and I_{XX} is the second moment of area

Forklift wheel generates two main kinds of loadings on the cross members. Pure bending response when wheel-load passes through the shear centre of beam. And, bending along with twisting loads when the load is not passing through the shear centre of the cross member. Maximum model (panel) displacement was expected when the forklift wheel was at the centre of the span in figure 4.2. As, the aim was to consider a loading case that would generate maximum plywood deflection.

A nonlinear static analysis was performed. Boundary conditions were same as in the partial support models described in section 3.3.1.2. The load was applied at the centre of the model.

Comparative study of different profiles showed that model displacement using RHS profiles as cross beams had the lowest value as shown in figure 4.3. Whereas, response with I-profile cross beams was close to RHS. The model displacement with I-profile as cross beams had a 1.32% higher deflection in comparison to the RHS at the span of 300 mm.

As mentioned earlier, the selection of profile was based on model stiffness, mass, shape factor and resistance to twisting loads (I_Z). Referring to table 4.1 and figure 4.2, it was concluded that I-profile would be the most suitable option for the small and medium span i.e. 300 mm and 400 mm. As, I-profile had a highest shape factor (Φ^e_b = 30.56), lowest mass per length and reasonable model stiffness.

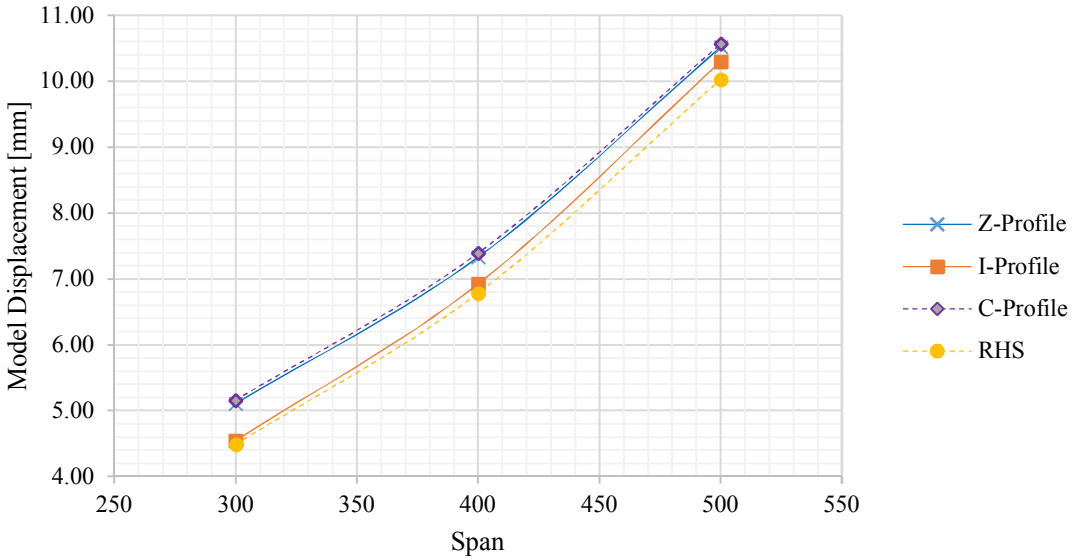

Figure 4.3: The graph showing model displacements (Uz) versus span of the different beam profile

Referring to figure 4.3 and table 4.2, it was also observed that as the span is increased, the relative difference of model displacement decreases. The relative difference between RHS and Z-profile is shown in table 4.2.

Table 4.2: Percent difference between model displacements of two profiles at various span

Span [mm]	**Model displacement [mm]**		**Deflection Increment [%]**
	RHS	Z-Profile	
300	4.49	5.11	13.82
400	6.79	7.33	8.05
500	10.03	10.52	4.89

Therefore, it was concluded that at higher span i.e. 500 mm, Z-profile would be a suitable option due to its significantly high shape factor i.e. $\Phi^{e}_{b} = 26.96$. Furthermore, Z-profile has the highest resistance to twisting loads ($I_Z = 10.17 \times 10^5$ mm^4) for the open profiles which about 38.21% more than the I-profile. As semi-trailer undergoes various loading conditions such as twisting due to road variations. It is important to use cross members with high torsional moment of inertia.

4.3 Application of Lightweight Materials for Weight Optimization

The choice of structural material plays a significant role on the performance of semi-trailer. Therefore, a comparative study was performed to comprehend the response of scaled-down model between two structural materials i.e. steel and aluminium. The material performance study was performed using I-profile as cross members. The model displacement was recorded at three different spans as stated in section 4.2.

A nonlinear static analysis was performed. Boundary conditions were same as in the partial support models described in section 3.3.1.2. Load was applied at the centre of the model. Figure 4.4 shows comparison of model displacement for steel (right) and aluminium (left) at the span of 300 mm.

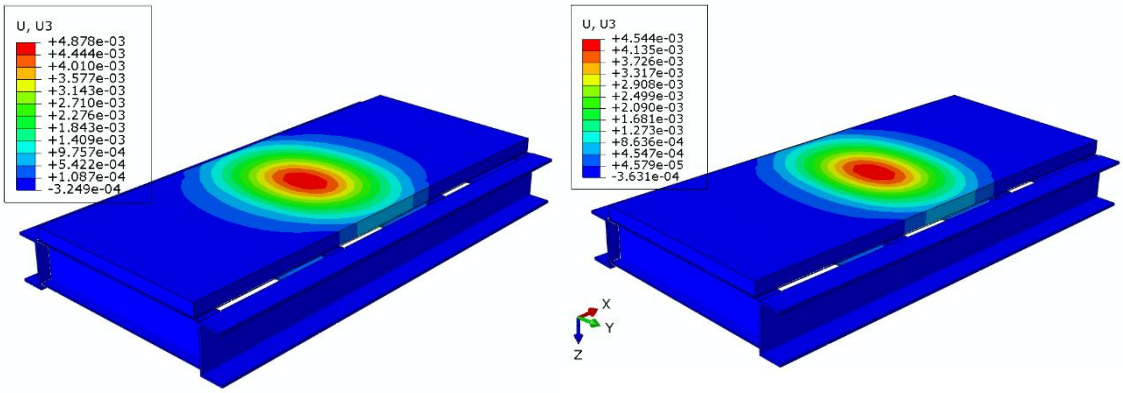

Figure 4.4: Aluminium frame (left) having 7.35% more model displacement in comparison to steel frame (right) at the span of 300 mm.

Plot for the model displacements at varying span is shown in figure 4.5.

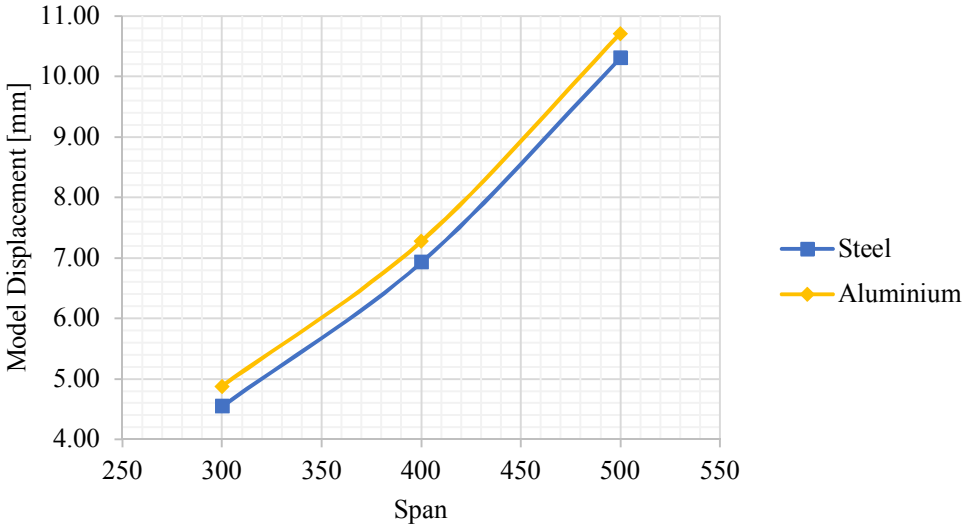

Figure 4.5: The plot showing displacement comparison between model frames made of steel and aluminium material. The aluminium frame experiences 7.35% at small span (300 mm), 5.05% at medium span (400 mm) and 3.98% less deflection at long span (500 mm) as compared to steel.

The frame displacement for aluminium and steel chassis are shown in figure 4.6. It shows that the plywood panel has significant contribution in model displacement than the frame material.

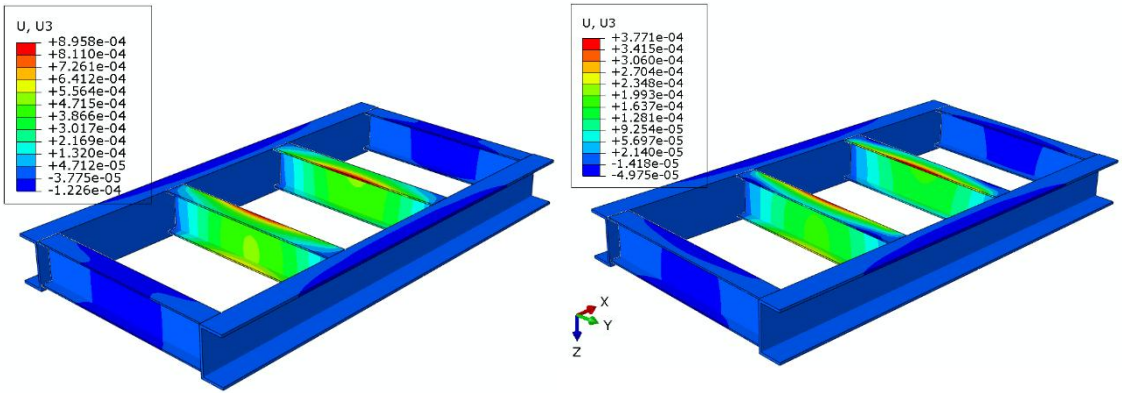

Figure 4.6: Aluminium frame (left) has 137.55% more frame displacement in comparison to steel frame (right) at the span of 300 mm.

In these comparison studies, ThyssenKrupp PAS Structural Steel 355 with cold forming was used to compare with the aluminium 6082-T6 as it is typically used in the truck frames (MatWeb, 2017). Aluminium 6082-T6 was considered as it is used in the transport applications as well (Zehnder, et al., 2011). Aluminium 6082-T6 has the yield strength of 250 MPa and ultimate tensile strength of 290 MPa for profiles having a thickness less than 5 mm (MatWeb, 2017). The stress distribution comparison of aluminium and steel frames in figure 4.7 shows that the aluminium frame is the below the yield strength with FOS of around 2.

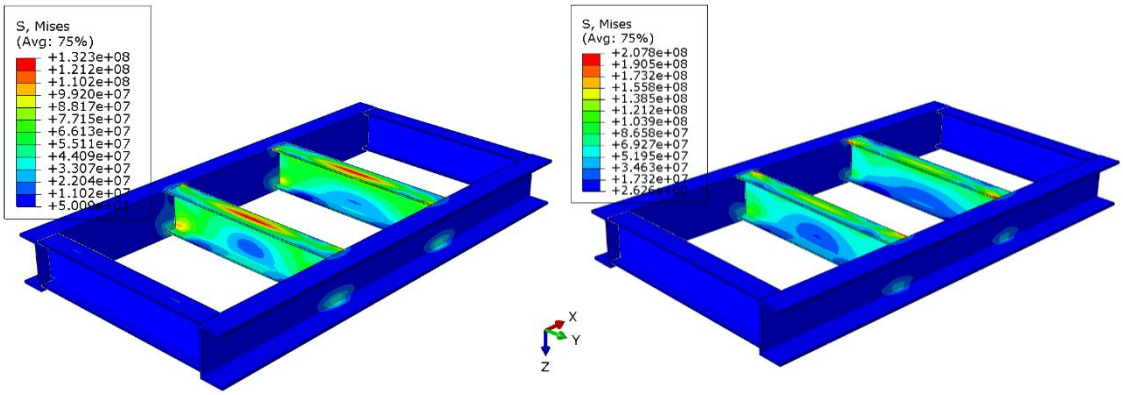

Figure 4.7: Von-Mises stress at the cross member for steel frame (right) and aluminium frame (left).

Table 4.3 shows that the aluminium frame 2.91 times lighter than steel frame. It can be used to effectively design lightweight semi-trailers with increased number of cross members to improve floor stiffness.

Table 4.3: Material properties and weight of the scaled-down model frames

Sr. No.	Material	Density	Yield Strength	Ultimate Strength	Mass (Frame)
		[kgm^{-3}]	[MPa]	[MPa]	[kg]
1	Structural Steel S355	7850	355	430-550	23.14
2	Aluminium 6082-T6	2700	250	290	7.96

According to the Ashby (2005), the efficiency of the materials can be measured by the material indices such as specific stiffness of the beam/shaft under bending/twisting loads.

Table 4.4 and 4.5 shows the comparison of S355 and 6082-T6 material with stiffness-limited (minimising elastic deformations) as a design criterion to achieve minimum mass and minimum cost. Stiffness-limited design for beam in bending at minimum mass can be calculated as

$$\text{Beam}_{\text{minimum mass}} = \frac{E^{1/2}}{\rho}$$

Similarly, stiffness-limited design for beam/shaft in torsion at minimum mass can be calculated as

$$\text{Beam}_{\text{minimum mass}} = \frac{G^{1/2}}{\rho}$$

The above equations are valid for the beam when elastic modulus, length of the beam and shape of the section is specified. But, section area can vary.

Table 4.4: Structural steel S355 and aluminium 6082-T6 for stiffness-limited design at minimum mass

Sr. No.	Material	Stiffness Limited Design	
		Bending	Torsion
1	Structural Steel S355	56.97	36.03
2	Aluminium 6082-T6	97.22	60.29

The table 4.4 shows that Aluminium 6080-T6 has higher performance index compared to structural steel S355 in bending as well as in torsion to achieve minimum mass which is also validated by Seyfried, et al. (2015) in their research.

Stiffness-limited design for beam in bending at minimum cost can be calculated as

$$\text{Beam}_{\text{minimum mass}} = \frac{E^{1/2}}{C_m \rho}$$

where C_m is the cost of material

Similarly, stiffness-limited design for beam/shaft in torsion at minimum cost can be calculated as

$$\text{Beam}_{\text{minimum mass}} = \frac{G^{1/2}}{C_m \rho}$$

Table 4.5: Structural steel S355 and aluminium 6080-T6 for stiffness-limited design at minimum cost

Sr. No.	Material	Cost of material *	Stiffness Limited Design	
		€ / kg	Bending	Torsion
1	Structural Steel S355	0.54	105.30	66.60
2	Aluminium 6082-T6	2.03-2.33	40.72	25.88

** as per CES software*

From, table 4.5, it was concluded that aluminium 6082-T6 is a costlier solution to develop a semi-trailer. But, it can be more economically viable option in the product life-cycle due to lower fuel consumption and higher payload. It is also recommended that similar studies shall be performed for strength-limited (avoiding plastic failure) design to achieve more comprehensive data for the selection of the material.

4.4 Static Analysis of Partial (full-width) Semi-Trailer Chassis

Modelling approach developed in the chapter 3 was used to make partial (Full-width) models. Zone-3 of the semi-trailer was used to study full-width models based on its simple construction. In full-width models, transverse and longitudinal panel arrangement were simulated to study the displacement of the floor panel according to ISO 1496-1 (1990) forklift axle-load. Forklift axle-load used in these simulations was 72 kN that corresponds to 36 kN on each wheel. Axle width was slightly exaggerated from the currently available forklift models to place the forklift wheel exactly in the centre and centre-edge of the full-width model.

As concluded in section 3.6, oriented panel construction gave stiffer than special construction. Therefore, oriented panel construction was used in these simulations. It is also possible to optimise the plywood panel construction depending on the loading and boundary conditions. However, it was considered out of the scope of this thesis.

The frame of semi-trailer was modelled as accurately as possible. I-profile was used for the longitudinal beams and cross members. I-profile used in the cross members was standard component manufactured by ArcelorMittal (one of the largest steel producer) as shown in figure 4.8. The side-rails and cover sheets were made of structural steel and aluminium respectively as commonly used in semi-trailer design.

The objective in these design studies was to perform exemplary model simulations for displacement. And, to perform weight optimization studies. It was assumed that the forklift loading produces local deformations and stress.

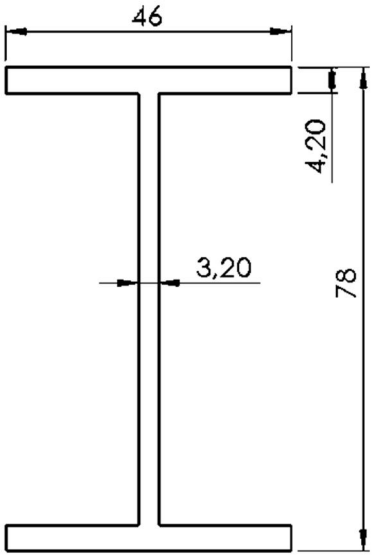

Figure 4.8: IPE AA 80 as manufactured by ArcelorMittal.

4.4.1 Partial (full-width) model with longitudinal panel arrangement

In the partial model with longitudinal panel arrangement, the centre to centre span of the cross members was 442.20 mm and the unsupported span for plywood flooring was 396.20 mm. Cross members were welded to the longitudinal beams and side-rail. The aluminium coversheet was in frictional contact with longitudinal beams, cross members, and plywood panel. Adhesive was only applied at the cross members to bond plywood panel with the chassis.

A 27.40 mm thick plywood panel was modelled having 20 veneers. The oriented construction with the face veneer in the Y-axis direction was used. Overall, the strongest panel direction was in the X-axis direction. The size of the plywood panel used in this model were based on the standard sizes manufactured by UPM Plywood Oy. The full-width (zone-3) model for longitudinal panel arrangement is shown in figure 4.9.

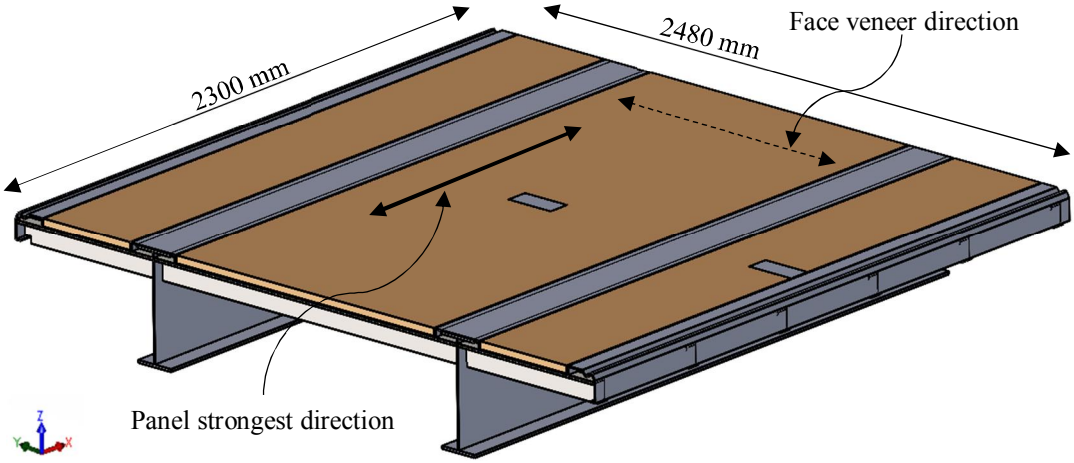

Figure 4.9: Zone-3 of the semi-trailer with longitudinal panel arrangement.

Exploded view of the zone-3 of the semi-trailer having longitudinal panel arrangement is shown in figure 4.10. The figure shows the material of various components as well. The elastic modulus of 68.9 GPa and Poisson's ratio of 0.33 was used for aluminium cover-sheets (Prucz, et al., 2013).

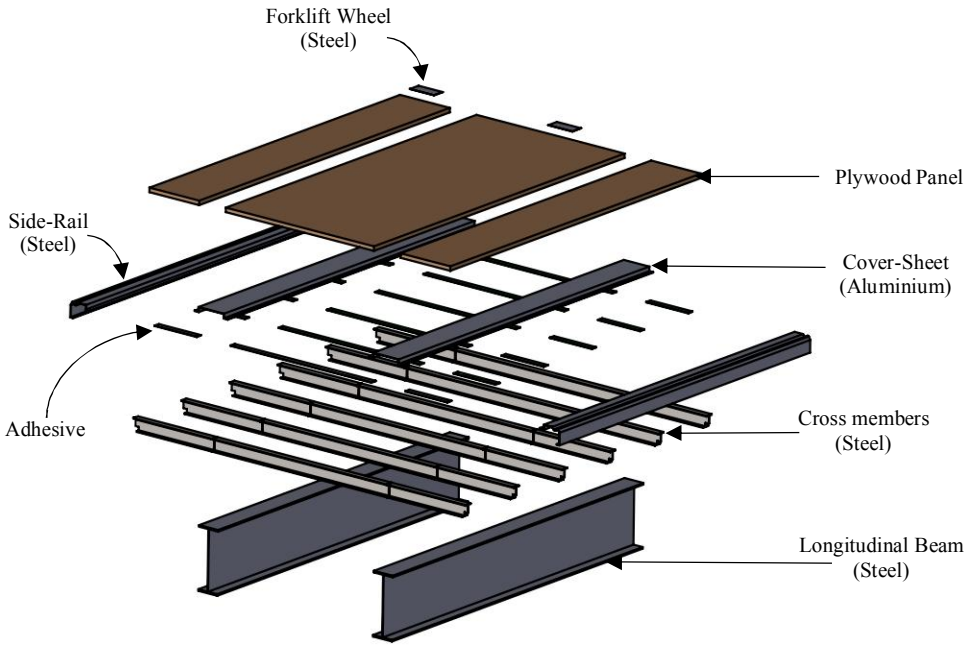

Figure 4.10: Exploded view of the zone-3 of the semi-trailer with longitudinal panel arrangement.

A nonlinear static analysis was performed similar to section 3.3.1.2. The frictional contacts were created between plywood and cover-sheets, plywood and side-rails, cover-sheet, and cross members, and between cover-sheet and longitudinal beams. It was observed that addition of frictional contacts increased the computational time of the model. And, rest of the model is connected using 'Tie' constraint showing the perfect

bonding condition. Partial (full-width) model was loaded with 72 kN axle-load i.e. 36 kN on each wheel plate. Ends of the semi-trailer section were constrained using pinned boundary conditions i.e. $U_X = U_Y = U_Z = 0$ as shown in figure 4.11.

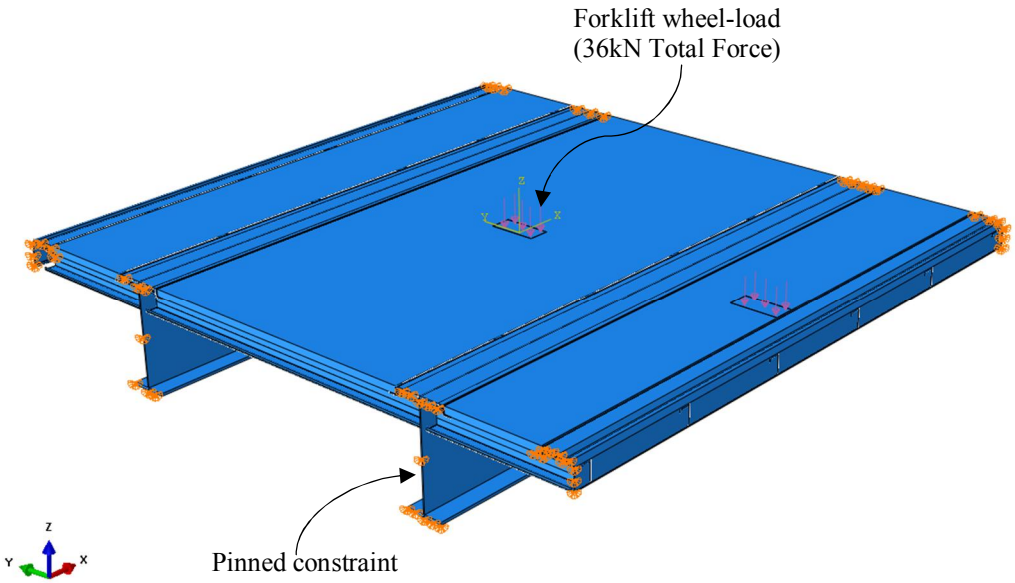

Figure 4.11: 36kN of wheel-load (each wheel) is applied on the centre and centre-edge of the plywood panel to get the maximum panel displacement. The end of the structure is pinned ($U_X=U_Y=U_Z=0$) as the load generates local effects.

Figure 4.11 shows the meshed model and location for frictional contacts. The adhesive component and side-rail were modelled using quadratic brick (C3D20R) elements.

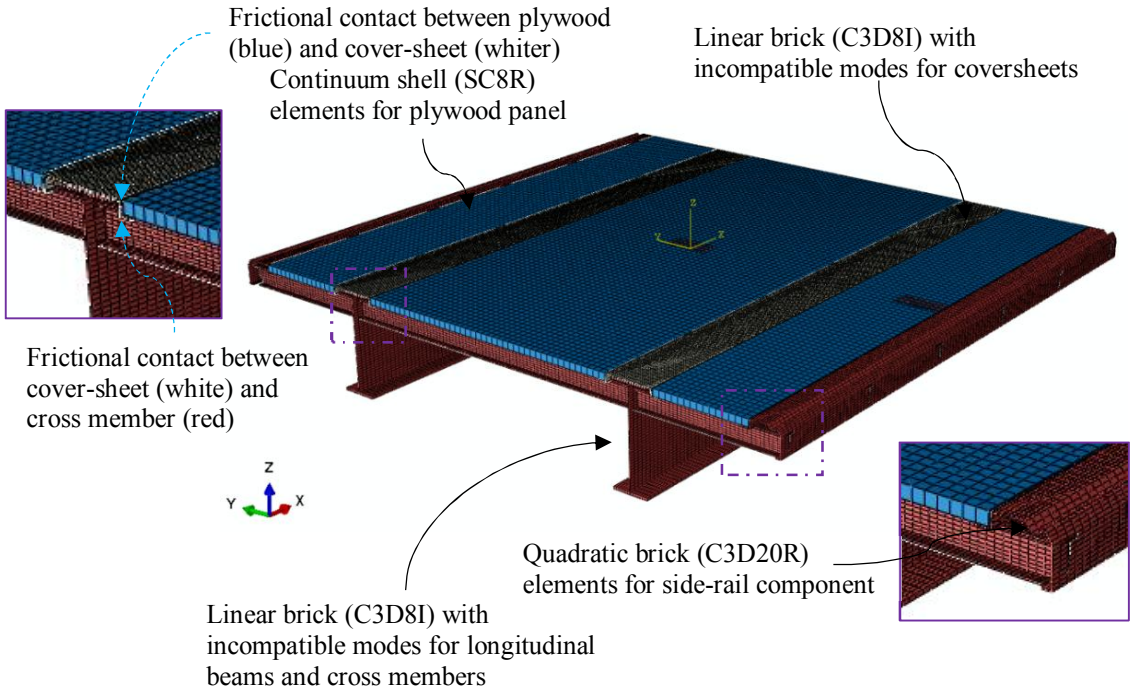

Figure 4.12: Meshed Full-width model (zone-3) with longitudinal panel arrangement.

Vertical displacement for the partial model (longitudinal panel arrangement) came out to be 10.21 mm as shown in figure 4.13. Model displacement is comparable to the scaled-down model displacements for I-profile cross beams in section 4.2. Deviation in the results is due to different boundary conditions and wider plywood panel (1102 mm instead

of 385 mm). Also, longitudinal beams could bend and twist. Whereas, in the scaled-down models, longitudinal beams were more rigidly supported from bottom-face. However, the simulations show that partial model can be used to predict the floor displacements. It is important to perform detail analysis on the critical locations to comprehend complete response of bonded floor semi-trailers.

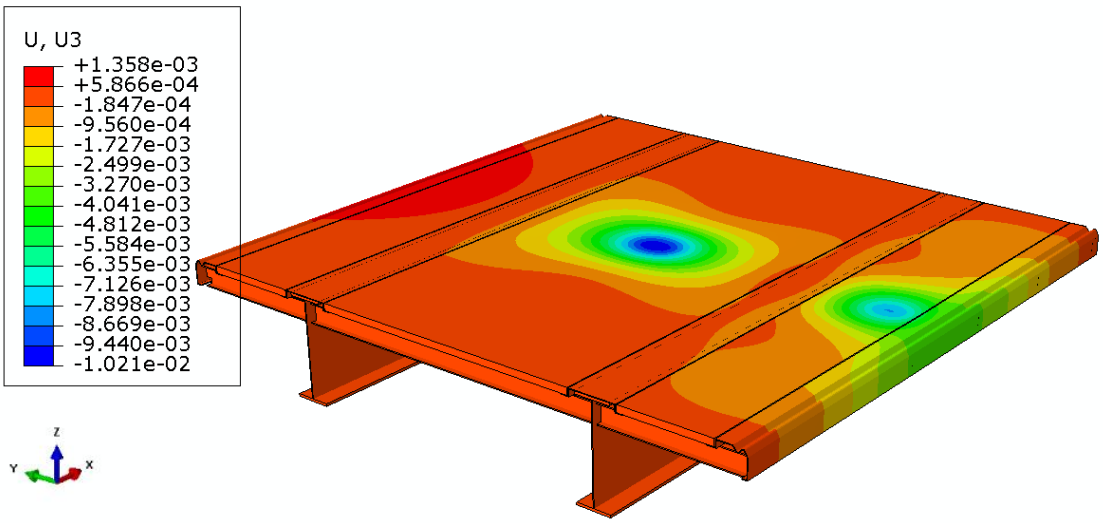

Figure 4.13: Vertical displacement (U_Z) for longitudinal panel arrangement comes out to be 10.21 mm.

4.4.2 Partial (full-width) model with transverse panel arrangement

In the partial model with transverse panel arrangement, the centre to centre span of the cross members was 400 mm. Cross members were welded to the longitudinal beams and side-rail. The plywood panel was in frictional contact with the side-rails. Adhesive was applied at the cross members and longitudinal beams to bond plywood panel with the chassis.

In this transverse panel arrangement, the size of the panels is usually around 1200 x 2100 mm^2 or 1500 x 2100 mm^2. In this model, face veneer is in X-axis direction and panel stronger direction is in Y-axis direction. Figure 4.14 shows the exploded view of the zone-3 of semi-trailer with transverse panel arrangement.

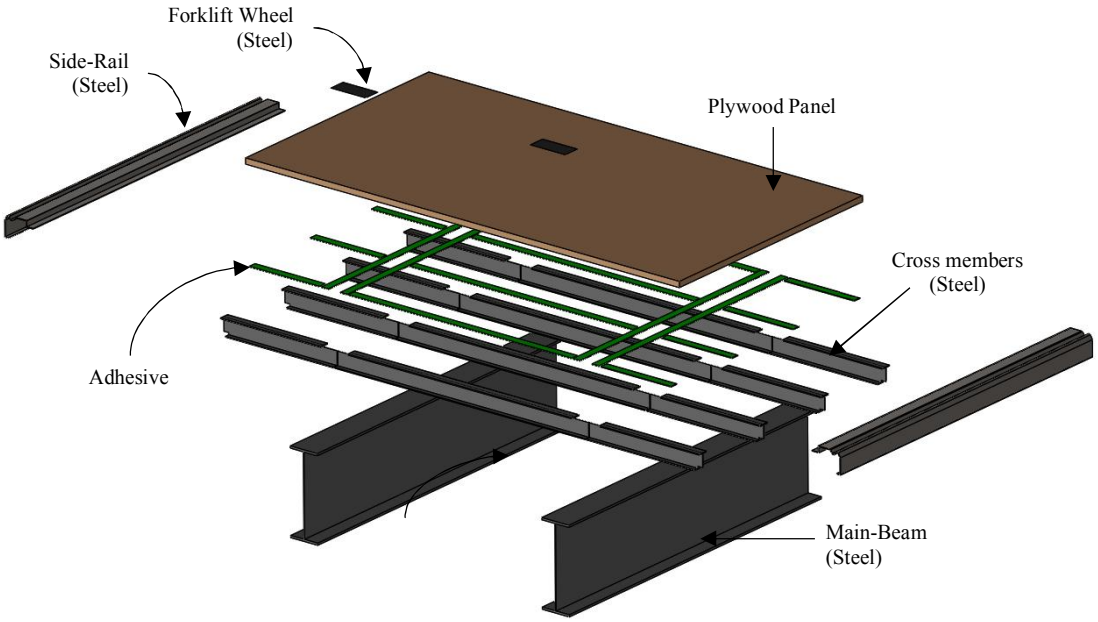

Figure 4.14: Exploded view of the zone-3 of the semi-trailer with transverse panel arrangement.

A detailed drawing of the partial (zone-3) for transverse panel arrangement is shown in appendix 6. Also, a simplified model of cross member-longitudinal beam interface was analysed to comprehend our modelling simplification. The results of the simulation are documented in appendix 7.

A nonlinear static analysis was performed similar to section 4.4.1. The frictional contact was made between plywood and side-rails. Rest of the model was connected using 'Tie' constraint to establish perfect bonding condition.

The partial model was loaded with 72 kN axle-load i.e. 36 kN on each wheel plate. The ends of the semi-trailer section were constrained using pinned boundary conditions i.e. $U_X = U_Y = U_Z = 0$ as shown in figure 4.15.

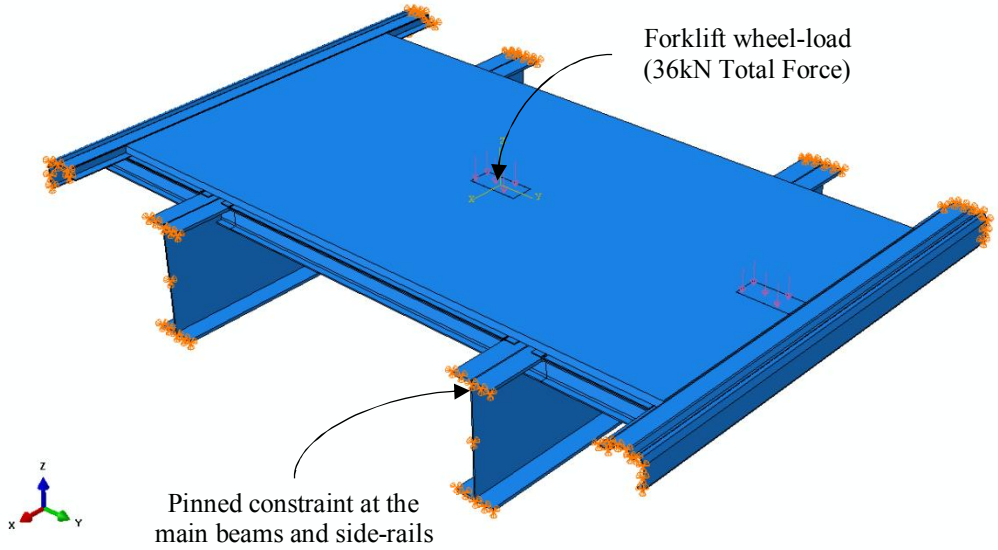

Figure 4.15: 36kN of wheel-load (each wheel) is applied on the centre and centre-edge of the plywood panel to get the maximum panel displacement. The end of the structure is pinned ($U_X=U_Y=U_Z=0$).

Figure 4.16 shows the meshed model and location for frictional contacts. The adhesive component and side-rail were modelled using quadratic brick (C3D20R) elements.

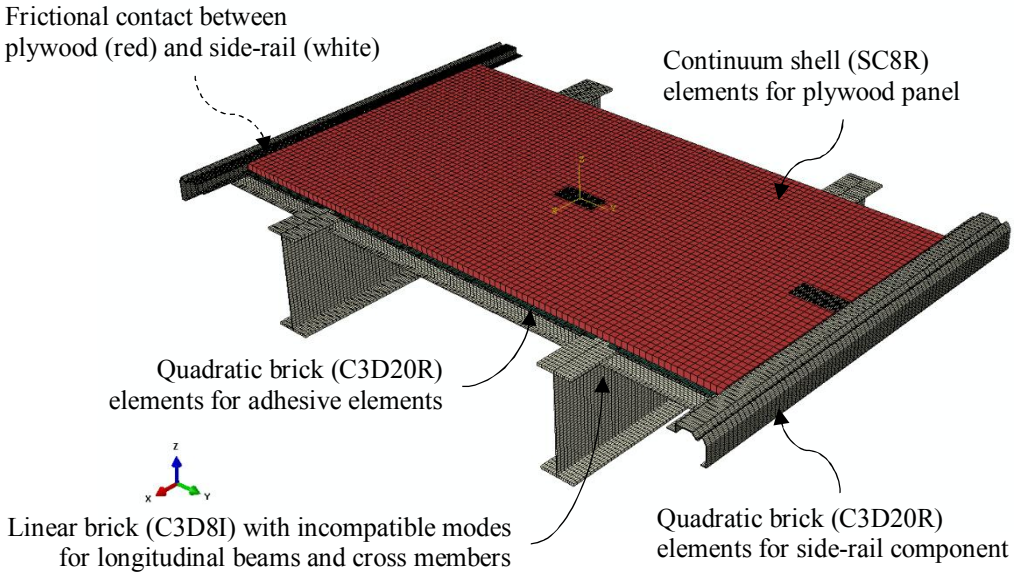

Figure 4.16: Meshed model (zone-3) with transverse panel arrangement.

Vertical displacement for the partial model (transverse panel arrangement) came out to be 11.13 mm as shown in figure 4.17. It was noticed that the longitudinal panel arrangement performs better in comparison to transverse panel arrangement. The longitudinal panel arrangement gives lowers displacements despite having larger span i.e. 436.20 in comparison to 400 mm. This is due to better supports by cover-shits in longitudinal panel arrangement.

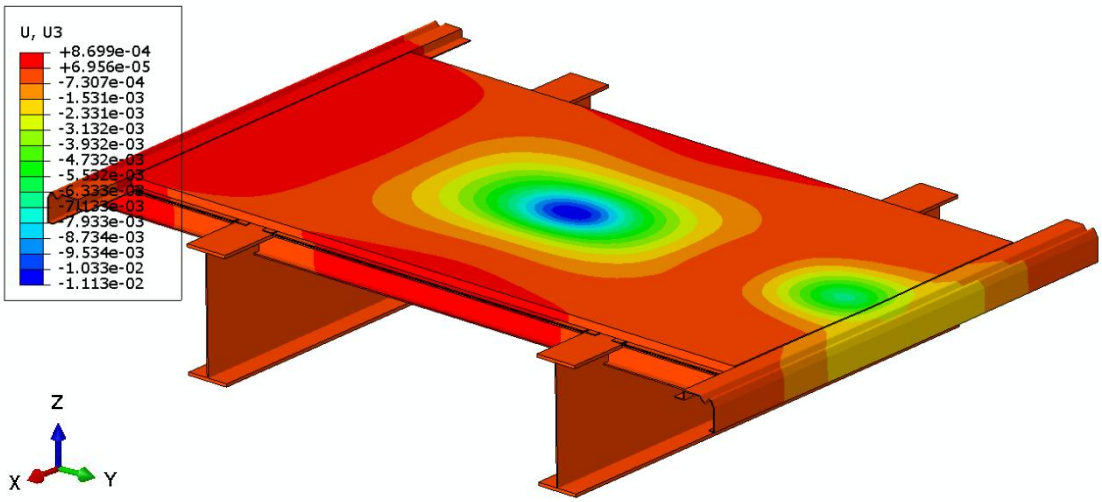

Figure 4.17: Vertical displacement (U_Z) for transverse panel arrangement comes out to be 11.13 mm.

4.5 Optimization of the Partial (full-width) Semi-Trailer Model

The optimisation studies were performed on the zone-3 of the semi-trailer chassis under forklift wheel-load. Transverse panel arrangement was selected to perform exemplary studies. A nonlinear static analysis with loading and boundary conditions similar to section 4.4.2 was performed. The optimization of the bonded flooring structure was performed by two different optimization strategies.

1. Optimization of the structure by removing the non-critical structural mass.
2. Redesign the arrangement of semi-trailer cross members to improve structural efficiency.

4.5.1 Mass optimization by removing non-critical mass

In this optimization technique, the intention was to remove mass from the cross members and longitudinal beams to reduce structure mass. Three iterations were performed as shown in figure 4.18, 4.19 and 4.20. Iteration – 1 was done by creating cut-outs in the cross members, iteration – 2 by increasing the number of cut-outs in the cross members and iteration – 3 by adding cut-outs the longitudinal beam as well.

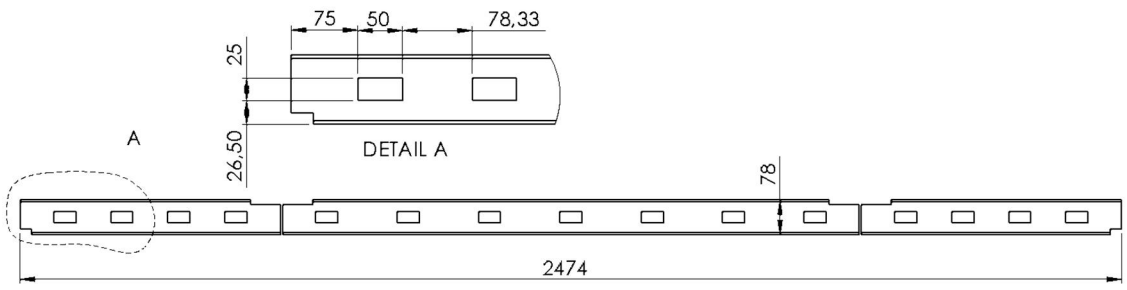

Figure 4.18: Iteration-1 with rectangular cut-outs of 50 × 25 mm with a gap of 78.33 mm.

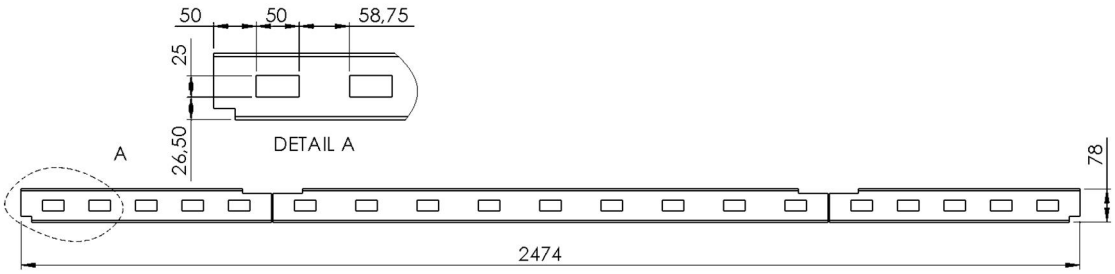

Figure 4.19: Iteration-2 with increasing number of the cut-outs and the gap reduced to 58.75 mm.

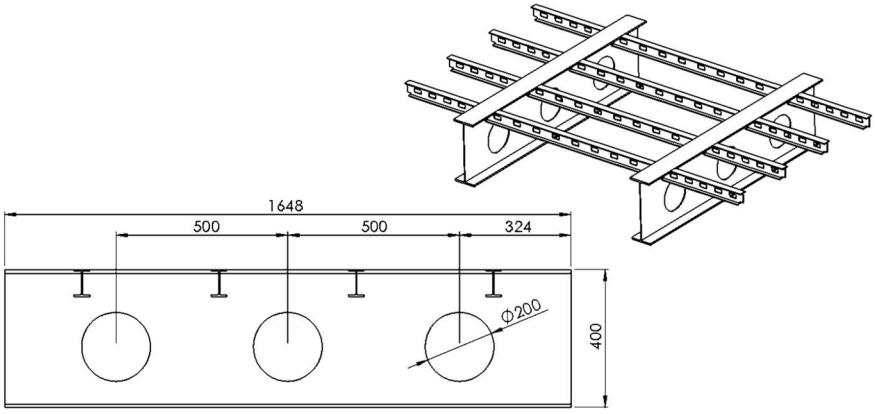

Figure 4.20: Iteration-3 was inclusion of cut-out in the longitudinal beam of the frame.

The plot in figure 4.21 shows model displacement versus the mass of the frame for different iterations.

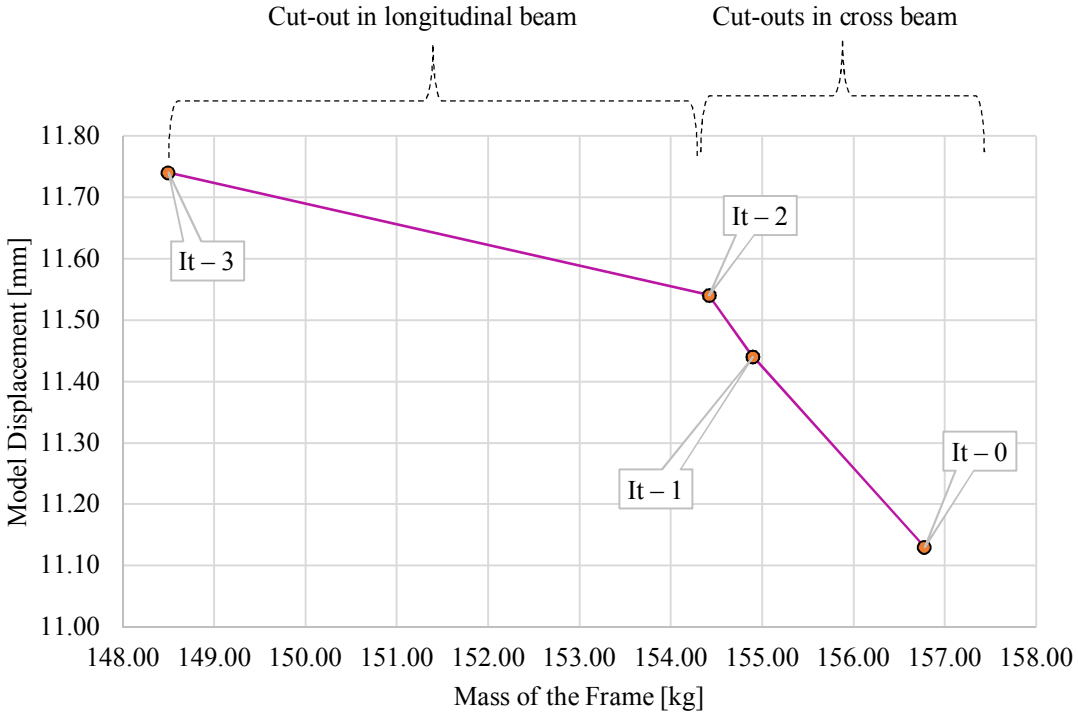

Figure 4.21: The plot showing reduction in the structure mass versus model displacement.

From figure 4.21, it was noticed that the optimisation of the cross members by adding cut-outs contributed to the maximum of 5.24% weight reduction i.e. approximately 20 kilograms in the complete chassis. But, model displacement also increased by

3.68%. Increase in the deflection due to bending and twisting loads generated by forklift wheel. And, it might be noted that the addition of cut-out reduces resistance against twisting loads.

It was also noticed that the addition of cut-outs in the longitudinal beam reduces the percentage weight of frame by 5.28% i.e. approx. 25 kilograms in the whole chassis while resulting in 5.48% increase of model displacement. The model displacement and stress distribution in the model frame are shown in figure 4.21 and 4.22.

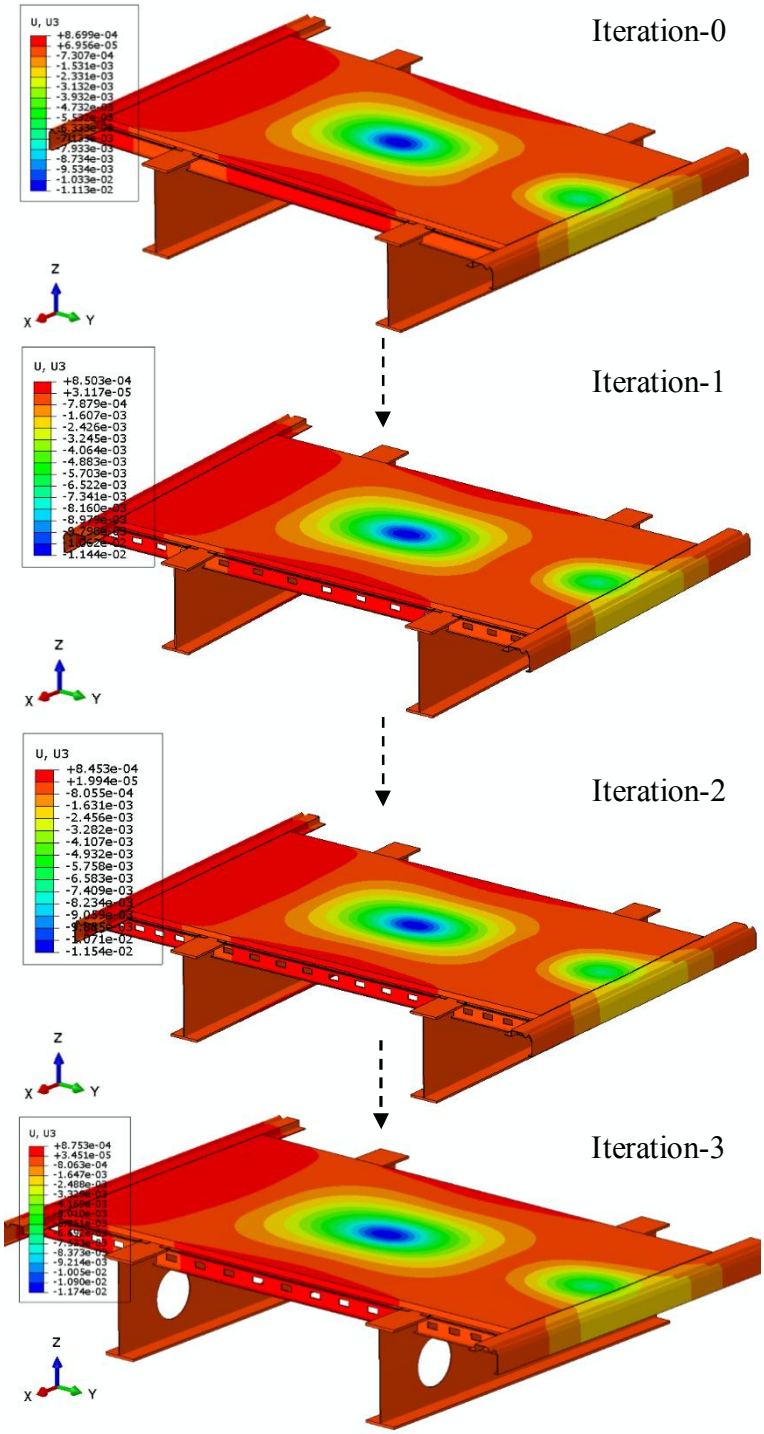

Figure 4.22: Model displacement (U_Z) of the different iterations performed in order reduced the weight of semi-trailer section.

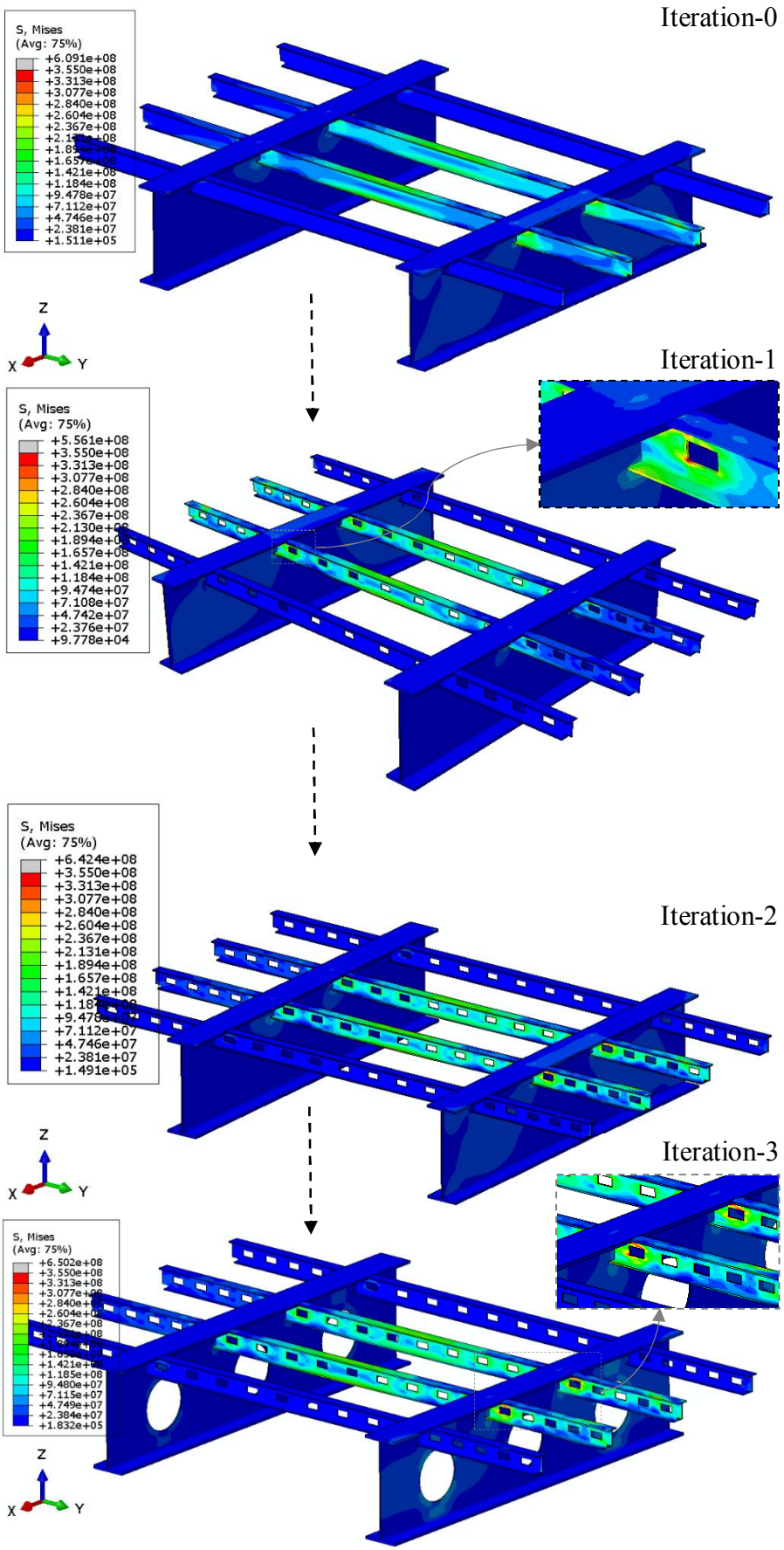

Figure 4.23: Von-mises stress distribution of the different iterations performed in order reduced the weight of semi-trailer section.

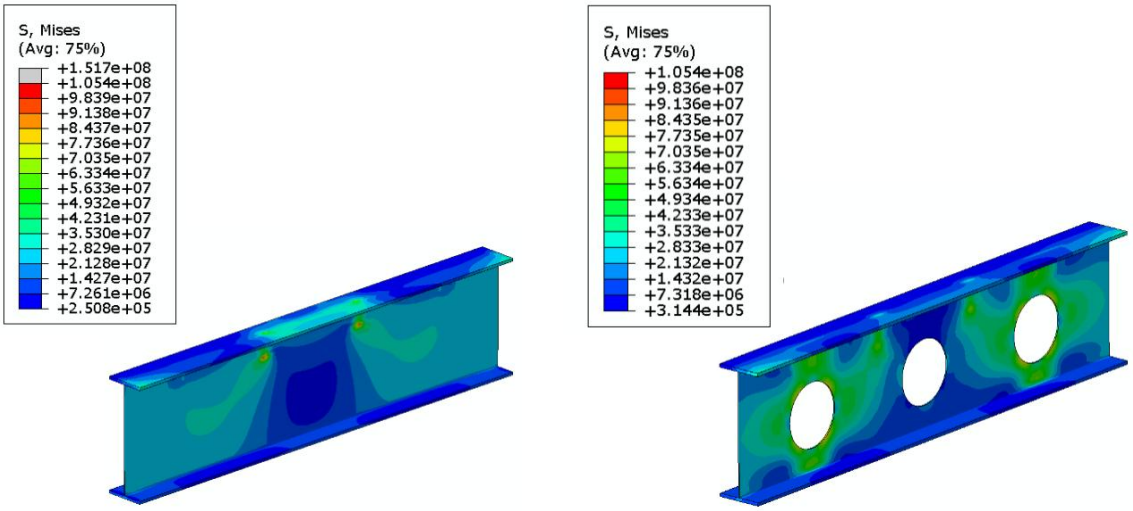

Figure 4.24: The addition of cut-outs in the longitudinal beam improves the stress distribution and utilization on the material increases.

From figure 4.18 and 4.24, it was comprehended that longitudinal beams have a higher impact in the weight reduction of the overall semi-trailer. Therefore, it was concluded that cut-out study shall also be performed on the longitudinal beam in full-scale models.

4.5.2 Optimization by redesigning cross members arrangement

The redesigning of frame structure was performed to better support the plywood panel for wheel-load or axle-load. The redesigned frame structure is shown in figure 4.25.

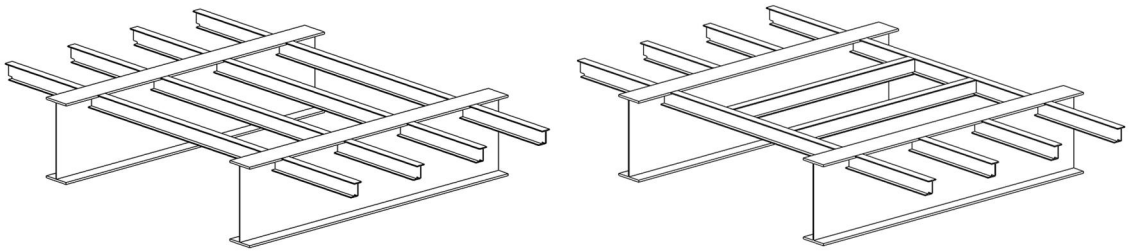

Figure 4.25: Original frame structure (left) for transverse panel arrangement. Redesign version of the frame structure (right) for transverse panel arrangement.

It was noticed that the redesigned model was 3.82% lighter than the original ladder frame design as shown in figure 4.25 i.e. approx. 14 kg.

The plot in figure 4.26 shows that model displacements for the new frame design has 2.88% lower as compared to the original design. It was concluded that redesigning of semi-trailer in the bonded flooring structures may be studied in detail for further optimisation.

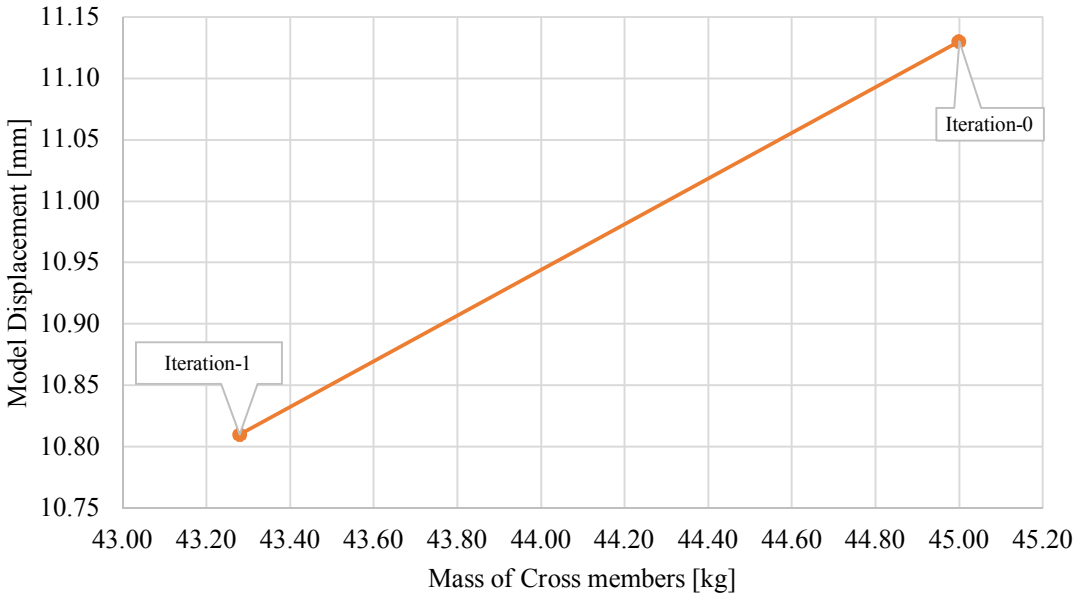

Figure 4.26: The plot shows that redesigned model improves model stiffness against forklift loading and reduces the structure weight as well.

Vertical displacements for the redesigned frame performed better as compared to original design as shown in figure 4.26.

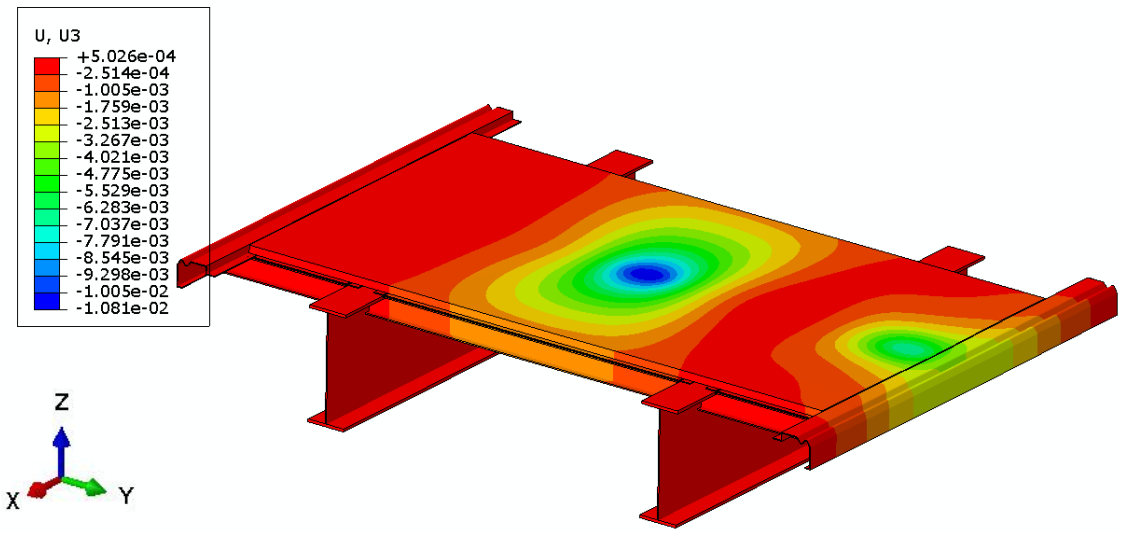

Figure 4.27: Model displacement (U_Z) of the redesigned semi-trailer (zone-3) section is 2.88% less compared to the original model.

The stress distribution is shown in figure 4.28. It can be seen in the figure that peak stress location has been change due to twisting effects generated by forklift wheel-load in the centre.

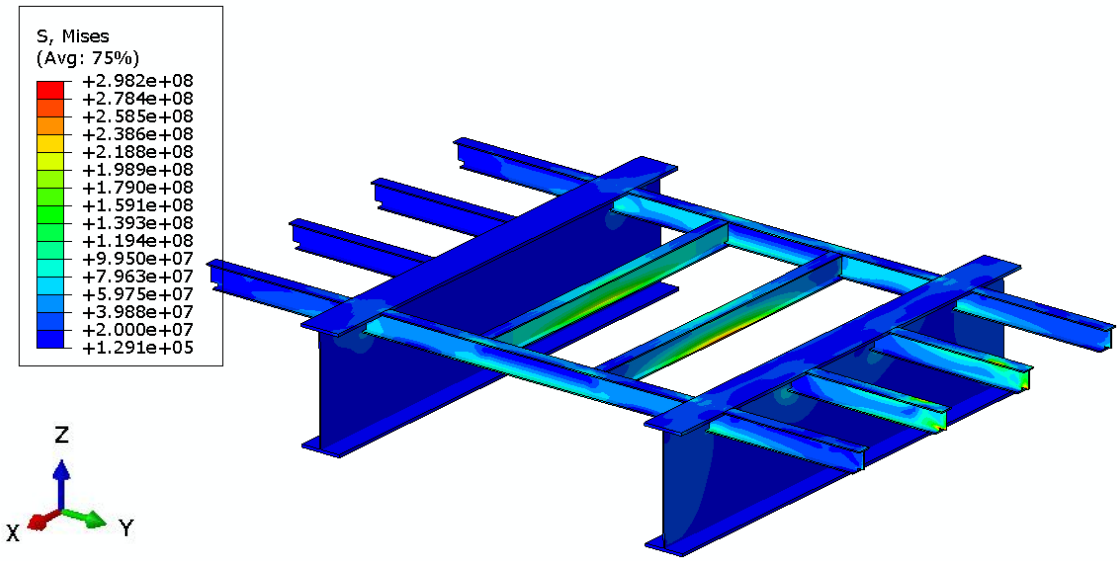

Figure 4.28: Von-mises stress distributions shows that the redesigned model has slightly higher stresses compared to original design (figure 4.18, iteration-0) but still under the same limit.

In this study, further reduction of weight by introducing cut-outs was not studied but it can be implemented to increase weight reduction.

4.6 Static Analysis of Full-Scale Semi-Trailer

The chassis structure contributes to a major weight portion of the flatbed semi-trailer as shown in figure 4.29. It creates a viable opportunity to investigate the effect of bonded flooring in the full-scale semi-trailer and optimise the weight of the longitudinal beams.

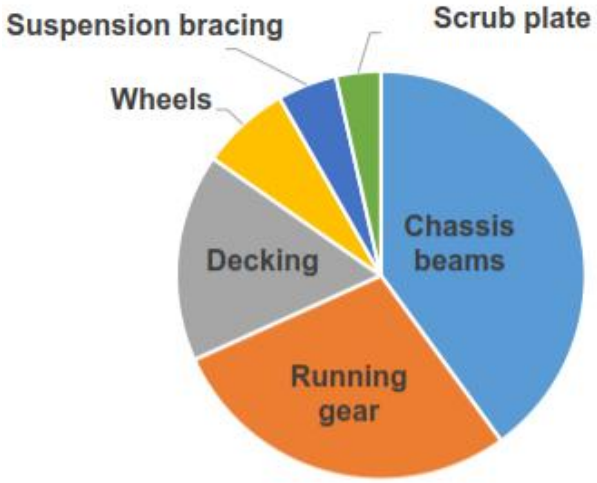

Figure 4.29: Weight distribution of a standard 13.50 m long flatbed semi-trailer (Galos, et al., 2016).

In this study, comparative studies were performed to comprehend the effect of bonded flooring on the model stiffness. Typical load case selected for these studies was pressure applied by the 40-ft. freight container load on the 13.50 m long semi-trailer chassis as shown in figure 30.

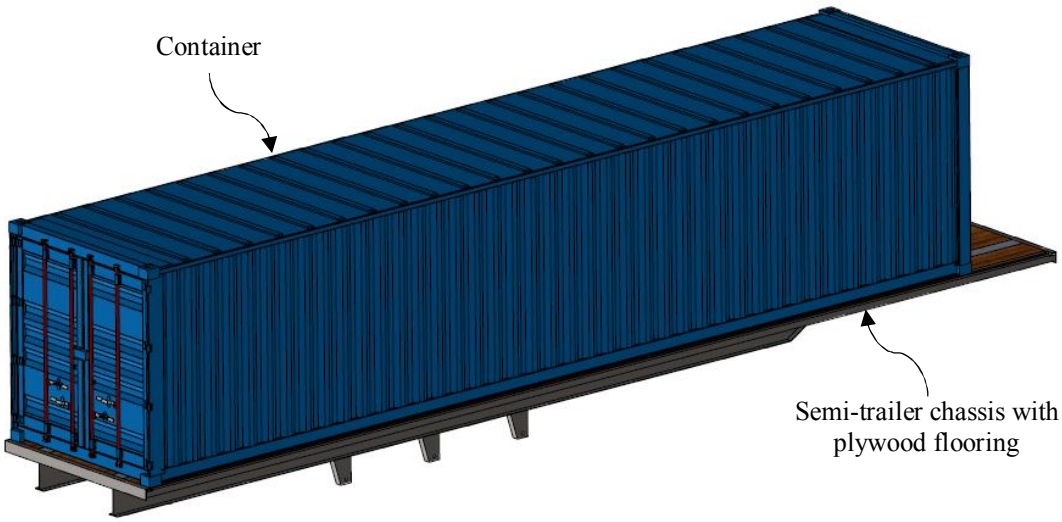

Figure 4.30: CAD model of the bonded floor semi-trailer with 40 ft. ISO container.

Figure 31 shows the detail view of the bonded floor semi-trailer. The adhesive material was applied on the cross members' similar to partial model in section 4.4.1 and on the kingpin region.

The detailed drawing of full-scale semi-trailer is attached in appendix 8.

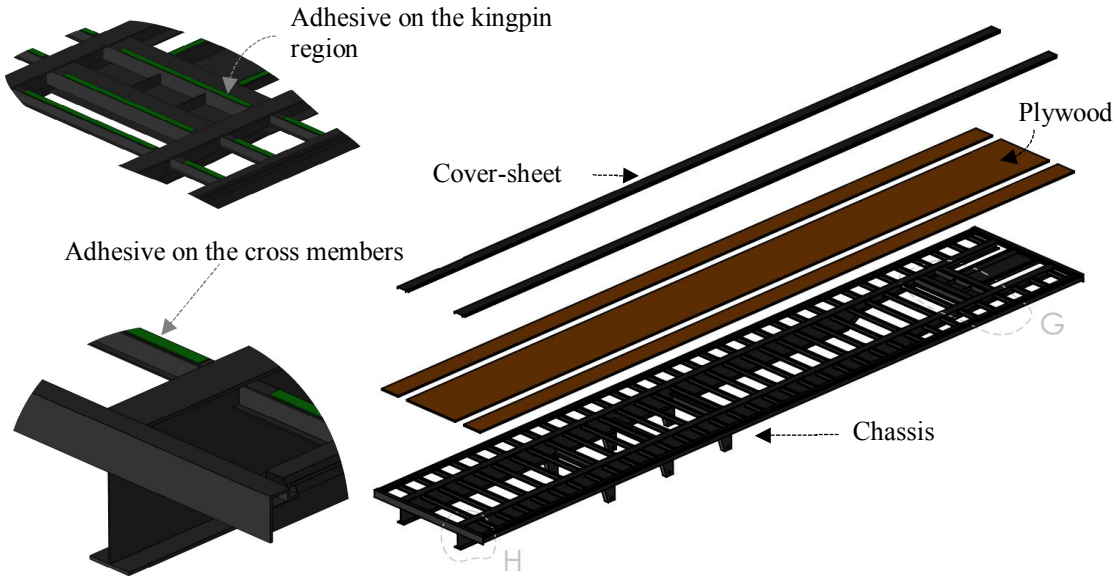

Figure 4.31: Exploded view of the semi-trailer chassis and its connection details.

The CAD model was simplified for FEA to improve computational time. And, to generate superior quality mesh. Semi-trailer model was divided in half along to longitudinal plane (XZ) due to model symmetry as shown in figure 4.32.

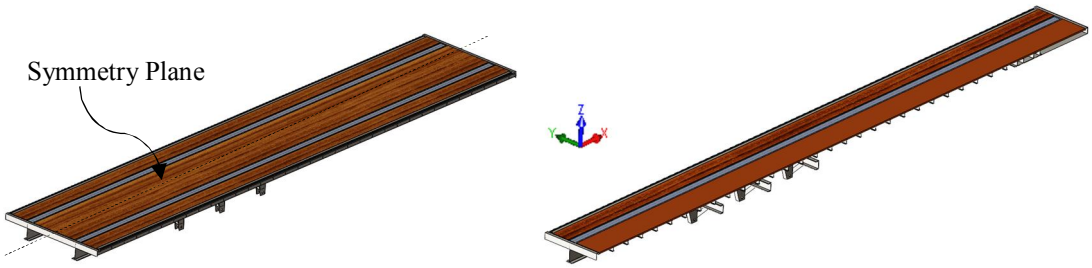

Figure 4.32: Semi-trailer (bonded floor) chassis simplified around the symmetric plane (XZ) to reduce computational time. Original model (left) and simplified model (right).

Geometric simplifications were performed at the kingpin area and axle support brackets as shown in figure 4.33 and 4.34. The kingpin cut-out was replaced with a flat continuum area to improve mesh element shape. Also, the kingpin support plate draft angle was removed for a similar reason. At the support area, axle support bracket was modified for complex sheet metal design to a solid body as shown in figure 4.34.

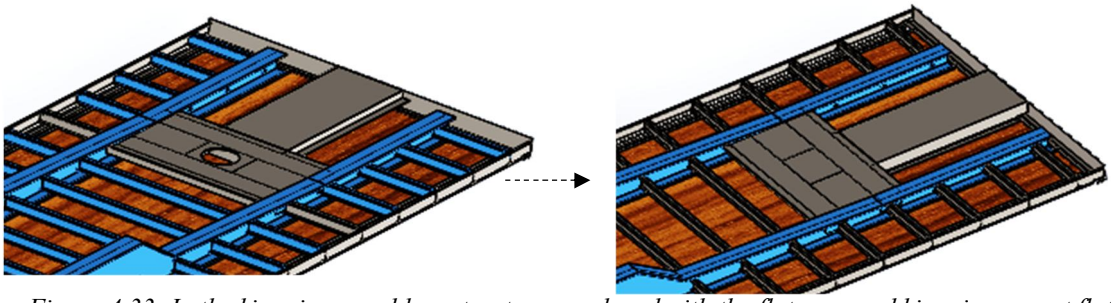

Figure 4.33: In the kingpin assembly, cut-out was replaced with the flat area and kingpin support flat draft was removed for the ease of meshing.

At the support area, axle support bracket was modified for complex sheet metal design to a solid body as shown in figure 4.34.

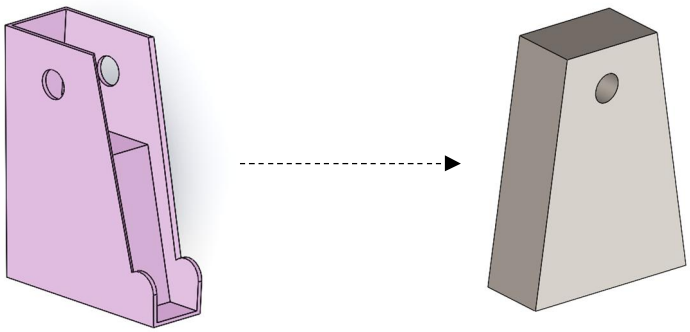

Figure 4.34: Axle support bracket was changed from complex sheet metal assembly to simple solid design that was later mesh with solid mesh elements.

4.6.1 Comparative study of bonded floor semi-trailer vs. chassis-only

A comparative study of the bonded floor semi-trailer chassis and without bonded floor semi-trailer chassis were performed to comprehend to the model displacements. And, to visualise the stress distribution in the longitudinal beam.

A nonlinear static analysis was performed. Loading and boundary condition of the bonded semi-trailer and chassis-only cases are shown in figure 4.35 and 4.36. According to the studies performed by Eckerlid, et al. (2010) for the design of flatbed semi-trailer, the total weight of the 40 feet ISO container is about 30480 kg. Therefore, 149504.40 N of pressure load (total force) was applied on the top-side of the trailer model (region covered by container). And, axle support bracket were restricted in the vertical direction.

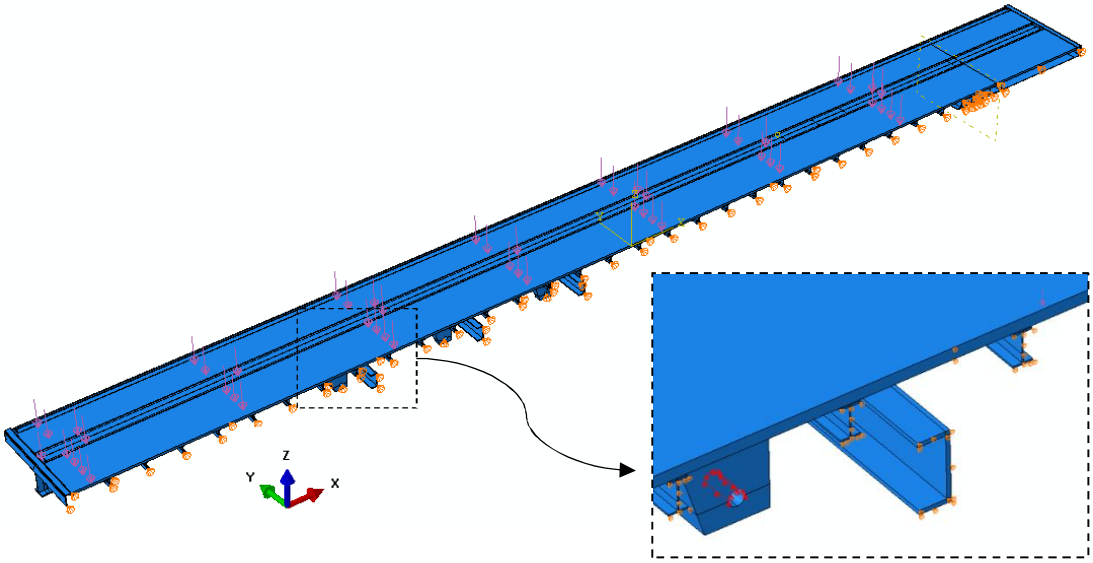

Figure 4.35: The pressure load of 149504.40 N was applied on the container face area. Axle supports were restraint in vertical direction (U_Z = 0) and kingpin region was restraint using pinned constraint (U_X=U_Y=U_Z=0). The symmetry plane was restrained only in the U_Y = 0 as solid elements are used.

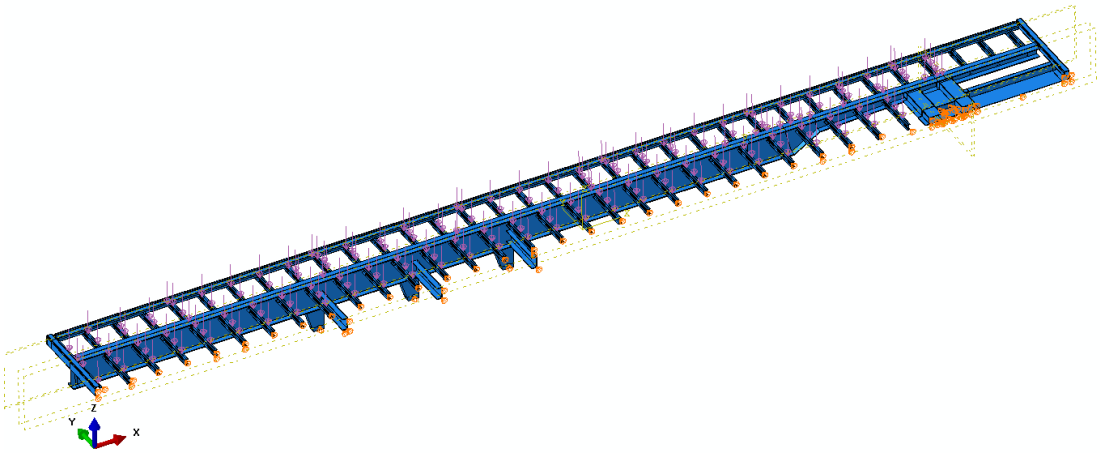

Figure 4.36: The pressure load of 149504.40 N was applied on the chassis beams that were under container face area. Axle supports were restraint in vertical direction (U_Z = 0) and kingpin region was restraint using pinned constraint (U_X=U_Y=U_Z=0). The symmetry plane was restrained only in the U_Y =0.

Longitudinal beam for the full-scale model was meshed with 'continuum shell elements'. And, interaction of the plywood with the chassis components (cover-sheets, side-rails, and end-beams) were in frictional contact as demonstrated in section 4.4.1.

Vertical displacements for bonded floor semi-trailer and chassis-only are shown in figure 4.37 and 4.38. It shows that the application of bonded floors decrease vertical displacements by 9.47%. Therefore, it is concluded to use complete model to optimise the chassis construction.

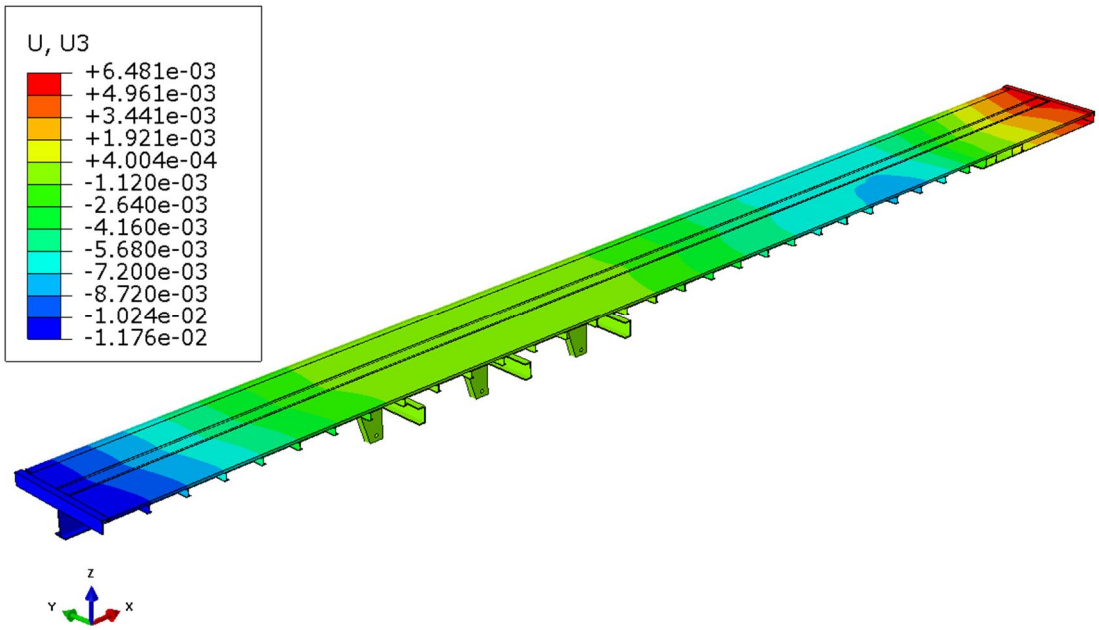

Figure 4.37: The model displacement (U_Z) for the bonded flooring structure came out to be 11.76 mm.

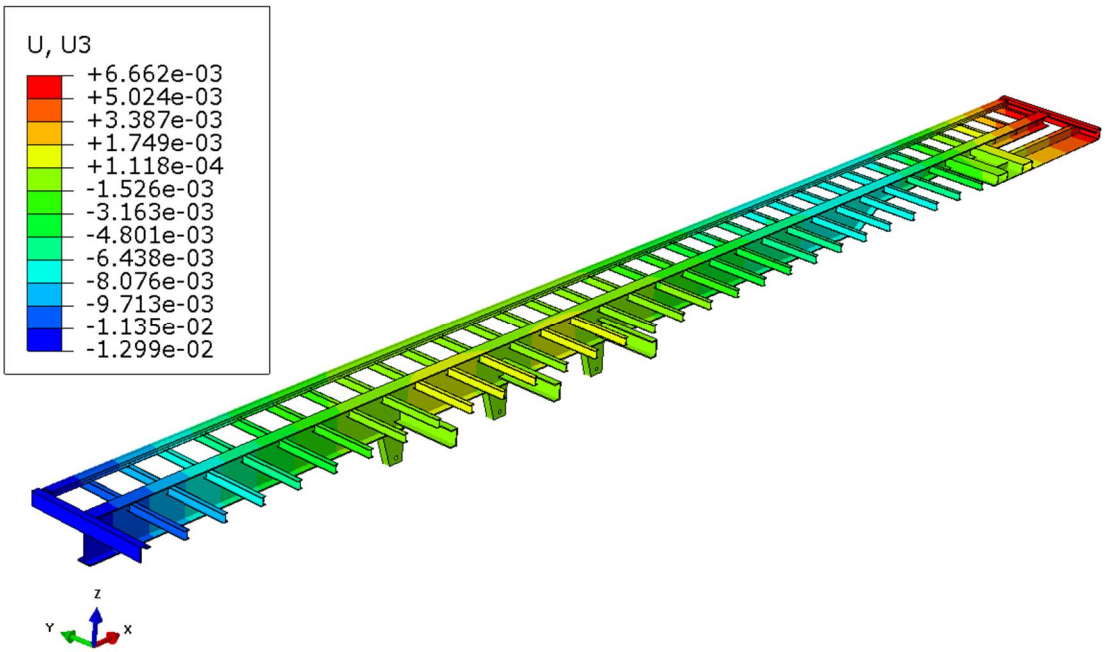

Figure 4.38: The model displacement (U_Z) for the chassis-only condition came out to be 12.99 mm.

Stress distribution of the bonded floor chassis and chassis-only are shown in figure 4.39. The stress distribution for both models were almost similar.

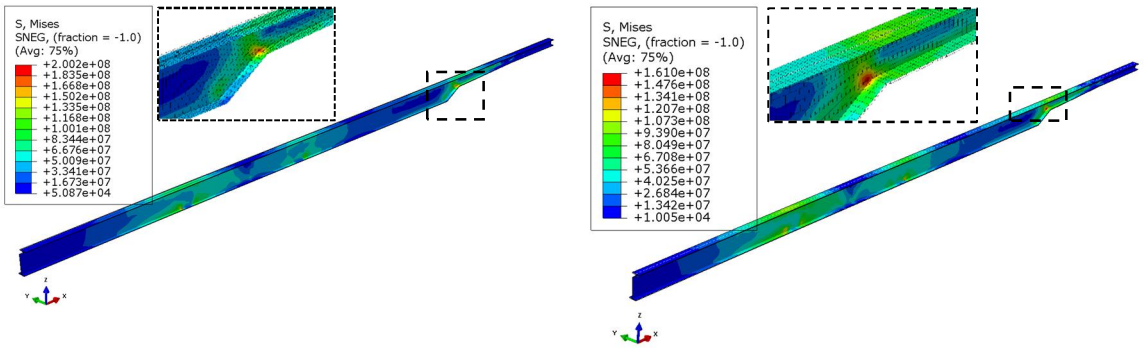

Figure 4.39: Von-mises stress distribution of the bonded floored longitudinal beam (left) versus chassis-only longitudinal beam (right). Stress distribution is comparable.

4.6.2 Optimisation of longitudinal beams for bonded floor semi-trailer

To achieve a higher percentage of weight reduction, two different profiles of the longitudinal beam were compared as shown in figure 4.40. The difference between the two profiles was flange thickness and overall height of the I-profile.

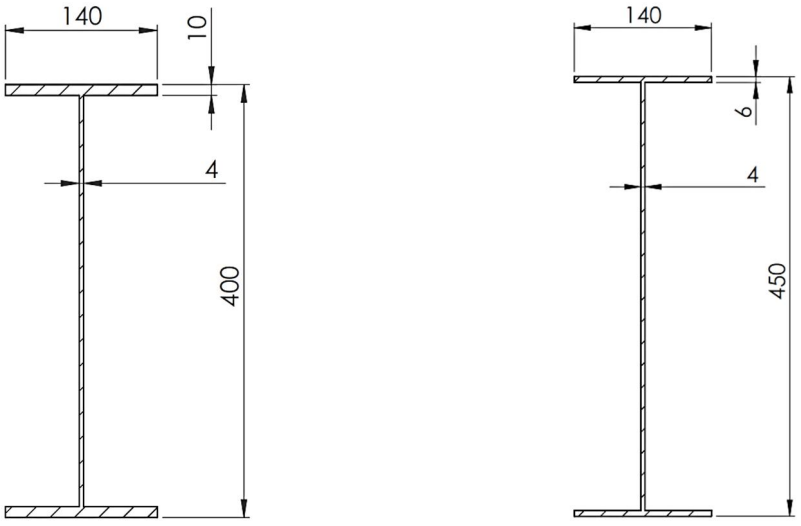

Figure 4.40: Two different profile used in the optimization studies of longitudinal beams in the bonded floor semi-trailer. Profile-1 (left) and Profile – 2 (right).

The geometrical properties of the two profiles used in the simulations are shown in table 4.6. Three simulations were simulations were performed. The third simulation was with the profile – 2 with cut-outs to further reduce the weight.

Table 4.6: Properties of the longitudinal profile used in the comparative studies of semi-trailer

Iteration	**Profile**	**Dimensions**	**Section Area**	**Mass**	**% Mass saving**	$I_{XX} \times 10^7$	ϕ^e_b
No.	[I-Profile]	[mm]	[mm^2]	[kg]		[mm^4]	
1.0	Profile – 1	400×140×10×4	4320	428.45	-	12.48	83.98
2.0	Profile – 2	450×140×6×4	3432	329.80	23.03	11.08	118.16
3.0	Profile – 2 (with cut-outs)	450×140×6×4	-	316.95	26.02		

Bending stiffness is directly related to the moment of inertia whereas bending shape factor is related to the optimum use of the material. Table 4.6 shows that profile-2 have a high shape factor. But, slightly lower moment of inertia which explains the lower stiffness in the simulations.

4.6.2.1 Longitudinal beam optimization in the bonded floor semi-trailer

A nonlinear static analysis was performed. Loading and boundary conditions were similar to bonded floor semi-trailer in section 4.6.1. And, a Tie constraints were used in the complete model to reduce computational time and comprehend the effect of using fully-tied model i.e. using tie constraints for plywood – chassis interface. The vertical displacements for all three iterations are shown in figure 4.41, 4.42 and 4.43.

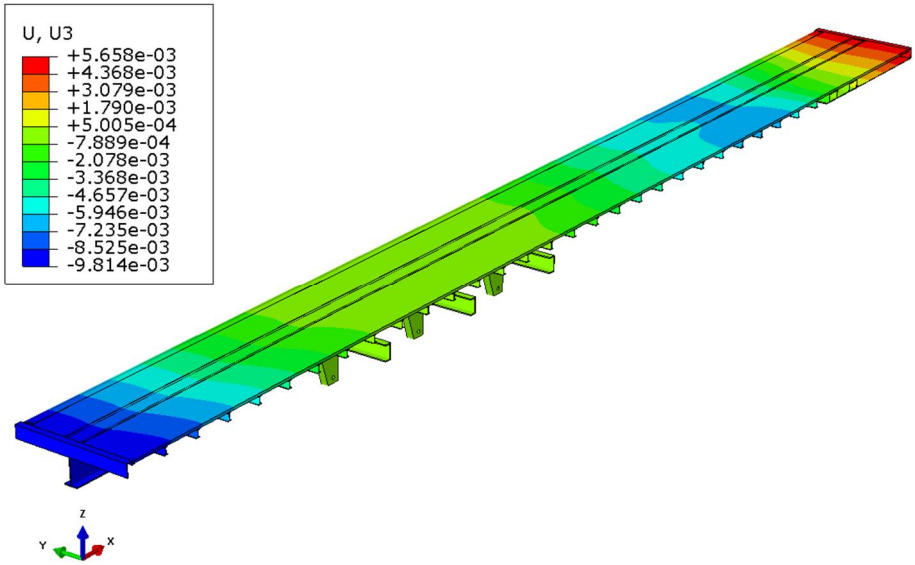

Figure 4.41: Displacement for the semi-trailer model with profile – 1 came out to be 9.81 mm.

Comparing figure 4.41 with figure 4.37 (full-scale model with frictional contact) shows that the use of tie constraints results in 16.55% lower displacement values. It should be considered while making a comprise between computational time and accuracy.

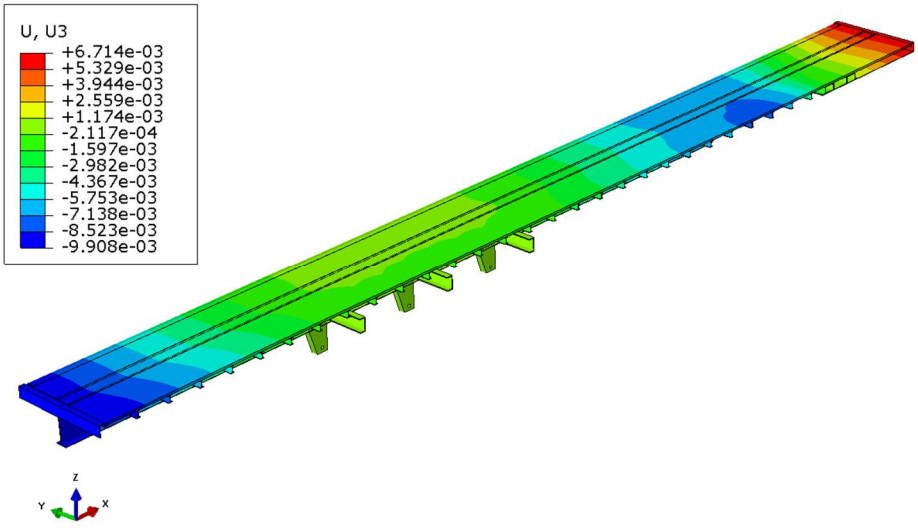

Figure 4.42: Displacement for the semi-trailer model with profile – 2 was 9.91 mm.

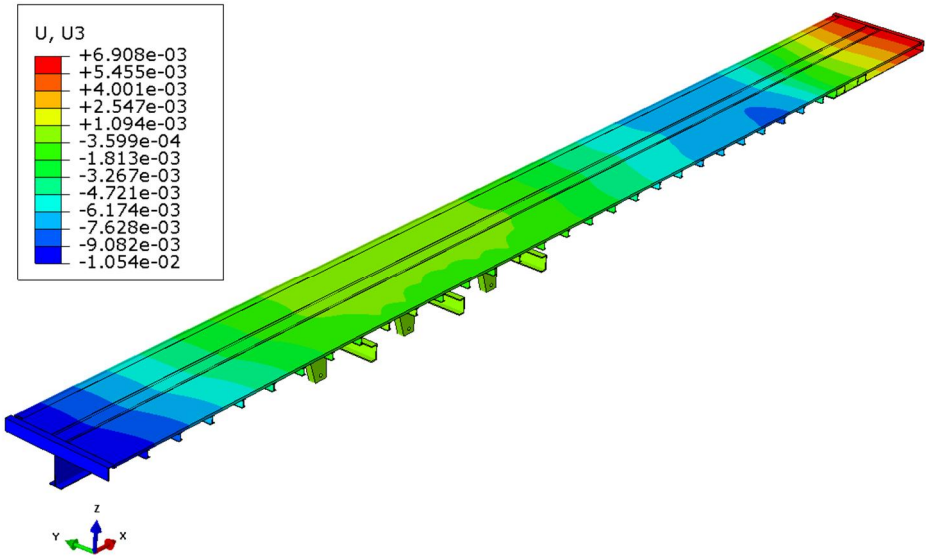

Figure 4.43: Displacement for the semi-trailer model with profile – 2 with cut-outs was 10.54 mm.

The simulation results in figure 4.44 shows that the profile-2 is more suitable profile in this loading case as it reduces the weight of the longitudinal beam by 23.03% which is around 197.30 kg in the complete chassis. And, the resulting profile only increases the model vertical displacement by 0.96%.

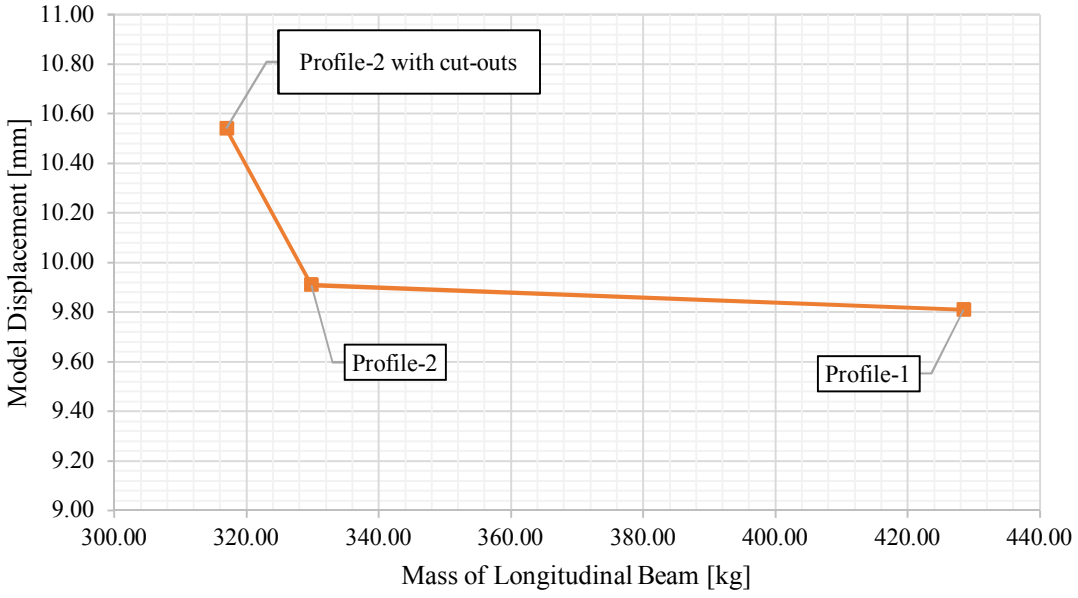

Figure 4.44: Plot showing model displacement (U_Z) with different longitudinal beams. The longitudinal beams have different mass.

5 Conclusions and Recommendations

5.1 Conclusions

An extensive review of the finite elements available in the ABAQUS CAE for FEA of the bonded flooring structure was carried out in this thesis. The selection of the elements was based on literature material. And, couple of comparative studies were performed to verify the element selection process. During the course of this study, it was realised that continuum shell elements (SC8R) works well for layered composite plywood panel and provides two-sided contact option. Second-order continuum elements (C3D20R) for adhesive material is recommended. And, mesh convergence studies confirmed that it was an optimum element type for these studies. The frame components of the chassis were modelled using Incompatible-mode linear brick elements (C3D8I) in the situation where mesh elements were rectangular shaped i.e. chassis structure of scaled-down and partial models excluding side-rails. But, the longitudinal beam in the full-scale model were simulated using continuum shell elements due to geometrically irregular profile.

A comparative analysis was carried out between the FE simulations of scaled-down models for ISO 1496-1 (1990) and their experimental validations. It provided good insight into the bonded flooring structures. The trend of the FE simulations resembled closely to the experimental results with some constant difference. The percentage error between the experiments and FE simulations was between 20-30%. The investigation of various FEM parameters was performed to evaluate critical parameters in the FE modelling such as the effect of material properties of plywood, adhesive, and frictional coefficient between the components. It was noted that the material properties of plywood had a significant role in the model displacement for forklift wheel-load case. The model displacements were moderately affected by the material properties of adhesive material (elastic modulus). It was recorded that the application of stiffer adhesive material increased the percentage difference between FEM and experiments model displacement from 23.91% to 29.13%. But, it also suggests that using adhesive material with higher elastic modulus will improve the stiffness of flooring structure. Lastly, the frictional coefficient between the components had trivial effect on the model displacements. During the scaled-down model simulations, it was observed that the plywood layup had a considerable effect on the model displacement under forklift wheel-load case. The oriented ply arrangement gave 2.82% lower model displacements as compared to special ply arrangement.

In the development of design models for the selection of structural profiles for bonded floor structures, a study was performed using different profile with varying span. It was concluded from the simulation results that I-Profile (cross-beams) provide an optimum trade-off between model displacement and weight of the structure at short and medium span i.e. 300 mm and 400 mm. It was observed that I-Profiles had the highest shape efficiency in the bending dominated condition i.e. $\Phi_e^b = 30.56$. It was also concluded that Z-profile was a suitable choice at long-span i.e. 500 mm due to its second-highest structural efficiency ($\Phi_e^b = 29.96$) after I-profile. And, it has a good resistance to twisting. Percentage difference between the I_Z value of Z-profile and I-Profile was 38.17%. Based on the literature review, closed profiles are preferable due to their higher torsion resistance. In these studies, it was noted that the selected Z-profile was quite comparable to I_Z value of RHS.

The application of advanced materials such as Aluminium 6082-T6 provided an additional parameter that can be used in the development of lightweight semi-trailers. It was also realised that the use of aluminium alloy instead of structural steel S355 reduced the weight of scaled-down model by 65.60%. The stiffness-limited design at minimum mass also suggested the use of aluminium material. It was noted that the structural steel outperforms aluminium 6082-T6 in cost comparison. But, in the development of the high-performance semi-trailers, it is important the use of advanced materials to achieve lightweight structures.

Design optimisation studies of the partial (full-width) and full-scale models showed good potential in the weight reduction using bonded flooring structure. It was noted that redesigning of the chassis frame along with cut-outs has further improve for weight reduction. It was observed that the optimization of cross members provided weight reduction of about 5.28%. And, the application of longitudinal beam with higher shape efficiency reduced its weight by 23.03%. The weight reduction of longitudinal beam with cut-outs reached to 26.02% with little loss in stiffness. Comparative studies of bonded floor semi-trailer and chassis-only model showed that the presence of plywood panel in the FE simulations generated a stiffer response. The model displacements were reduced by 9.47% with the incorporation of bonded plywood flooring. In the end, it was concluded that the bonded flooring provides higher stiffness values. However, the development method shall include complete structure to maximise its optimisation process.

5.2 Recommendations

The development of the optimised flooring solutions for semi-trailers needs to be considered from various aspects. In this regard, the following are recommended:

a. FE models may be further refined to improve the computational cost and efficiency of the design process e.g. using spring elements for adhesive components. Or, the use of solid shell (continuum shell) elements in the chassis structure to improve the model response while reducing computational as recommended by LEAP Australia (2017).

b. FEA may be performed on the different loading conditions experienced by semi-trailers. The complete design optimization shall include all the loading conditions for reliable results.

c. Effects of using thicker plywood of 30 mm and thinner cross members in the bonded flooring structure may be studied. It might require minor redesigning the existing frame which may have the potential to reduce weight of semi-trailer.

d. Effects of adhesive material location and dimensions on the model displacement may be studied and optimised to improve structural performance.

e. Plywood layup (construction) had a significant effect on the model displacements. Therefore, optimisation studies for the plywood ply layup may be performed as it is an important parameter for ISO 1496-1 (1990) floor strength test.

f. Experimental methods play a significant role in the development of the FE models as it acts as a reference case. Hence, the repeatability of experimental process may be verified.

References

ABAQUS, 2016. *ABAQUS Documentation,* Providence, RI, USA: Dassault Systèmes.

Adhesives & Sealants Industry, 2010. *Advancing Adhesives: Advanced High-Strength Solution for Trailer Flooring.* [Online]
Available at: http://www.adhesivesmag.com/articles/89262-advancing-adhesives-advanced-high-strength-solution-for-trailer-flooring

Aghayere, A. & Vigil, J., 2009. *Structural Steel Design (A Practice-Oriented Approach).* Special International ed. New Jersey: Pearson Education.

Ashby, M., 2005. *Materials Selection in Mechanical Design.* 3rd ed. Oxford: Elsevier Butterworth Heinemann.

Ashby, M. F., 1991. Materials and Shape. *Acta Metallurgica et Materialia ,* 39(6), pp. 1025-1039.

Assembly, 2009. *Adhesives for Trailer Assembly.* [Online]
Available at: http://www.assemblymag.com/articles/86655-adhesives-for-trailer-assembly

Assembly, 2011. *Adhesive Bonding: The Hidden Costs of Instant Assembly.* [Online]
Available at: http://www.assemblymag.com/articles/88628-adhesive-bonding-the-hidden-costs-of-instant-assembly

AustubeMills, 2015. *Design Capacity Tables - Profiles structural steel angles, channels and flats,* Newcastle: AustubeMills.

Baguley, D. & Hose, D. R., 1997. *How to - Interpret Finite Element Results,* Glasgow: NAFEMS Ltd.

Bassler, H. I., El-Sebakhy, I. & Malik, D. J., 1992. *Weldbonding of Structural Adhesives for Body Stiffening.* Michigan, Society of Automotive Engineers, pp. 39-55.
Bogdanovich, A. & Kizhakkethara, I., 1999. Three-dimensional finite element analysis of double-lap composite adhesive bonded joint using submodeling approach. *Composites Part B: Engineering,* 30(6), pp. 537-551.

Braess, H.-H. & Seiffert, U., 2005. *Handbook of Automotive Engineering.* 2nd ed. Warrendale: SAE International.

Brooke, L. & Evans, H., 2009. Lighten up!. *Automotive Engineering International,* 117(3), p. Society of Automotive Engineers.

Canex Group, 2010. *Veneer Cutting Method and Pattern.* [Online]
Available at: www.canex-group.com/tech-info3.html

Couchman, D. G. H., Toma, I. A. W., Brehelmans, I. J. W. P. M. & Van deb Brande, I. E. L. M. G., 1999. *Steel-Board Composite Floors.* Espoo, Elsevier.

Department for Transport, 2012. *Transport Statistics Great Britain.* [Online]
Available at: https://www.gov.uk/government/collections/transport-statistics-great-britain

Diehl, T., 2004. *Modelling Surface-Bonded Structures with ABAQUS Cohesive Elements: Beam-Type Solutions.* Wilmington, ABAQUS Users' Conference.

Dow Automotive Systems, 2017. *WISA Bonded Floor Solution.* [Online]
Available at: http://www.dow.com/en-us/products/WISABondedFloorSolution

Eckerlid, J., Åsell, M. & Ohlsson, A., 2010. *Use of Vanadium High-Strength Low-Alloy Steels in Trailers.* [Online]
Available at: http://www.hsla-v.org/hsla_casedetail.php?View=3&ID=16

EN 789, 2004. *Timber structures - Test methods - Determination of mechanical properties of wood based panels.* Brussels: European Committee for Standardization.

Federation of Aluminium Consumers in Europe, 2010. *Aluminium, the best choice in automotive.* [Online]
Available at:
http://www.facealuminium.com/ENG/Hot_topics/Techical_papers/Aluminium_the_best_choice_in_automotive.asp

Fenton, J., 1976. *Handbook of Automotive Design Analysis.* Plymouth: Butterworth & Co.

Fenton, J., 1996. *Handbook of Vehicle Design Analysis.* Warrendale: SAE International.

Finnish Forest Industries Federation, 2002. *Handbook of Finnish Plywood.* Lahti: Kirjapaino Markprint Oy.

Fitch, J. W., 1994. *Motor Truck Engineering Handbook.* 4th ed. Pennsylvania: Society of Automotive Engineers, Inc.

Frisch, K. & Reegen, S., 1984. *Advances in urethane science and technology.* 1 - 9 ed. Westport: Technomic.

Galos, J. L., 2017. *Lightweight Composite Trailer Design,* s.l.: University of Cambridge.

Galos, J., Sutcliffe, D. M. & Cebon, P. D., 2014. *Design of a Lightweight Heavy Goods Vehicle Trailer.* Frankfurt, Association for European Transport.

Galos, J., Sutcliffe, M. & Newaz, G., 2016. Design, fabrication and testing of sandwich panel decking for use in road freight trailers. *Journal of Sandwich Structures and Materials.*

Ghazaly, N. M., 2014. Applications of Finite Element Stress Analysis of Heavy Truck Chassis: Survey and Recent Development. *Journal of Mechanical Design and Vibration,* 2(3), pp. 69-73.

Happian-Smith, J., 2002. *An Introduction to Modern Vehicle Design.* 1st ed. Warrendale: SAE International.

Henkel Corporation, 2013. *Structural Adhesives and NVH Selector Guide,* Connecticut: Henkel Corporation.

Hughes, A. F., Iles, D. C. & Malik, A. S., 2011. *Design of Steel Beams in Torsion,* Berkshire: The Steel Construction Institute.

ISO 1496-1, 1990. *Series 1 Freight Containers - Specification & Testing - Part 1, General Cargo Containers.* Washington DC: International Organization for Standardization.

Ivanov, I. V., Sadowski, T., Filipiak, M. & Kneć, M., 2008. Experimental and numerical investigation of plywood progressive failure in CT tests. *Budownictwo i Architektura ,* 2(1), pp. 79-94.

Keeler, S. & Kimchi, M., 2014. *Advanced High-Strength Steels Application Guidelines.* 5.0 ed. s.l.:World Steel Association.

Krone, 2017. *http://www.krone-trailer.com.* [Online]
Available at: http://www.krone-trailer.com/english/products/curtainsider/paper-liner/

Labans, E. & Kalniņš, K., 2011. *Numerical versus Experimental Investigation of Plywood Sandwich Panels with Corrugated Core.* Jelgava, Latvia University of Agriculture.

LEAP Australia, 2017. *LEAP Australia.* [Online]
Available at: https://www.finiteelementanalysis.com.au/featured/simulation-driving-the-transport-industry/

Madenci, E. & Guven, I., 2015. *The Finite Element Method and Applications in Engineering Using ANSYS.* 2nd ed. New York: Springer International Publishing.

Mallick, P. K., 2010. *Materials, design and manufacturing for lightweight vehicles.* 1st ed. Cambridge: Woodhead Publishing Limited.

MatWeb, 2017. *Aluminum 6082-T6.* [Online]
Available at:
http://www.matweb.com/search/datasheet_print.aspx?matguid=fad29be6e64d4e95a241690f1f6e1eb7

MatWeb, 2017. *ThyssenKrupp PAS 355 Structural Steel for Cold Forming.* [Online]
Available at:
http://www.matweb.com/search/DataSheet.aspx?MatGUID=8eab8a0ca2d7405fbfc59f6de5b7a827&ckck=1

National Research Council, 2003. *Use of Lightweight Materials in 21st Century Army Trucks,* Washington, DC: The National Academies Press.

Patil, K. Y. & Deore, E. R., 2015. Stress Analysis of Ladder Chassis with Various Cross Sections. *IOSR Journal of Mechanical and Civil Engineering,* 12(4), pp. 111-116.

Peng, W. & Yong-hai, W., 2010. *Fatigue Life Analysis of a New Semi-Trailer Frame Based on FEA Method.* IEEE, Yiwu.

Prucz, J. C., Shoukry, S. N., Shoukry, M. S. & William, G. W., 2013. *Lightweight Composite Materials for Heavy Duty Vehicles,* West Virginia: Department of Mechanical and Aerospace Engineering, College of Engineering and Mineral Resources, West Virginia University.

Qiuli Sun, E., 2006. *Shear Locking and Hourglassing in MSC Nastran, ABAQUS, and ANSYS.* California, MSC Software.

Rahman, R. A., Tamin, M. N. & Kurdi, O., 2008. Stress Analysis of Heavy Duty Truck Chassis as a Preliminary Data for its Fatigue Life Prediction using FEM. *Jurnal Mekanikal,* pp. 76-85 .

Rees, D. W. A., 2009. *Mechanics of Optimal Structural Design: Minimum Weight Structures.* 1st ed. Uxbridge: A John Wiley and Sons, Ltd., Publication.

Robson Forensic, 2017. *Robson Forensic.* [Online]
Available at: http://www.robsonforensic.com/articles/trailer-collapse-expert-investigates-semi-trailer-that-collapsed-under-weig

Sadowski, T., Golewski, P. & Zarzeka-Raczkowska, E., 2011. Damage and failure processes of hybrid joints: Adhesive bonded aluminium plates reinforced by rivets. *Computational Materials Science,* 50(4), pp. 1256-1262.

Seiffert, U. & Walzer, P., 1984. *The Future for Automotive Technology.* 1st ed. Wolfburg: Frances Pinter.

Seyfried, P. et al., 2015. Light weighting opportunities and material choice for commercial vehicle frame structures from a design point of view. *Springerlink,* Volume 3, pp. 19-26.

Sika Services AG, 2006. *Elastic Bonding - The basic principles of adhesive technology and a guide to its cost-effective use in industry,* Munich: Die Bibliothek der Technik.

SSAB, 2015. *Trailer Design Guideline ,* Borlänge: s.n.

UPM Plywood, 2017. *About plywood.* [Online]
Available at: http://www.wisaplywood.com/Products/about-plywood/Pages/Default.aspx

UPM Plywood, 2017. *Sizes, thicknesses and weights.* [Online]
Available at: http://www.wisaplywood.com/Products/about-plywood/Pages/Sizes-thicknesses-and-weights.aspx

UPM Plywood, 2017. *Technical Information,* Lahti: WISA plywood.

UPM Plywood, 2017. *WISA-Trans.* [Online]
Available at: http://www.wisaplywood.com/Products/product-catalogue/wisa-trans/Pages/Default.aspx

Veistinen, J. & Pennala, E., 1999. *Finnforest Plywood Handbook.* Lahti: Finnforest OY.

WISA Plywood, 2013. *Eight months with WISA Bonded Floor pilot trailer.* [Online]
Available at: http://www.wisaplywood.com/Applications/References/Pages/eight-months-with-wisa-bonded-floor-pilot-trailer.aspx

Yu, W.-W., 1991. *Cold-Formed Steel Design.* 2nd ed. Rolla, Missouri: John Wiley & Sons. Inc,.

Zachariah, A. T., 2006. *Finite Element Modelling of Adhesive Interface between Steel and CFRP,* Göteborg: Department of Civil and Environmental Engineering, Chalmers University of Technology.

Zehnder, J., Pritzlaff, R., Lundberg, S. & Gilmont, B., 2011. *Aluminium in Commercial Vehicles,* Brussels: European Aluminium Association AISBL.

Öchsner, A. & Merkel, M., 2013. *One-Dimensional Finite Elements: An Introduction to the FE Method.* Berlin: Springer.

Appendices

1 Comparative study of plywood modelling in ABAQUS and ANSYS

A comparative study was performed to comprehend the response of conventional shell (S4R) and continuum shell (SC8R) elements. A simply supported plywood panel (size: 1000 × 400 × 36mm) having 26 birch veneer plies with an oriented ply arrangement under 47kN wheel load (size: 180 × 80mm) was simulated.

The results were compared with the reference (ANSYS) model provided by UPM. The results of the FE simulations are summarised in table 1.

Table 1: Model response of plywood panel with different finite elements

	Displacement [mm]	**Stress, S_{11} 1st Layer [MPa]**	**Stress, S_{11} 2nd Layer [MPa]**	**THSR13 Middle Layer [MPa]**
ANSYS (Reference)	6.07	57.16	86.66	4.28
ABAQUS Shell (Mid-Surface)	6.09	57.89	84.50	3.93
ABAQUS Shell (Top-Surface)	5.88	53.16	78.26	3.99
ABAQUS Continuum Shell	5.85	54.01	79.41	3.89

Figures 1 – 4 shows the comparison of ABAQUS conventional shell (top surface) vs. continuum shell elements.

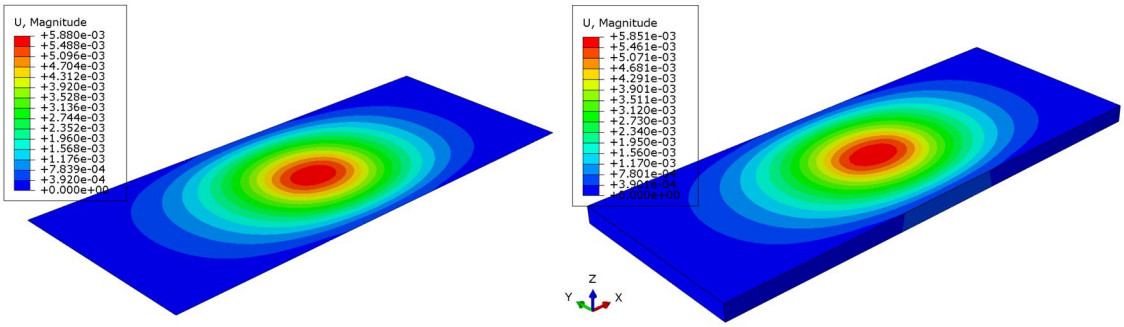

Figure 1.1: Displacement comparison between conventional shell elements (left) and continuum shell elements (right) for plywood panel

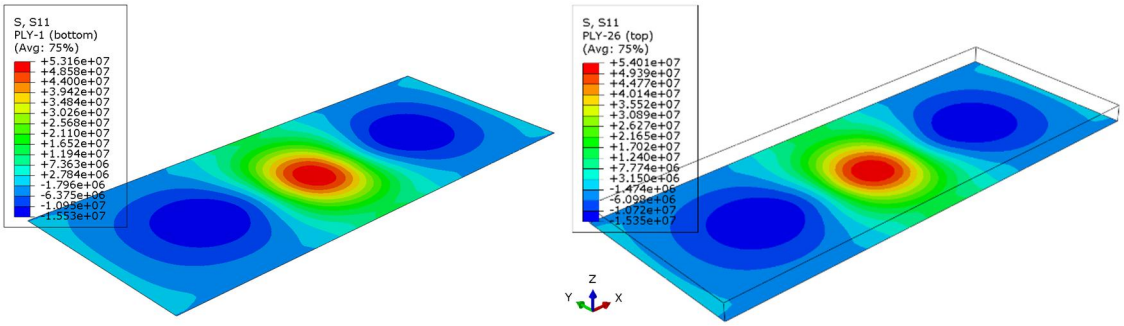

Figure 1.2: S_{11} (bottom ply) comparison between conventional shell elements (left) and continuum shell elements (right) for plywood panel

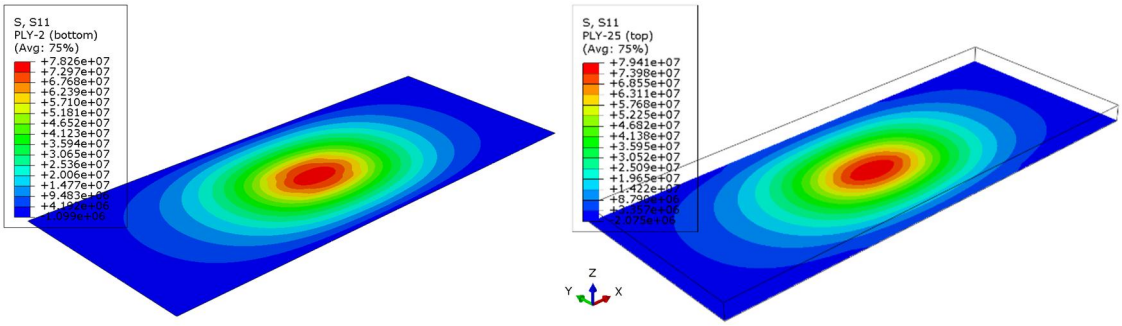

Figure 1.3: S_{11} (second bottom ply) comparison between conventional shell elements (left) and continuum shell elements (right) for plywood panel

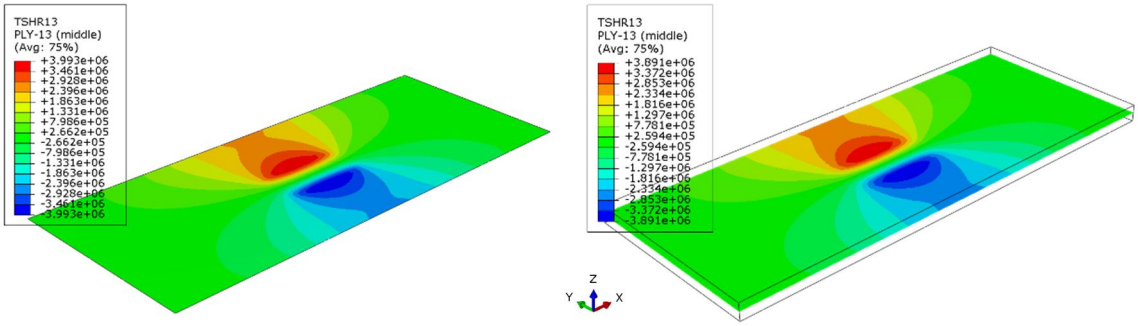

Figure 1.4: Transverse shear stress (second bottom ply) comparison between conventional shell elements (left) and continuum shell elements (right) for plywood panel

Conclusion

Referring to the table 1, it shall be noted that the reference surface for the conventional shell (S4R) elements plays a significant part on the overall displacements and stresses. It is common practice to model shell surfaces by the middle surface as a reference surface. Due to the presence of two-sided contact, the continuum shell is a preferred choice of the element in this modelling work.

2 Comparative study of adhesive material with cohesive and continuum elements

A comparative study was performed on the scaled-down model where the adhesive material was modelled with cohesive (continuum-based) element as well as a second-order brick element. The relative difference of model displacement between the element types was just 0.095% as shown in table 2.1.

Table 2.1: Response of scaled-down model using cohesive and 3D stress elements

Simulation Name	Element Type	Model Displacement
		[mm]
M1-SPL-PS-PL-C	COH3D8	6.286
M1-SPL-PS-PL-C	C3D20R	6.292

Figure 2.1 shows the model displacement between the two different element choices available i.e. cohesive and continuum (3D stress) elements. The scaled-down model used in this study was M1-SPL-PS-PL-C.

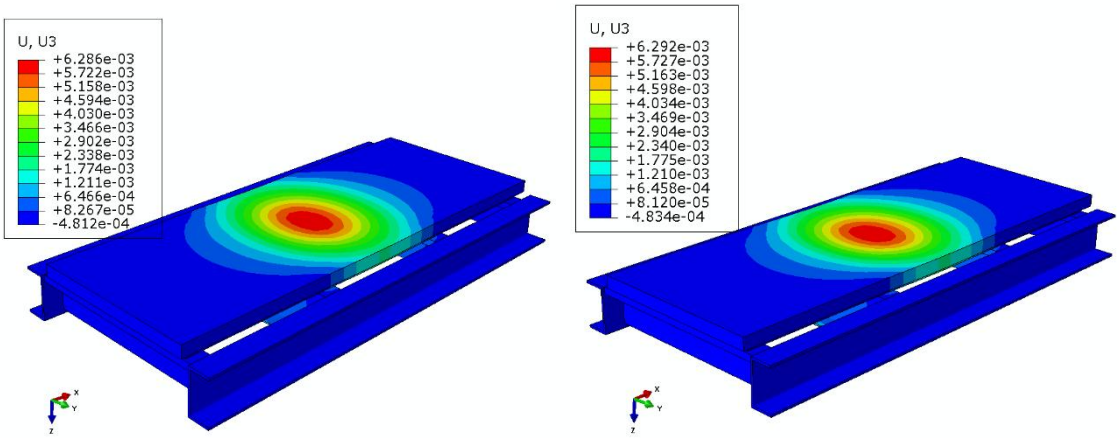

Figure 2.1: Comparison of model displacement with adhesive material model with cohesive elements (left) and 3D stress elements (right)

3 Comparative study of shell and solid FEM of frame components

To study the effect of modelling elements (solid or shell) of the steel components, three simulations were performed under ISO-1496-1 forklift wheel load case with 36 kN pressure load. The simulated model names are shown below:

1. M1-ORN-FS-PL-C
2. M1-SPL-FS-PL-C
3. M2-SPL-PS-PL-C

The solid elements used in the comparative studies for modelling of the steel components were incompatible mode linear elements i.e. C3D8I. The shell elements used in the modelling of steel components (longitudinal and cross beams) were S4R. According to the ABAQUS (2016), S4R are general-purpose robust elements. They are recommended for a wide range of applications as they avoid shear locking by uniformly reduced integration.

Figure 3.1 – 3.3 shows the simulation result comparisons between solid and shell modelling.

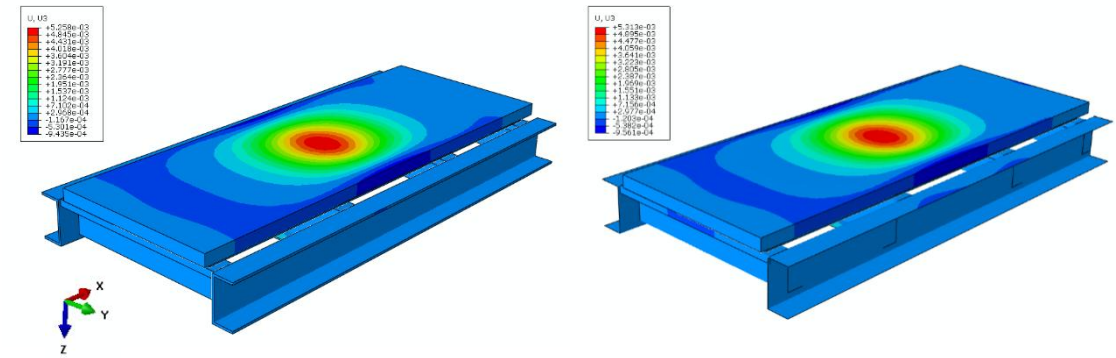

Figure 3.1: Displacement (U_Z) comparison between solid (left) and shell (right) modelling of steel components for M1-ORN-FS-PL-C.

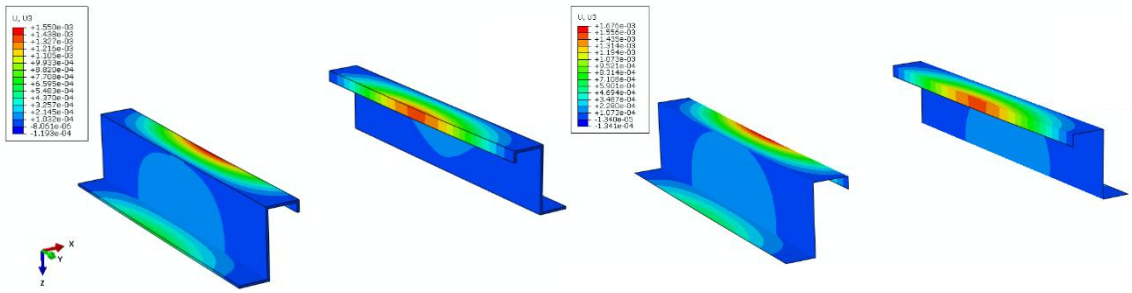

Figure 3.2: Cross member displacement (U_Z) comparison between solid (left) and shell (right) modelling of steel components for of M1-ORN-FS-PL-C.

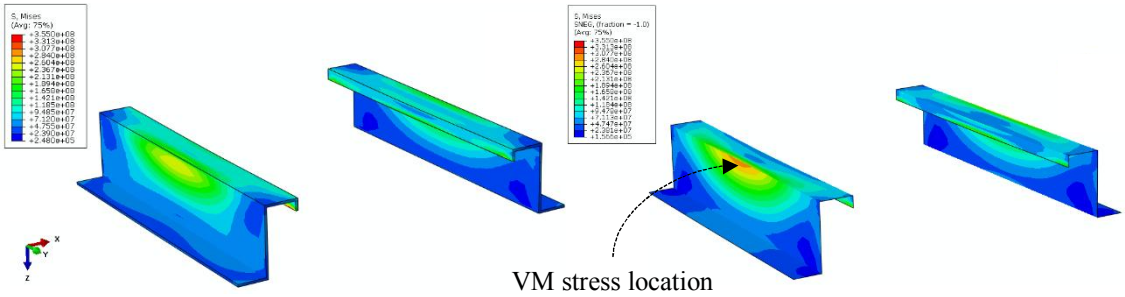

Figure 3.3: von-Mises stress distribution in the cross members. Solid (left) and shell (right) models of cross members for of M1-ORN-FS-PL-C.

It was observed that maximum percentage difference between the model displacement was around 3% where the maximum percentage difference between the cross members is close to 12%. In all cases, the shell elements were more responsive to applied loading compared to solid elements as shown in figure 3.4.

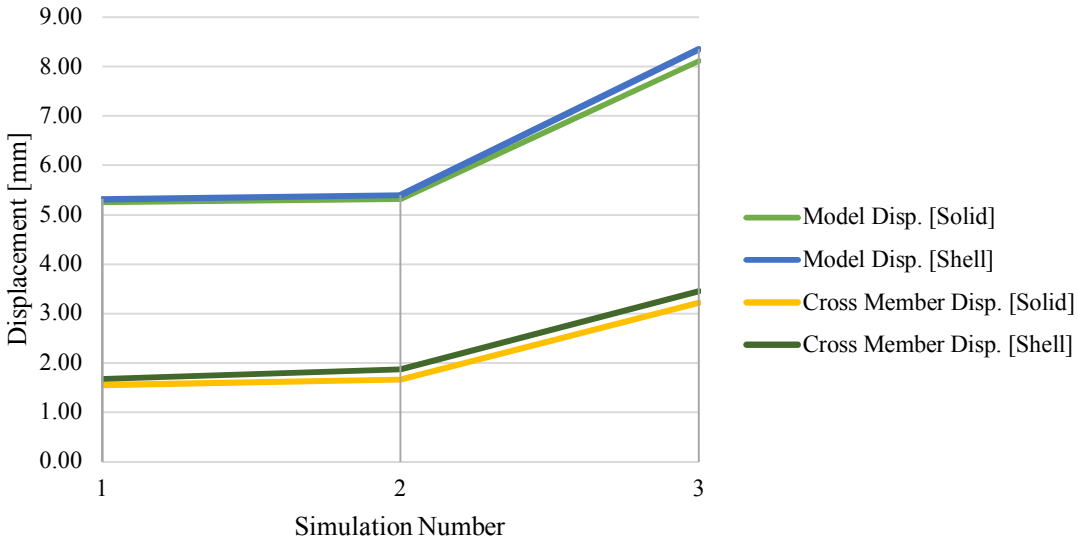

Figure 3.4: The plot showing displacements of the scale-down model meshed with solid and shell elements.

The maximum percentage difference for the von-Mises stress of cross members (solid vs. shell) is close to 3.3% as shown in figure 3.5. The stress values for shell elements in the cross members are interpolated to get the stress value approximately at the same location as in the solid model.

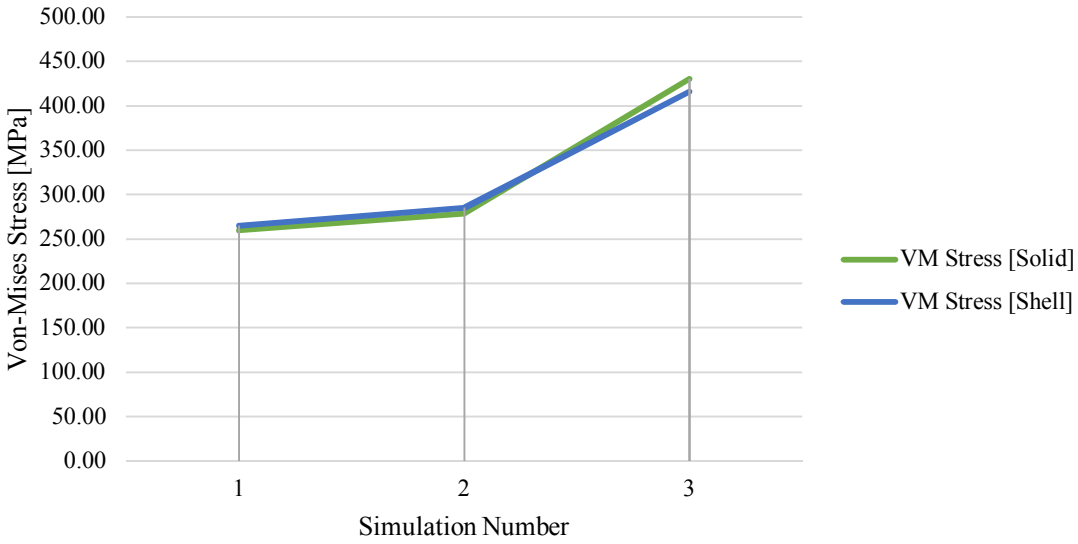

Figure 3.5: von-Mises stress comparison plots between solid (left) and shell (right) modelling of steel components.

A clock time comparison was also made for the same simulations as shown in figure 3.6. The clock time for the simulation 1 & 2 were quite similar as the shell has 6 degrees of freedom with a 4-node element and the solid element has 3 degrees of freedom with a 8-node element. As the mesh size was similar the computational time came out to be quite close.

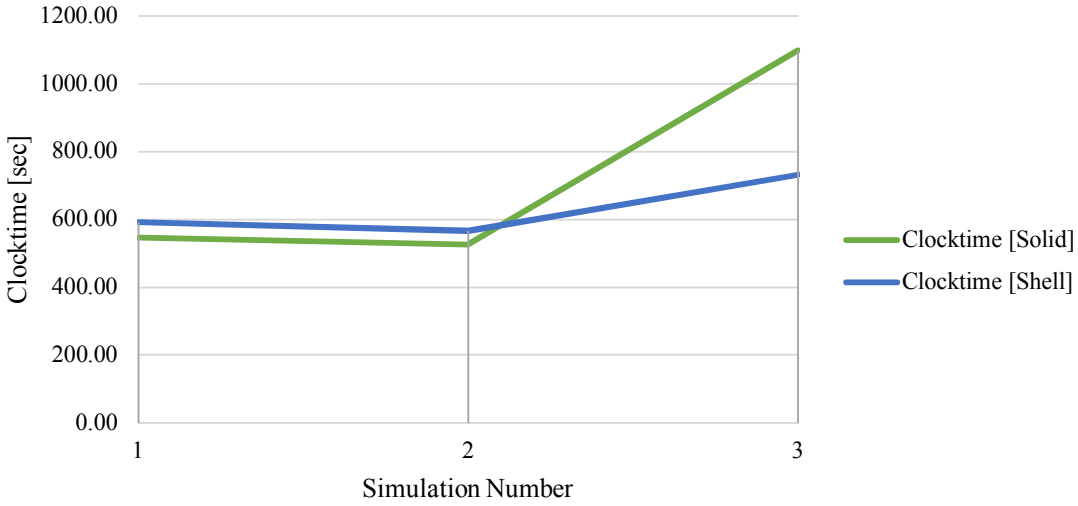

Figure 3.6: The clock time plot between solid (left) and shell (right) modelling of steel components showed as non-conclusive behaviour

The clock time of the third simulation gave indistinct results and it shall be evaluated in the further studies.

4. CAD of scaled-down models
Units : mm

Model Frame - 1

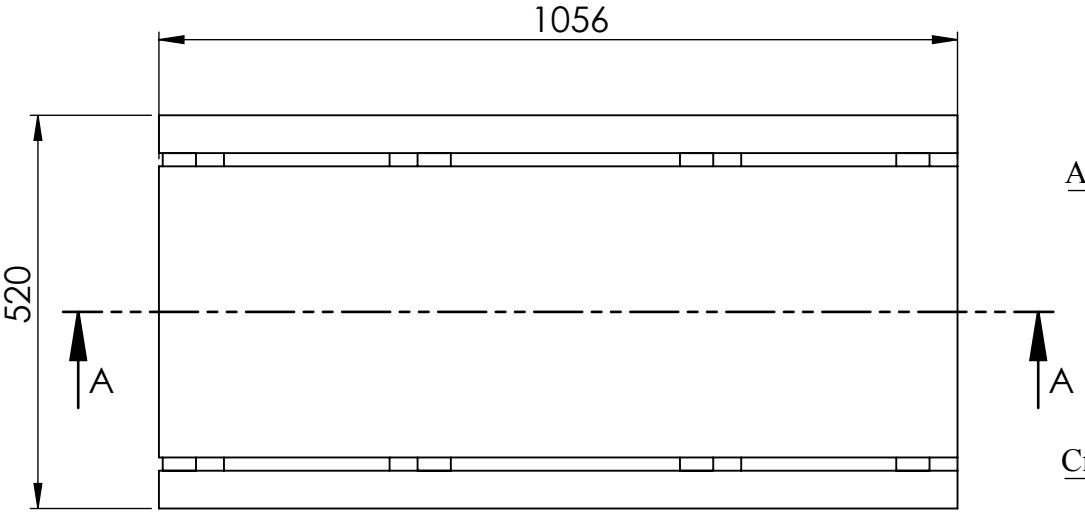

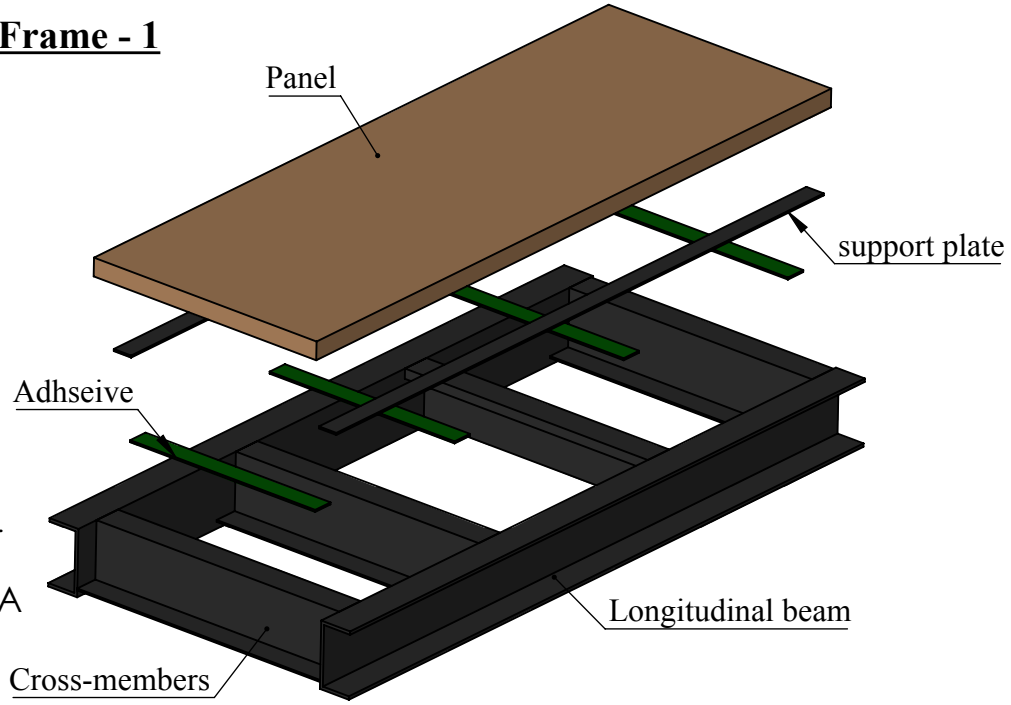

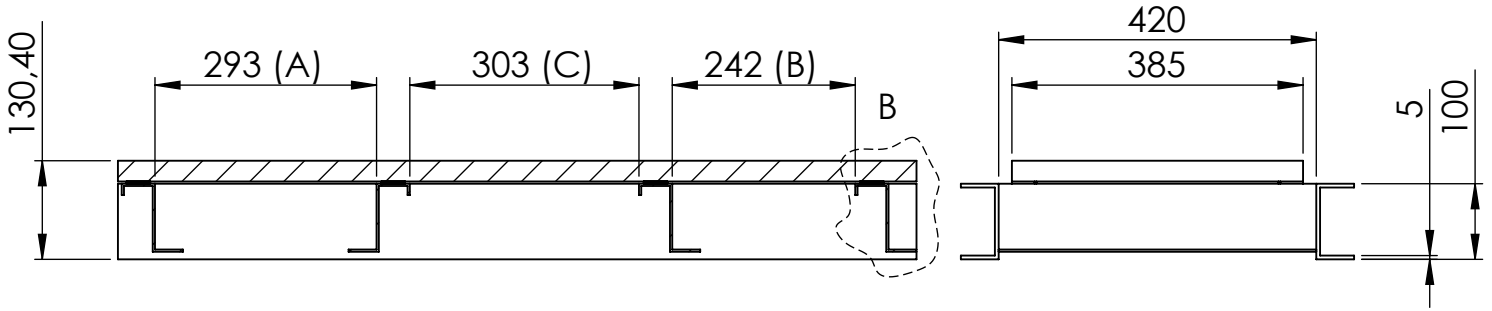

SECTION A-A

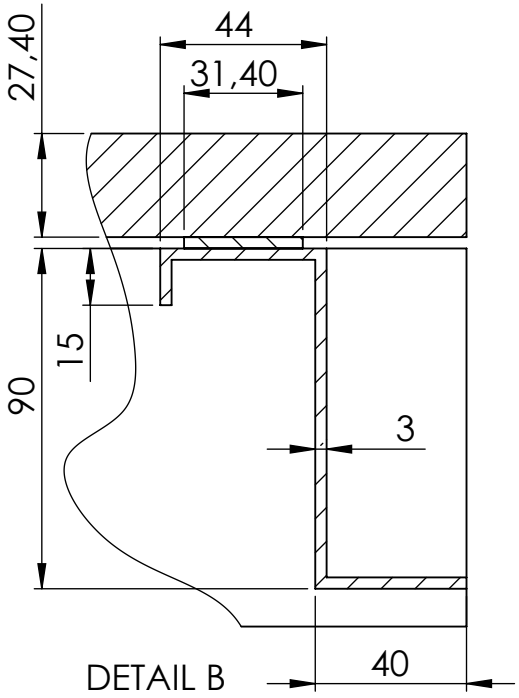

DETAIL B

Model Frame - 2

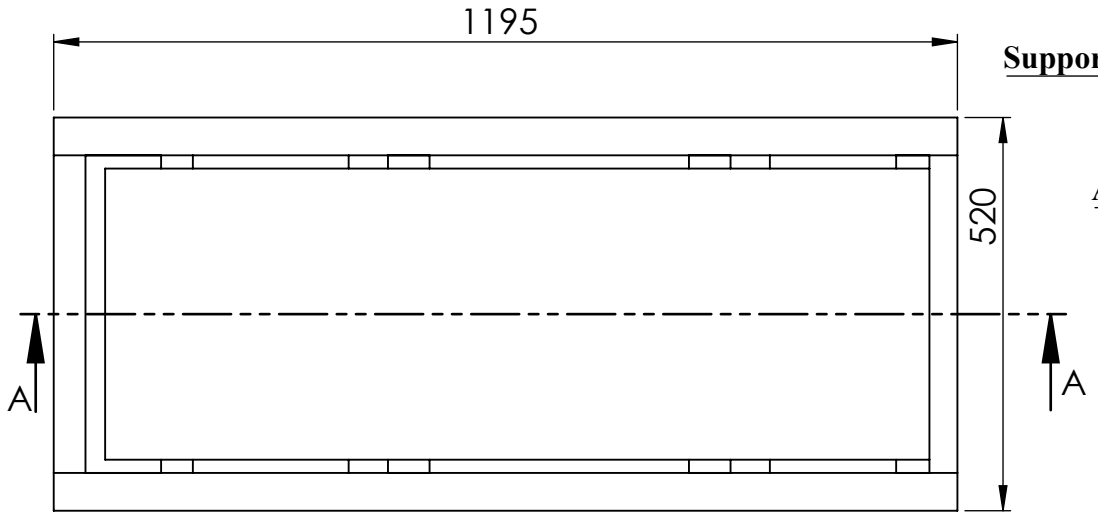

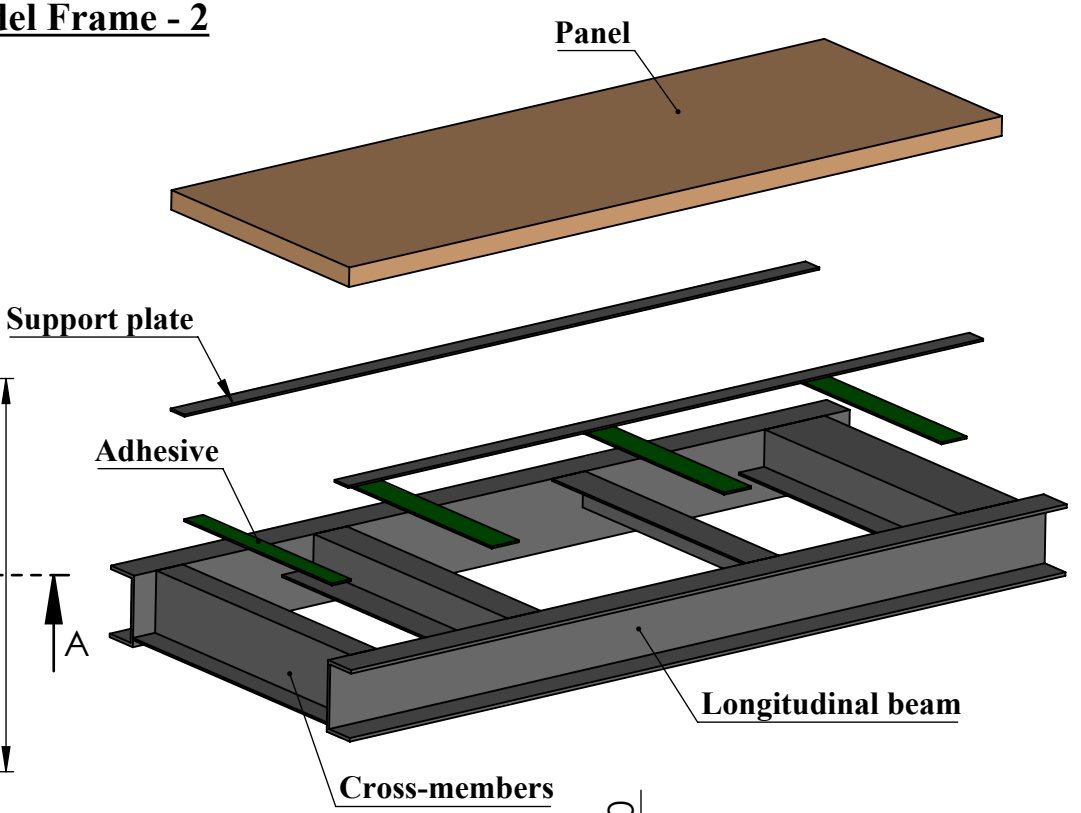

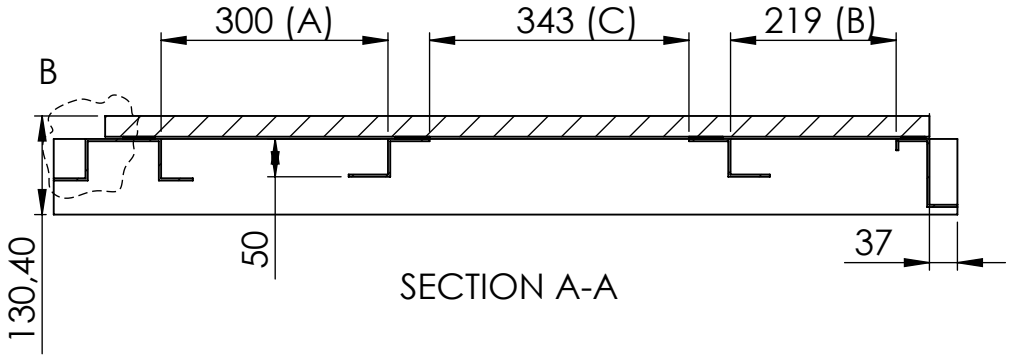

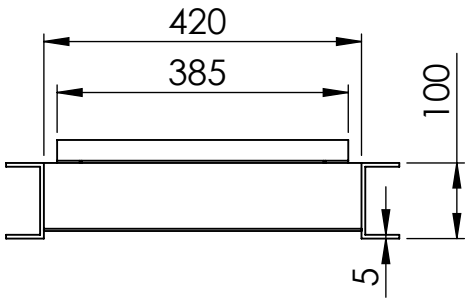

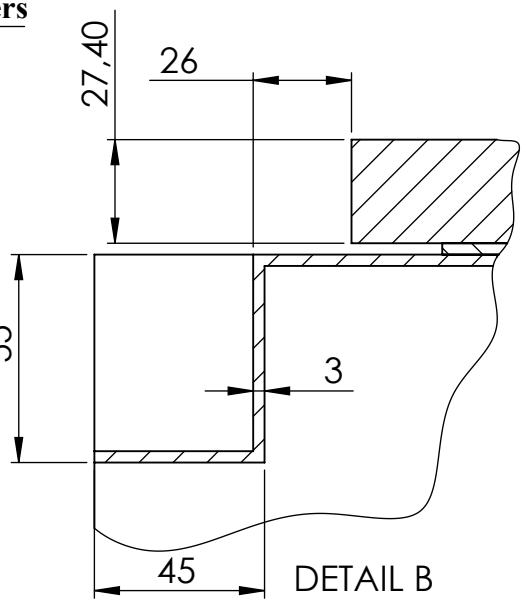

Unit: mm

Model Frame - 3

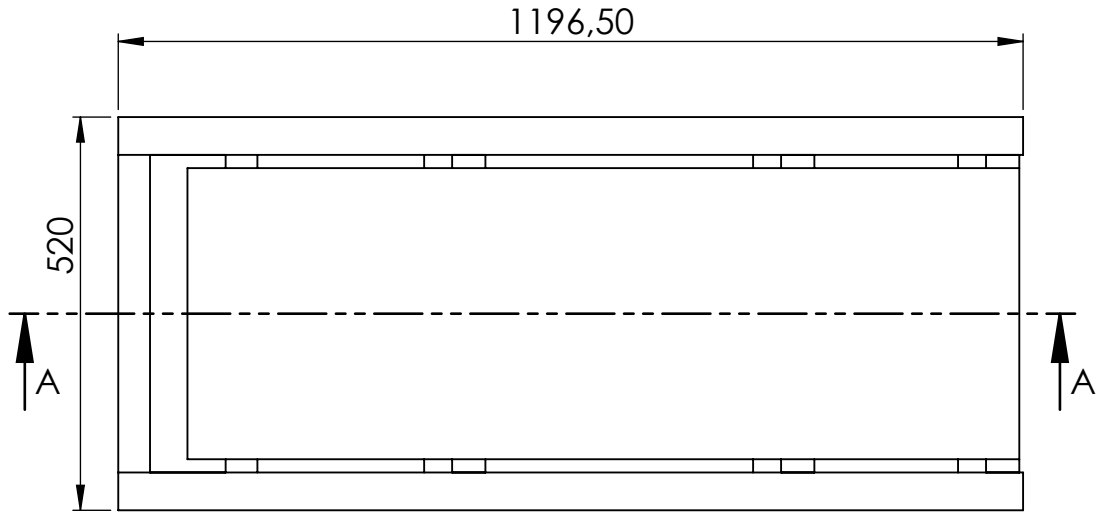

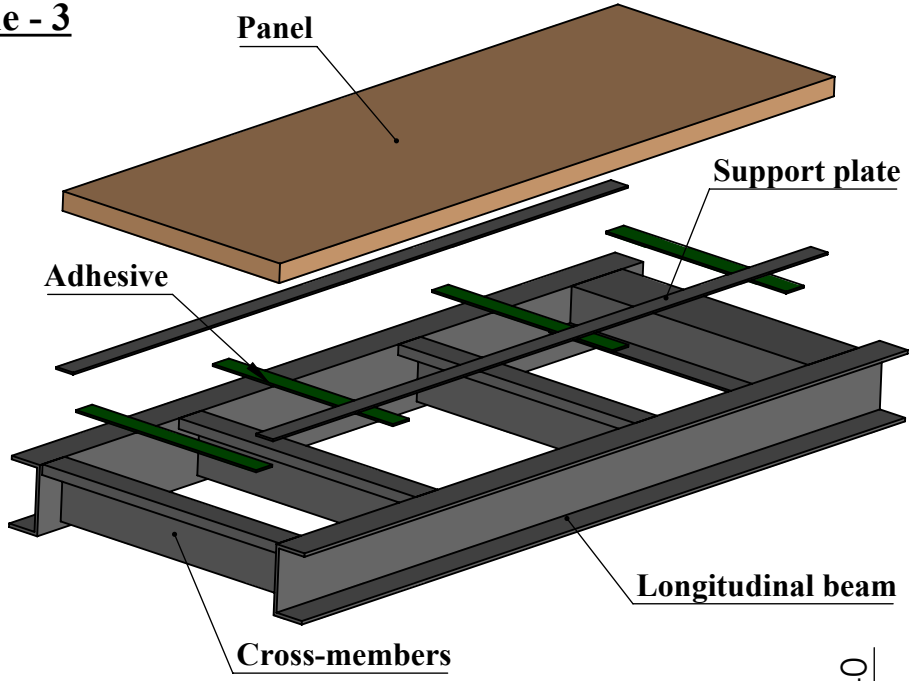

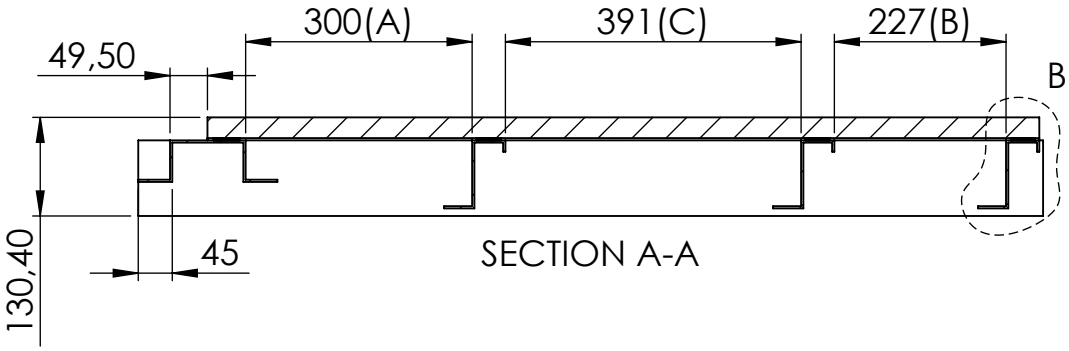

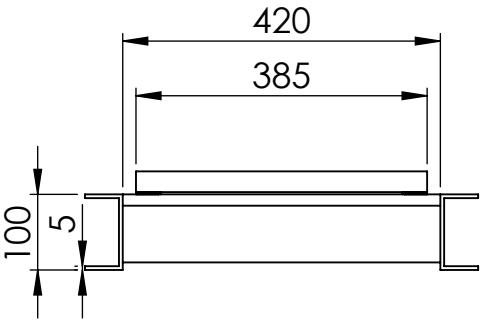

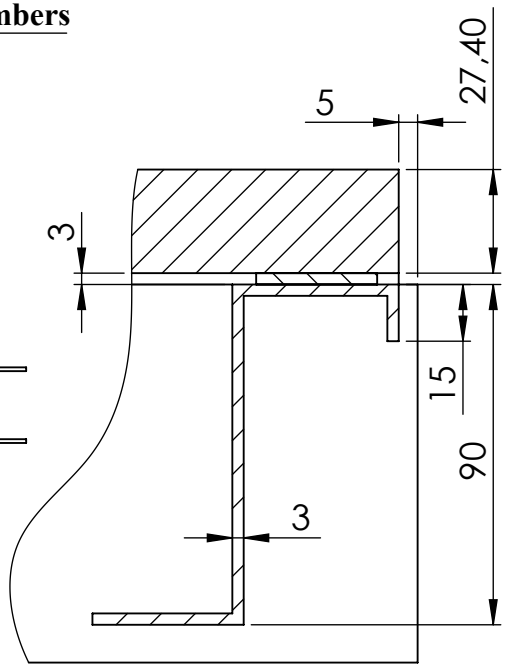

Units: mm

7 Longitudinal beam – cross member contact formulation study

In order to perform model simplification on the cross member – longitudinal beam contact interface, a small model was created to check the displacement and stress response. The objective of this modelling study was to create a simple model contact for ease in generating rectangular elements. The loading and boundary condition is shown in figure 7.1. In figure 7.1(left), the cross member is divided into two pieces and the profile face is in 'Tie' constraint with the longitudinal beam face whereas in figure 7.1(right), the cross member passes through the longitudinal beam and the vertical sides are in 'Tie' constraint.

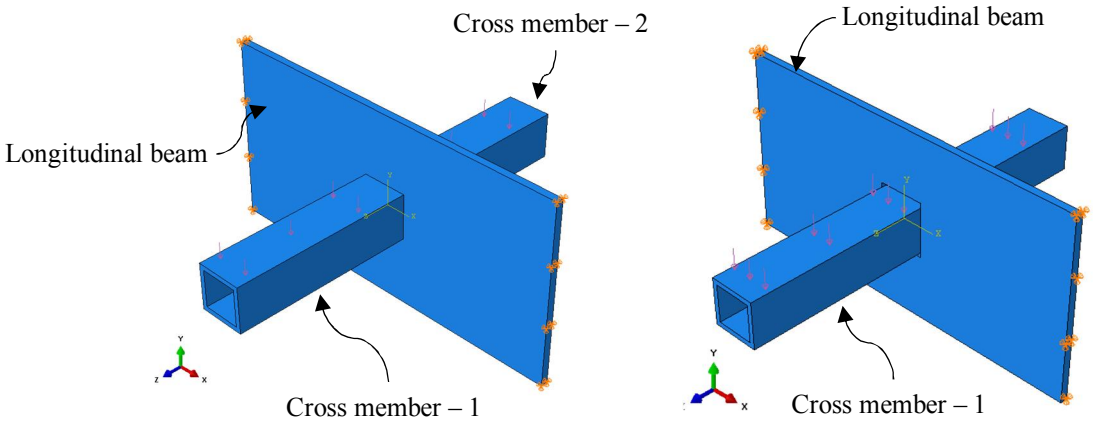

Figure 7.1: Loading and boundary conditions of the small model for contact formulations study

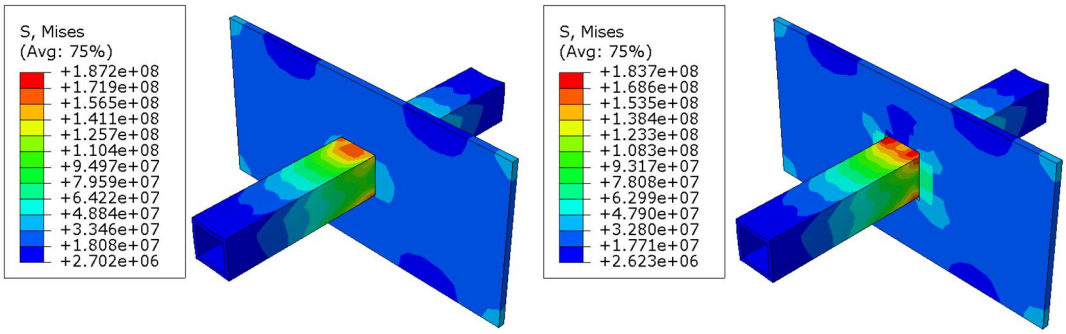

Figure 7.2: von Mises stress for simplified model (left) and original model (right)

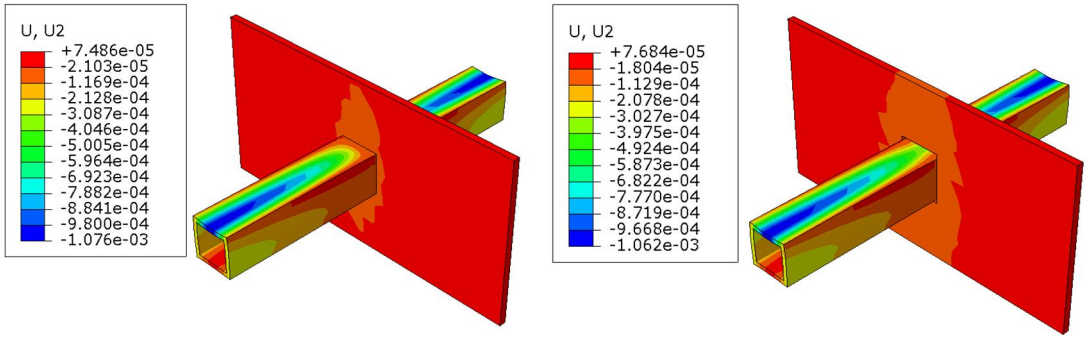

Figure 7.3: Model displacement for simplified model (left) and original model (right)

FE simulations showed that the relative difference in the stresses is 1.88% whereas the model displacements were only 1.31%.

8. FULL-SCALE MODEL

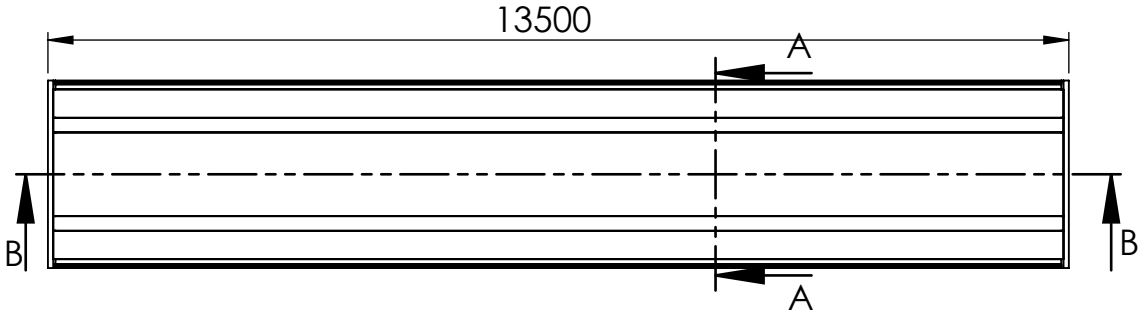

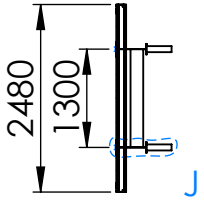

SECTION A-A

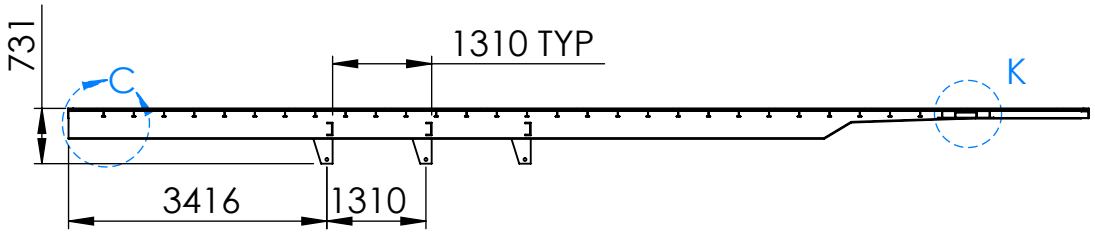

SECTION B-B

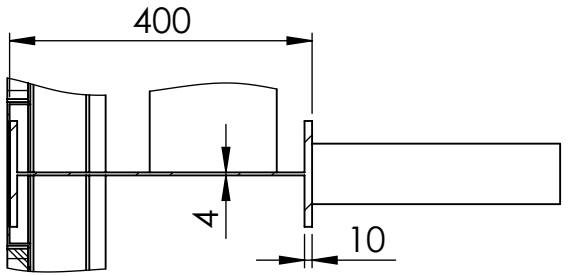

DETAIL J

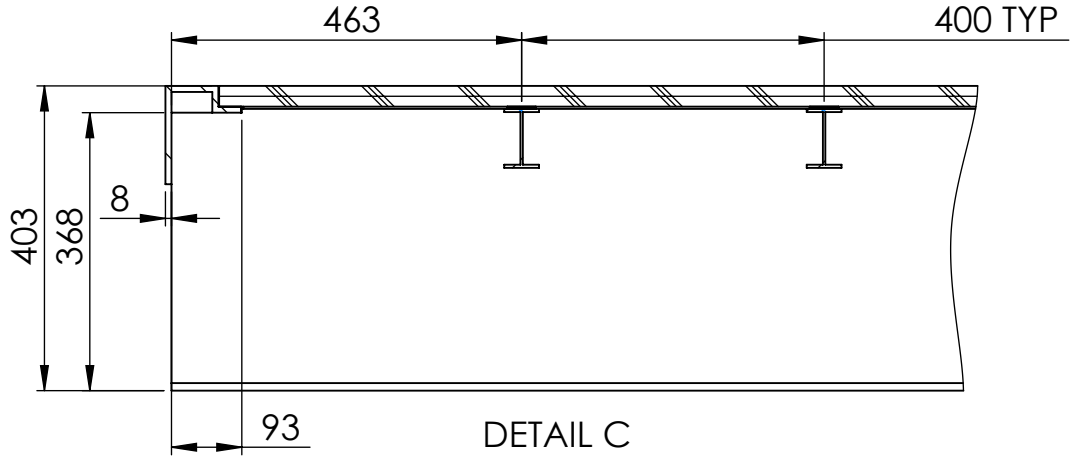

DETAIL C

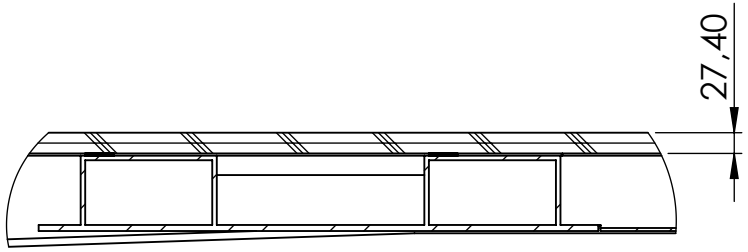

DETAIL K

9 Response of the full-scale semi-trailer under test bench loading case

Torsional and bending stiffness of semi-trailer is usually calculated on the test bench inside factory. A similar loading condition was created to test the bonded flooring structure for the bending stiffness of the bonded full-scale semi-trailer model. Loading and boundary condition as shown in figure 9.1 and 9.2.

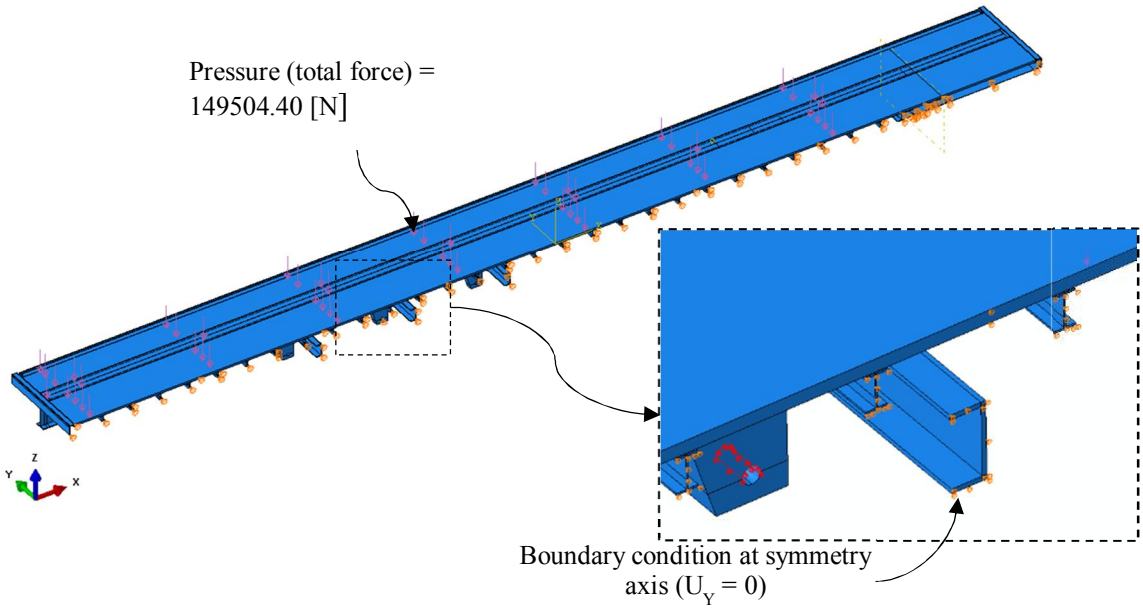

Figure 9.1: Loading and the boundary conditions of the full-scale model under test bench loading condition.

The middle axle support bracket is restricted in the U_Z axis.

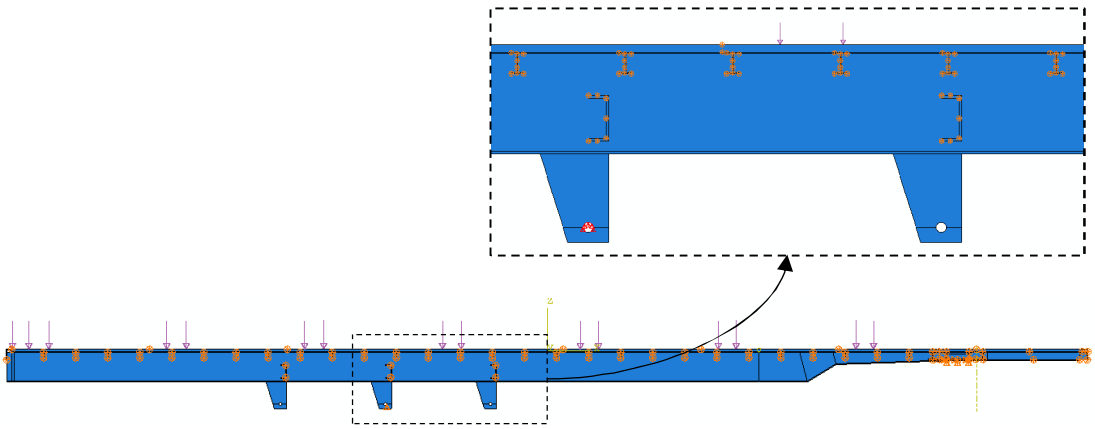

Figure 9.2: Loading and the boundary conditions of the full scale model under test bench loading condition. Only central axle is restricted in the vertical (U_Z) direction.

Figure 9.3 shows the model displacement under test bench boundary conditions. The model displacement was increased by 211.61% due to change in the boundary condition.

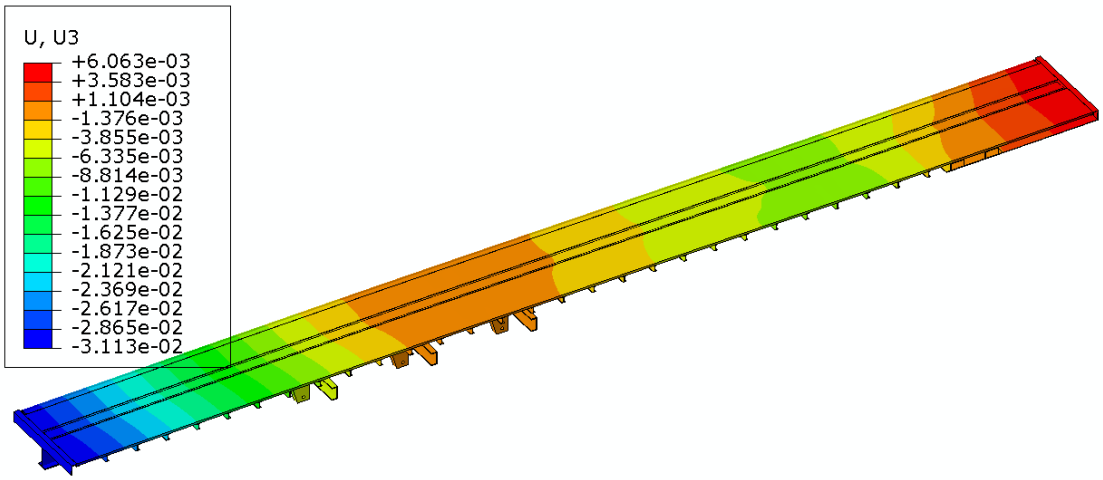

Figure 9.3: Model displacement in the test bench loading condition came out to be 31.13 mm

Figure 9.4 shows the vertical displacement of the chassis structure under test bench boundary conditions. The displacement came out to be 31.13 mm.

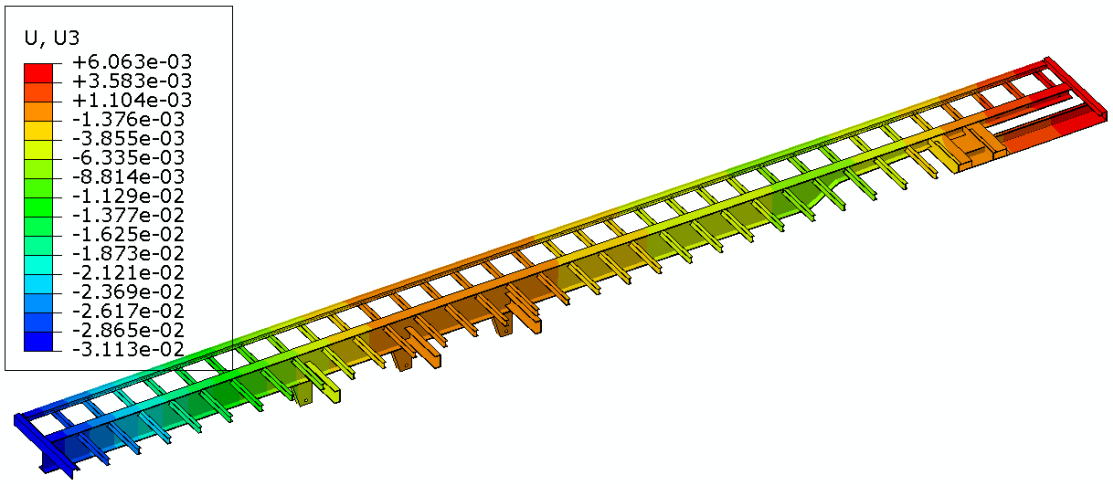

Figure 9.4: Model displacement in the test bench loading condition came out to be 31.13 mm

Figure 9.5 shows the von-Mises of the chassis structure under test bench boundary conditions. It shall be noted that kingpin region and longitudinal beam are the most stressed regions in the bending loads. Excluding the notch stresses, the model is in safe limit.

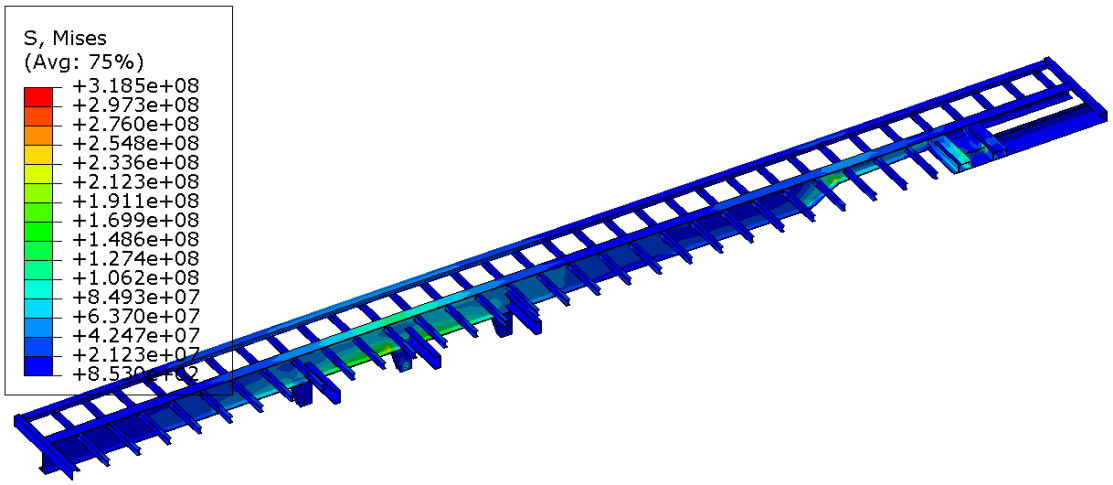

Figure 9.5: Stress distribution (von Mises) in the chassis of the semi-trailer. Peak stresses due to stress concentration at the edges

Figure 9.6 shows the von-Mises of the longitudinal beam under test bench boundary conditions. It shall be noted that the maximum stress in the legend is due to notch stresses.

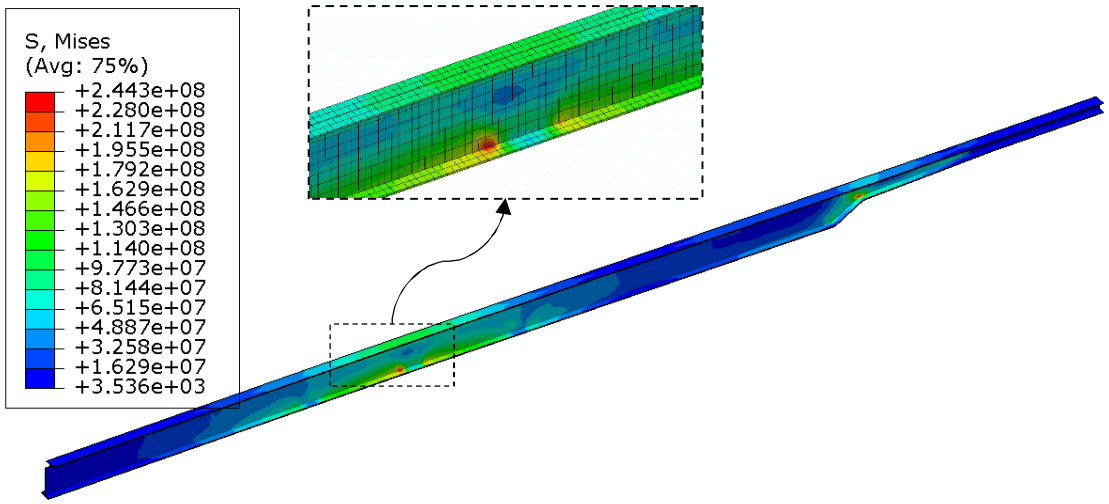

Figure 9.6: Stress distribution (von-Mises) of the longitudinal beam

These simulations can be used as a starting point to compare with industrial data available with the manufactures.